MODELING AND CONTROL OF FREE PISTON ENGINE

A DISSERTATION

SUBMITTED TO THE FACULTY OF THE GRADUATE SCHOOL

OF THE UNIVERSITY OF MINNESOTA

BY

Ke Li

IN PARTIAL FULFILLMENT OF THE REQUIREMENTS

FOR THE DEGREE OF

DOCTOR OF PHILOSOPHY

Professor Zongxuan Sun, Advisor

December, 2014

Acknowledgements

I owe my gratitude to all the people who have made this dissertation possible and because of whom I shall cherish the time at the University of Minnesota forever.

Foremost, I would like to thank my advisor, Professor Zongxuan Sun, for the training, guidance and care throughout my doctoral study. His passion, vision and dedication have always amazed and inspired me. I feel extremely fortunate to be one of his students, for both his technical and nontechnical teachings have and will benefit me through the rest of my career as a researcher.

Besides my advisor, I would like to thank the rest of my thesis committee: Professor Perry Li, Professor Peter Seiler, and Professor Kim Stelson. My gratitude goes to Professor Li and Professor Seiler for their interesting and informative control classes, and to Professor Stelson for his help and supports to this research.

I would like to acknowledge Ford Motor Company for donating the hydraulic free piston engine. I would specifically like to thank Mr. John Brevick for his technical and hardware supports to this research. I would also like to acknowledge the financial and hardware supports from the Center for Compact and Efficient Fluid Power at University of Minnesota. Especially, I would like to express my sincere gratitude to Mr. Mike Gust and Mr. Brad Bohlmann for their help on various aspects of the research.

Also, I would like to thank my colleagues in the Automotive Propulsion Control Laboratory and the Center for Compact and Efficient Fluid Power, for all the technical discussions and fun times. It is a privilege to work with these talented individuals on the exciting research subjects.

To my parents, Chunhui Li and Hong Liu.

Abstract

The free piston engine (FPE) as an alternative to the conventional internal combustion engine (ICE), has great potential for efficiency improvement and emissions reduction. The advantages of the FPE arise from the fact that its piston motion is free from the mechanical constraint, and therefore offers an effective way of controlling the combustion processes in the engine. However, wide application of the FPE technology has not been realized because the challenge of the FPE lies on the same fact that the piston motion can be affected by the combustion and load as well. The objective of this research is to offer a robust and effective solution to the fundamental challenge of the FPE: piston motion control, which can be applied to any FPE architecture so that the wide spread of this technology can be realized. To achieve the objective, the research has been divided into three parts.

First part of the research is to understand the FPE operation through modeling and stability analysis. A comprehensive model of a hydraulic FPE is built to study the characteristics of the engine operation. Additionally, to study the stability of the FPE operation in a systematic way, a novel stability analysis has been conducted based on a cycle-to-cycle model that describes the states that governs the FPE operation.

Second part of the research is the design of an active piston motion control. To leverage the advantages of the FPE but maintaining a stable and robust engine operation at the same time, the idea of piston trajectory tracking is proposed for the first time. An active piston motion control regulates the piston to follow a prescribed trajectory throughout the engine cycles. Essentially, the controller is seamlessly coordinating between the forces

acting on the piston in real time, to allow for the tracking of distinct reference trajectories. The uniqueness of the control is that it guarantees stable and reliable engine operation, and it also enables the design of distinct piston trajectories with respect to the operating conditions, so that engine operation can always be optimized. Because it acts as a crankshaft, but not mechanical, the active motion control is named the 'Virtual Crankshaft'. Precise motion control is critical in order to realize the unique advantages of the virtual crankshaft. Therefore, two feedforward control designs are proposed to assist the motion control and further improve the tracking performance. The virtual crankshaft is implemented on a hydraulic FPE, and the effectiveness of the control has been demonstrated by engine motoring tests. In this part of the research, the control of an alternative hydraulic FPE structure that utilizes digital hydraulic valves to reduce the production cost is investigated as well. The simulation results demonstrate the feasibility of such a design with the virtual crankshaft.

The third part of the research is to demonstrate the effectiveness of the proposed control on the FPE for combustion tests. Unlike engine motoring where the forces from combustion chambers are smooth and repeatable, the combustion force is rapid and varies from cycle to cycle. Therefore, when switching from engine motoring to engine firing, a transient period after the combustion cycle, especially when a strong combustion occurs, prevents the continuous engine operation. The transient period exists due to the fact that the coordination between the hydraulic force and piston motion is interfered by the combustion force. Therefore, a transient control algorithm is developed to eliminate the transient period after the combustion cycle. Essentially, the transient control modifies the

control signal to alter the hydraulic force, and restore the coordination with the combustion chamber, so that piston motion will be maintained. The advantage of the transient control lies on the fact that it retains the repetitive learning mechanism but can adjust intelligently to nonrepetitive disturbances such as motoring to firing transition, misfire and cycle-to-cycle combustion variations. The transient control is implemented on the hydraulic FPE for combustion tests, and its effectiveness has been demonstrated by various combustion scenarios. With the transient control, continuous firing tests are conducted. Detailed analysis of the combustion with various operating conditions is conducted to study the couplings between the combustion and piston motion.

Table of Contents

List of Tables ..... **viii**

List of Figures ..... **ix**

Chapter 1 Introduction **1**

1.1 Motivation 1

1.2 Background 4

1.3 Research Objectives 7

1.4 Dissertation Overview 10

Chapter 2 Modeling and Stability Analysis **13**

2.1 System Description 13

2.2 System Model 17

2.2.1 Thermodynamics 18

2.2.2 Gas Exchange 19

2.2.3 Combustion 21

2.2.4 Hydraulic system 23

2.2.5 Piston dynamics 25

2.2.6 Simulation results and discussions 26

2.3 Stability Analysis 31

2.3.1 Modeling approach 32

2.3.2 Dual chamber coupling 39

2.3.3 Cyclic states 40

2.3.4 Stability analysis 41

2.4 Conclusions 43

Chapter 3 Design of Active Piston Motion Control **45**

3.1 Control of Hydraulic and Piston Assembly 46

3.2 Repetitive Control Design of the hydraulic FPE 55

3.3 Feedforward Control Design 64

3.3.1 Linear feedforward control design 67

3.3.2 Nonlinear feedforward design 69

3.3.3 Experimental and simulation results 73
3.4 Digital Hydraulic Control 82
3.5 Conclusions 91
Chapter 4 Transient Control and Combustion Analysis 93
4.1 Introduction 94
4.2 Combustion Transient 97
4.3 Transient Control 100
4.3.1 Combustion detection 103
4.3.2 Shifting 106
4.3.3 Experimental results 111
4.3.4 Discussions 116
4.4 Combustion Analysis 116
4.4.1 Fuel injection pressure 117
4.4.2 Fuel injection timing 120
4.4.3 Centerline position 124
4.5 Conclusions 129
Chapter 5 Summary and Future Work 132
5.1 Conclusions 132
5.2 Contribution Summary 134
5.3 Future Work 135
Bibliography 137
Appendix 1 147
Appendix 2 149

List of Tables

Table 2.1.Hydraulic free piston engine specifications 17
Table 2.2.Parameter values for system model 31
Table 3.1.Parameter values for feedforward derivation 73
Table 4.1.Combustion data of three centerline positions 129

List of Figures

Fig. 1.1 Crankshaft-based ICE with rotational hydraulic pump 3

Fig. 2.1 The OPOC hydraulic free piston engine system 15

Fig. 2.2. Gas exchange phase diagram of the new Benson's model 19

Fig. 2.3. Free body diagram of inner piston pair (top) and outer piston pair (bottom).....25

Fig. 2.4. Simulated hydraulic pressure, combustion chamber pressure and piston position (from top to bottom) are validated against engine motoring data 26

Fig. 2.5. Block diagram of dynamic couplings of the hydraulic FPE 27

Fig. 2.6. FPE piston dynamics and conventional ICE piston dynamics 29

Fig. 2.7. Steady state combustion chamber pressure, hydraulic chamber pressure and piston position (from top to bottom) at two operating points 29

Fig. 2.8. Transient combustion chamber pressure, hydraulic chamber pressure and piston position (from top to bottom) after a sudden decrease of load 30

Fig. 2.9. Hydraulic FPE piston velocity versus position diagram 36

Fig. 2.10. Arrhenius integrand value versus the piston position 37

Fig. 2.11.TDC position of the left chamber with a small perturbation from the discrete and continuous model 42

Fig. 3.1.Hydraulic subsystem and piston assembly 46

Fig. 3.2 Control system configuration 50

Fig. 3.3 Transient response of the robust repetitive controller 50

Fig. 3.4.Steady state response of the robust repetitive controller 50

Fig. 3.5 Velocity vs. Position diagram of various stroke and speed 51

Fig. 3.6.Control and HIL system configuration 52

Fig. 3.7. a) HIL tracking performance. b) Net force acts on the piston pair from combustion chambers.....54

Fig. 3.8. Frequency response of the system and the estimated linear model 56

Fig. 3.9. Frequency response of Q filter and multiplicative uncertainty 57

Fig. 3.10. Sensitivity function of the repetitive controller design 57

Fig. 3.11. Experimental set-up in test cell: control system (top), free piston engine (left) and charging/loading system (right) 59

Fig. 3.12. Detailed schematic of test cell set up 60

Fig. 3.13. Optimal trajectory and the corresponding hydraulic input 63

Fig. 3.14. Motoring: Gas pressure, hydraulic chamber pressure and piston tracking performance (from top to bottom) 64

Fig. 3.15. Configuration of the control systems with linear and nonlinear feedforward control 67

Fig. 3.16. Inversion of the unstable zero based on the ZPET and Series expansion schemes 69

Fig. 3.17. Tracking performance of the three controllers at 30 mm and 44 mm displacement (from top to bottom: piston trajectory, control signal and tracking error)...74

Fig. 3.18. Transient tracking errors of the three control systems 76

Fig. 3.19. Tracking performance of the three control systems at 50 mm piston displacement (from top to bottom: piston trajectory, control signal and tracking error)...77

Fig. 3.20. Required net hydraulic force to track the references at three piston displacement ranges 78

Fig. 3.21. Simulated tracking performance of the three controllers at 50 mm sinusoid piston trajectory with 414 bar supply pressure (Top left: piston trajectory, top right: control signal; Bottom left: net hydraulic pressure, bottom right: tracking error).....80

Fig. 3.22. Simulated tracking performance of the three controllers with a modified sinusoid piston trajectory (Top left: piston trajectory, top right: control signal; Bottom left: net hydraulic force, bottom right: tracking error).....81

Fig. 3.23 Comparison of the configuration of the current design and the digital hydraulic design 84

Fig. 3.24 Block diagram of the control system of the digital hydraulic design 86

Fig. 3.25 Duty cycles of the two valve modes versus the control signal 87

Fig. 3.26 Simulated tracking performance of the proportional control with a 25 Hz signal 89

Fig. 3.27 Simulated tracking performance of the repetitive control with a 25 Hz signal .90

Fig. 3.28 An alternative PWM valve pulsing scheme 91

Fig. 4.1. Control structure of the HFPE 96

Fig. 4.2. Photograph of the experimental set-up 97

Fig. 4.3 Piston motion, net hydraulic force and control signals of a weak combustion ...98

Fig. 4.4 Piston motion, net hydraulic force and control signals of a strong combustion 100

Fig. 4.5 Diagram of piston motion versus the direction of hydraulic force of in engine motoring and single combustion cases 101

Fig. 4.6. Pressure sensor signal and filtered pressure signal 105

Fig. 4.7 Piston position, combustion chamber pressure and calculated rate of heat release from engine motoring to firing 106

Fig. 4.8 Hydraulic force shifting diagram 109

Fig. 4.9 Control signal shifting diagram 110

Fig. 4.10. Configuration of the hydraulic FPE motion control system 111

Fig. 4.11. Flow chart of the transient control algorithm 112

Fig. 4.12 Piston motion, net hydraulic force and control signals of a single-injection combustion with transient control 114

Fig. 4.13. Piston motion, pressure, heat release and control signals of a multiple-injection combustion with transient control 115

Fig. 4.14. Piston trajectory with the transient control in the case of continuous engine opeation 116

Fig. 4.15 Combustion data at 120 psi fuel injection pressure (from top to bottom: combustion chamber pressure versus displacement, heat release rate versus displacement, and pressure versus volume).....119

Fig. 4.16 Configuration of high pressure fuel injection system.....121

Fig. 4.17 Combustion data at 500 psi fuel injection pressure (from top to bottom: combustion chamber pressure versus displacement, heat release rate versus displacement, and pressure versus volume) 122

Fig. 4.18 Fuel injection timing signal with respect to piston motion 123

Fig. 4.19 Combustion data at -46 mm fuel injection timing (from top to bottom: combustion chamber pressure versus displacement, heat release rate versus displacement, and pressure versus volume).....125

Fig. 4.20 Combustion data at 54 mm fuel injection timing (from top to bottom: combustion chamber pressure versus displacement, heat release rate versus displacement, and pressure versus volume) 126

Fig. 4.21 Intake and exhaust ports location with respect to the combustion chamber centerline 128

Fig. 4.22 Combustion chamber pressure and scavenging pump pressure during continuous engine operation 130

Fig. 5.1. Schematic diagram of the HFPE-in-the-loop test setup with load-emulating system 136

Fig. A1.1 Optimal piston trajectory compared to a modified sinusoid trajectory (position and chamber pressure) 147

Fig. A2.1 Schematic of the scavenging pump 150

Chapter 1

Introduction

1.1 Motivation

Fossil fuels have been the major source of energy for our society since the 19th century. Currently, 78% of the world's energy is produced from fossil fuels. While the energy consumption soars year by year, the fossil fuel reserves are depleting. Furthermore, climate change related to the burning of fossil fuels is becoming a pressing issue. The transportation sector accounts for the largest share of the total growth in world consumption of petroleum, and world energy consumption in the transportation sector continue growing by an average of 2.2 percent per year [1]. Internal combustion engine (ICE) has been the main power source for mobile applications since its invention in the late 19th century. Conventional ICE features reciprocating pistons attached to crankshafts to produce rotational mechanical power. Significant improvement has been made to the engine design to achieve higher efficiency and reduced emissions since the last century. However, as a mature technology, the room left for the improvement on the conventional ICEs is limited. On the other hand, the free piston engine (FPE) as an alternative to the conventional ICE, has great potential for efficiency improvement and emission reduction. The FPE removes the crankshaft that constrains the movement of the piston, therefore it features linear piston motion that is determined by the combustion force and load in real time. The advantages of the FPE design are:

- **Variable compression ratio**: Engine efficiency is found to be closely related to the engine compression ratio [2]. By applying proper compression ratios to different loading conditions, the overall efficiency of the ICE can be significantly improved. The ability to vary compression ratio allows the engine to operate on various fuels as well. Different variable compression ratio mechanisms have been proposed. Most of them suggest modification of the crank/connecting rod mechanism with mechanical linkages and an actuation system [3-5]. Even though the designs offer some flexibility of variable compression ratio control, the improvement of engine performance is limited by the operating range of the mechanism. The large inertia limits the response time of the mechanism, which leads to undesired engine transient behavior, thus degrades the engine performance. What's more, modification of current engine parts and addition of extra components increase the system cost and complexity. The FPE on the other hand offers the ultimate flexibility for variable compression ratio control by eliminating the crankshaft, therefore enables advanced combustions such as low-temperature combustion, which provides better fuel economy and less NOx emission. Initial testing of a FPE, conducted by Sandia National Laboratory, has demonstrated an indicated thermal efficiency of 56% with near zero NOx emissions in a single-cycle experiment [6].
- **Reduced friction loss**: By removing the crankshaft, the crankshaft bearing friction and piston side friction are eliminated as well.

- **Simpler design**: Compared to its crankshaft-based counterpart, FPE carries a simpler design with fewer moving parts, resulting in a compact engine with low production and maintenance costs.
- **Modularity**: For mobile applications including both highway vehicles and mobile heavy equipments, fluid power is currently generated onboard using a crankshaft-based ICE (either gasoline or diesel) with a rotational hydraulic pump (Fig. 1.1). The main drawbacks of this configuration are its relatively low efficiency and complex design of both the ICE and the hydraulic pumping system due to the dynamic operating requirements. The FPE does not connect to load mechanically, which results in a modular design with high flexibility. For a particular application, several FPE units can be combined to provide the power required. However, unlike conventional ICEs, these units can be placed at different locations because they are not interconnected by mechanical linkages. More importantly, they can be turned on and off individually with respect to the loading conditions to ensure optimal efficiency.

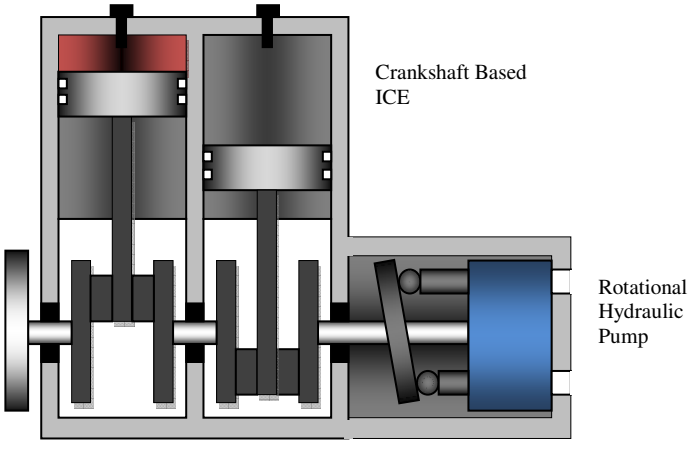

Fig. 1.1 Crankshaft-based ICE with rotational hydraulic pump

The advantages of the FPE come from its flexible design, which enables the engine to adjust to the dynamic operation conditions. Nevertheless, the extra degree of freedom reduces the robustness of the engine operation. By removing the crankshaft, the mechanism that ensures consistent piston motion is dismissed as well. The major technical barrier for mass production of this technology is the large cycle-to-cycle variation, which induces engine misfire, especially during transient operation. For a conventional ICE, the crankshaft is the mechanism, which maintains the piston motion if misfire occurs. However, for a FPE, the combustion, load and the piston dynamics are heavily coupled. The piston motion is determined by the combustion force and load, at the same time, the piston motion is affecting the gas mixing, heat transfer, chemical kinetics of the combustion processes. A misfire or a weak combustion from the last cycle can result in engine stall in the following cycle because the force is not enough to overcome the load. A violent combustion exerts excessive force on the piston that could lead to mechanical damage. Therefore, being able to have a controlled piston motion is the key to the success of this technology.

1.2 Background

FPE can be designed with three different architectures: single piston, opposed piston, and opposed chamber arrangement. Single piston architecture is simple and relatively easy to operate. Opposed piston architecture is self-balanced, therefore produces no vibration. Opposed chamber design allows power to be extracted during each stroke of the engine cycle, and therefore possesses the highest power density. The original FPE patent was credited to Pescara. Pescara started his work on FPEs in 1922 and developed

prototypes for both spark ignition and diesel combustion [7]. More work on FPEs has been reported since then. During the 40s and 60s, many research works had been done on the development of free piston gas generators that produces hot gas to power turbines [8] Both Ford and General Motors developed prototype vehicles in the 1950s'with small scale free-piston gas generators, but none of these made it past the prototype stage. Multi-fuel operation on free piston engine has also been investigated by Flynn [9] and others [10]. The older FPEs rely on mechanical mechanisms [11] to regulate the piston movement, but the overall package of the machine (cost, performance, reliability etc.) was not as competitive as its rotational counterpart. However, as the sensing and computation technology advances, researchers around the globe begin to revisit the idea of FPE from a mechatronic perspective. Many of the modern FPEs are of electric [12] and hydraulic types. Several FPE motion control strategies have been published in the literature. Among them is the Pulse Pause modulation (PPM) control which has been implemented by a number of researchers on single-piston and opposed-piston FPEs [13, 14]. The main idea is to utilize hydraulic circuits as a bounce chamber which holds the piston at its bottom dead center (BDC) to achieve identical piston motion of each engine cycle. A flow control valve is used to adjust the waiting period between the consecutive cycles. Therefore, the output flow rate of the engine can be changed in real time by adjusting the timing of the flow control valve. Researchers from Beijing Institute of Technology have developed a single-chamber hydraulic FPE with 15 kW maximum power output [15]. The engine utilizes its hydraulic circuits and the pulse pause modulation technique [16] to control the operating frequency, and adapts the pause width

to the bottom dead center (BDC) position to minimize cycle-to-cycle variation. The hydraulic FPE is able to achieve stable engine operation with an indicated thermal efficiency of 41%. Due to the identical engine cycles, the PPM control produces nearly constant efficiencies across the engine power output range. However, this approach is only applicable to the single-chamber FPE architectures where continuous operation is not required. Johansen et al. [17] developed a control system for a FPE powered turbine with air bounce chamber. The control system utilizes PID controllers to regulate the location of the top dead center (TDC) by adjusting the air mass in the bounce chamber, while the location of the BDC is controlled by adjusting the fuel injection quantity. Stable engine operation was achieved at a specific operating condition with the proposed control. Mikalsen and Roskilly [18] investigated the motion control of a FPE linear generator with air bounce chamber. A pseudo-derivative feedback (PDF) control maintains the TDC and BDC at the reference by adjusting the fuel injection quantity and air mass of the bounce chamber. In addition, a feedforward control modifies the fuel quantity and air mass according to the load. Simulation results show that the PDF plus feedforward control have a better transient performance than PID control when handling load change. Researchers from Nanjing University of Science and Technology reported the prototype testing results of a single-chamber four-stroke FPE linear generator [19]. A PID control scheme is employed for top dead center (TDC) and BDC location control by adjusting the current and fuel injection quantity. The engine is able to realize Atkinson cycle with a generating efficiency of 32% at 2.2 kW. Researchers from Toyota Central R&D Laboratory [20, 21] have developed a piston motion control for a FPE linear

generator. The motion control consists of a PID control and a gain scheduling map to alter the loading force to regulate the piston motion. The experimental results demonstrate stable engine operation at a specific operating point with the control scheme. An energy-balance based feedback control strategy, which adjusts the fuel injection quantity each cycle by calculating the energy flows in and out from the combustion chamber, was proposed by Tikkanen and Vilenius [22] for a dual-chamber FPE. Simulation results showed that the control strategy was able to produce stable energy operation at various operation points, but it does not address the engine stall issue of the FPE in the case of a misfire. Researchers from the Germain Aerospace center have been developing a free piston linear generator (FPLG). A hydraulic test stand is utilized initially to test the components of the FPLG. With a flatness-based feedforward plus PID and PD repetitive feedback control structure, the hydraulic actuator is able to track high frequency and high amplitude trajectory without the presence of combustion chambers [23]. A demonstrator system (with a linear generator and two opposed air chamber) was then built along with the development of a piston motion control strategy, which is also energy-based, but derives the required instantaneous linear generator force to reach the TDC and BDC target [24].

Besides the limitation of being applicable to only a specific FPE architecture, many of the existing control strategies rely on calibration to be effective. However, the complex interactions between the gas dynamics and the load in real time make the calibration a tedious task, and the resulting controllers are sensitive to variation of the operating conditions and disturbances. This imposes a huge challenge on the engine operation

control and calls for systematic active control design that can precisely regulate the piston motion.

1.3 Research Objectives

Wide application of the FPE technology has not been realized because the challenge of the FPE lies on the same fact that the piston motion is not constrained and can be affected by the combustion and load. How to leverage the advantages of the FPE but maintaining a stable and robust engine operation at the same time? The answer has not yet been found in the literature. The objective of this research is to offer a robust and effective solution to the fundamental challenge of the FPE: piston motion control, which can be applied to any FPE architecture so that the wide spread of this technology can be realized. To achieve the objective, the research has been divided in to three parts.

First part of the research is to answer the following questions: Why is piston motion control important? And how does it affect the FPE operation? The engine operation is relatively complex in a way that the dynamics of the subsystems are heavily coupled. Specifically, the piston motion affects the loading dynamics, the mixing of the gas mixture and the combustion process. Combustion chamber pressure and load further determine the piston dynamics. The intrinsic feedback nature of the engine implies that piston motion control is essential to ensure stable operations. A comprehensive model of a hydraulic FPE is built to study the characteristics of the engine operation. Additionally, to study the stability of the FPE operation in a systematic way, a stability analysis has been conducted based on a cycle-to-cycle model that describes the states that governing the FPE operation.

Second part of the research is the design of an active piston motion control. To leverage the advantages of the FPE but maintaining a stable and robust engine operation at the same time, the idea of piston trajectory tracking is proposed for the first time. An active piston motion control regulates the piston to follow a prescribed trajectory throughout the engine cycles. Essentially, the controller is seamlessly coordinating between the forces acting on the piston in real time to allow for the tracking of distinct reference trajectories. Because the active motion control acts as a crankshaft but not mechanical, it is named the Virtual Crankshaft. The uniqueness of the control is that it guarantees stable and reliable engine operation, and it also enables the design of distinct piston trajectories with respect to the operating conditions, so that engine operation can always be optimized. It is obvious that precise motion control is necessary in order to realize the unique advantage of the virtual crankshaft. Therefore, two feedforward control designs are proposed to further improve the tracking performance. The proposed motion control is implemented on a hydraulic FPE, and the effectiveness of the control has been demonstrated by engine motoring tests. In this part of the research, the control of an alternative hydraulic FPE structure that utilizes digital hydraulic valves in place of the current servo valve plus check valves design is investigated as well. The alternative design offers can significantly reduce the production cost, and the simulation results demonstrate the feasibility of such a design with the virtual crankshaft.

The third part of the research is to demonstrate the effectiveness of the proposed control on the FPE for combustion test, and therefore continuous engine operation can be achieved. Unlike engine motoring where the forces from combustion chambers are

smooth and repeatable, the combustion force is rapid and varies from cycle to cycle. Therefore, when switching from engine motoring to engine firing, a transient period after the combustion cycle, especially when a strong combustion occurs, prevents the continuous engine operation. The transient period exists due to the fact that the coordination between the hydraulic force and piston motion is interfered by the combustion force. Therefore, a transient control algorithm is developed to eliminate the transient period after the combustion cycle. Essentially, the transient control modifies the control signal to alter the hydraulic force, and restore the coordination with the combustion chamber, so that piston motion will be maintained. The advantage of the transient control lies in the fact that it retains the repetitive learning mechanism but can adjust intelligently to nonrepetitive disturbances such as motoring to firing transition, misfire and cycle-to-cycle combustion variations. The transient control is implemented on the hydraulic FPE for combustion tests, and its effectiveness has been demonstrated by various combustion scenarios. With the transient control, continuous firing tests are conducted. Detailed analysis of the combustion with various operating conditions is conducted to study the couplings between the piston motion and combustion.

1.4 Dissertation Overview

All of the research achievements in the thesis will be presented in details as follows:

Chapter 2 (Modeling and stability analysis): In this chapter, a comprehensive model of the hydraulic FPE system is developed. The piston dynamics of the FPE is compared with the conventional ICE. A calibration-based piston motion control is investigated using the model, and simulation results demonstrate the limitation of the calibration-

based control when operating condition changes. In this chapter, stability analysis of the engine operation is also investigated. A cycle-to-cycle based model is derived and validated for this purpose. The model is linearized around equilibrium points with respect to a range of operating conditions for stability checking. The results demonstrate that feedback control is required to achieve stable engine operation.

Chapter 3 (Design of active piston motion control): In this chapter, an active piston motion control is proposed, designed and implemented. The motion control utilizes the energy in the storage unit to regulate the piston to follow a prescribed trajectory. Due to the repetitive motion of the piston, robust repetitive control is employed. Experimental results demonstrate the effectiveness of the proposed control. To further improve the tracking performance of the control system, a linear and nonlinear feedforward control are designed to assist the repetitive control. The combined control system demonstrates the tracking performance beyond the current state-of -the-art in electrohydraulic systems. Additionally, the control of a digital hydraulic FPE design is also investigated in this chapter. The simulation results demonstrate the feasibility of piston motion control with fast response hydraulic on-off valves.

Chapter 4 (Transient control and combustion analysis): In this chapter, a transient control algorithm which involves the modification of the repetitive control is developed. The transient control detects and automatically adjust the control signal to eliminate the transient piston motion caused by aperiodic phenomenon such as transition from motoring to firing or engine misfire (transition from firing to motoring), so that

continuous engine operation can be achieved. Detailed analysis on the effects of operating conditions on the combustion process is then conducted.

Chapter 5 (Conclusion): This chapter concludes the thesis with a summary of the research achievements and future work.

Chapter 2

Modeling and Stability Analysis

The focus of this chapter is to understand the FPE operation via simulation and stability analysis. Specifically, a physics-based model of a hydraulic FPE which includes models of the thermodynamics, scavenging, HCCI combustion and hydraulic system is developed and validated [25-26]. The coordination among combustion, scavenging, piston and hydraulic system under various loading conditions are investigated. Furthermore, a cycle-to-cycle based FPE model is developed to study the stability of the operation analytically [27]. Both the simulation results and stability analysis demonstrate the need for robust and effective piston motion control.

2.1 System Description

The FPE in this research is an opposed-piston opposed-cylinder (OPOC), two-stroke engine. The OPOC design offers the highest power density and scavenging efficiency among the FPE architectures. And the variable compression ratio feature makes it suitable for the low temperature combustion (LTC) implementation, such as the homogeneous charged compression ignition (HCCI). When combined with linear hydraulic pumps, the engine is a highly efficient and modular power generation unit for both on-highway and off-highway vehicles.

Photograph of the hydraulic FPE and its schematic diagram are shown in Fig. 2.1, and the engine specifications are summarized in Table 2.1. The main components of the engine consist of two combustion chambers (left and right), two piston pairs (inner and

outer) and a hydraulic block. The hydraulic block (Fig. 2.1(a)) houses three hydraulic pumps: two small pumps connected with the outer piston pair and a larger pump connected with the inner piston pair. And the plunger area of the larger pump is identical to the total plunger area of the two small pumps. Left chambers (1, 3 and 5) of the three hydraulic pumps are connected to the high pressure (HP) or low pressure (LP) accumulators through a servo valve and two pairs of check valves, whereas right chambers (2, 4 and 6) of the three pumps are interconnected as a synchronizing volume. The inner piston pair and the outer piston pair are designed to move in an opposed but synchronized fashion. However, during engine operation, synchronization will not be automatically guaranteed due to leakages of the hydraulic chambers and force unbalances between the two piston pairs. Unsynchronized piston motion creates undesired cycle-to-cycle variations and unbalanced operating conditions for the two combustion chambers, which will induce engine instability. Therefore, a pair of on-off valves, which connects the right chambers (2 and 6) of the outer piston pumps to LP and HP, is used for piston pair synchronization. A synchronization algorithm is also developed. It controls the open and close timing of the two on-off valves based on the position of the piston pairs (distance between piston head and center of the combustion chamber). When the outer piston position is larger than the inner piston position, the upper on-off valve will open to connect LP to chamber 2. When the outer piston position is smaller than the inner piston position, the lower on-off valve will open to connect HP to chamber 6. The increase or decrease of the chamber pressure will accelerate or decelerate the outer piston accordingly to eliminate the position error between the two piston pairs.

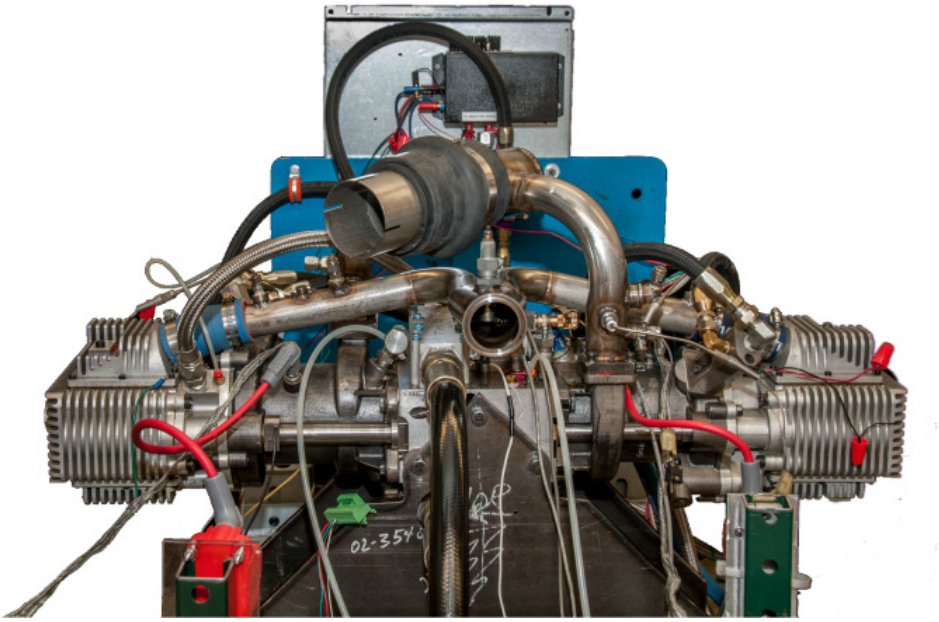

(a)

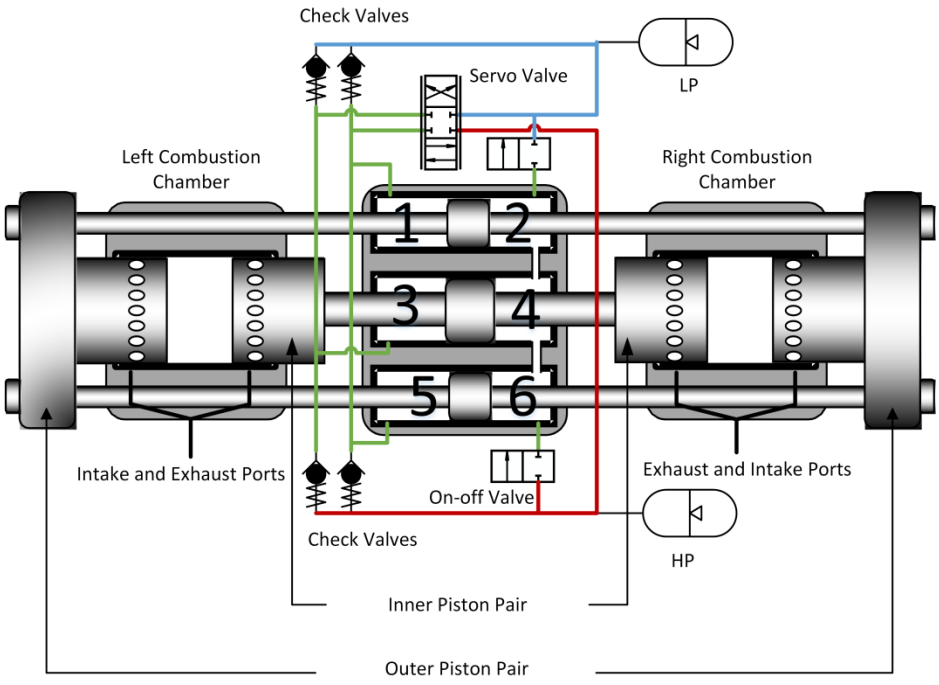

(b)

Fig. 2.1 (a) Photograph of the OPOC hydraulic FPE with a charging/loading unit
(b) Schematics of the Hydraulic FPE

The servo valve as shown in Fig. 2.1(b) is a 4-way 3-position proportional valve, whose position and opening are determined by the sign and magnitude of the input voltage (with 5 ms response time). When the servo valve is at its top position, chamber 3 is connected to HP and chamber 1, 5 are connected to LP. The pressure difference causes the inner piston to move toward the right, and the outer piston toward the left. However, when the valve is at its bottom position, hydraulic force will change direction and move the pistons in the opposite direction. When the servo valve is at its middle position, no fluid flow will go through the servo valve. Instead, check valves will open and close according to the piston motion to pump fluid into HP or withdraw fluid from LP. This correlation between the piston dynamics and the servo valve positioning implies that piston motion control can be realized by manipulating the input voltage to the servo valve.

The engine operation begins with a motoring stage, when energy stored in the HP accumulator is utilized to bring the piston pairs to a repeatable motion, so that combustion can occur smoothly. During engine firing, the piston motion is mainly driven by the combustion force, whereas the hydraulic force is only controlled to compensate for the cycle-to-cycle variations. In Fig. 2.1(b), assume combustion has just occurred at the TDC of the right combustion chamber (at this instant, left chamber is at its BDC). Gas expansion in the right combustion chamber causes the inner piston to move toward the left, and the outer piston toward the right. This motion compresses the gas in the left combustion chamber toward its TDC where the gas mixture will be ignited. Meanwhile, fluid in chamber 3 is being pushed into the HP accumulator, whereas fluid in the LP accumulator is being drawn into chamber 1 and chamber 5. After the gas mixture

combusts at TDC of the left combustion chamber, the inner piston will be pushed toward the right and the outer piston will be pushed toward the left. This motion compresses the gas in the right combustion chamber. Meanwhile, fluid in chamber 1 and chamber 5 are being pushed into the HP accumulator, whereas fluid in the LP accumulator is being drawn into chamber 3. An engine cycle is completed when the pistons reach the TDC of the right combustion chamber.

Table 2.1.Hydraulic Free-Piston Engine Specifications

Item	Specification
Engine	
Bore	79.5 mm
Stroke	120 mm
Displacement/Cylinder	0.6 L
Hydraulic system	
Inner plunger diameter	13.4 mm
Outer plunger diameter	9.48 mm
Piston Mass	9 kg

2.2 System Model

Majority of the modeling work [28-41] on FPE in the literature are of single piston, opposed chamber, and opposed piston types. The OPOC structure of the hydraulic FPE offers unique advantages while adding complexity to the system dynamics. A control oriented model is developed to study the characteristic of the engine operation and the dynamics couplings among the engine subsystems.

2.2.1 Thermodynamics

The gas mixture in the cylinder is assumed to be homogeneous and ideal. States of the in-cylinder gas mixture are determined by the first law of thermodynamics with the effects of kinetic and potential energy been neglected:

$$\dot{U} = \dot{Q} - \dot{W} + \sum \dot{m}_i \cdot h_i - \sum \dot{m}_e \cdot h_e \tag{2.1}$$

where U is the internal energy, Q is the heat transfer, W is the work done by the in-cylinder gas, m_i and m_e are the intake mass flow and exhaust mass flow, h_i and h_e are the enthalpy of the intake mass flow and exhaust mass flow respectively. The rate of change of in-cylinder gas temperature can be obtained by rearranging both sides of (2.1):

$$\dot{P} = \frac{\gamma - 1}{V}\left[\dot{Q} - \frac{\gamma}{\gamma - 1} P\dot{V} + \frac{R\gamma}{\gamma - 1} T_i \dot{m}_i - \frac{R\gamma}{\gamma - 1} T\dot{m}_e\right] \tag{2.2}$$

where P is the cylinder gas pressure, T and T_i are the cylinder gas and the intake manifold temperature. Chamber volume is denoted by V, γ is the specific heat ratio and R is the gas constant. And the cylinder gas pressure can be calculated by integrating (2.2), then apply the ideal gas law we will have the gas temperature

$$T = \frac{P \cdot V}{m \cdot R} \tag{2.3}$$

The heat transfer between gas mixture and engine wall is defined as

$$\dot{Q} = h \cdot A_{wall} \cdot \left(T - T_{wall}\right) \tag{2.4}$$

where A_{wall} is the engine wall surface area, T_{wall} is the wall temperature and h is the heat transfer coefficient, which is derived from a modified coefficient formula for HCCI engine [42].

2.2.2 Gas exchange

The exhaust ports of the combustion chambers are located near the inner piston pair whereas the intake ports are located near the outer piston pair (Fig. 2.1(b)).

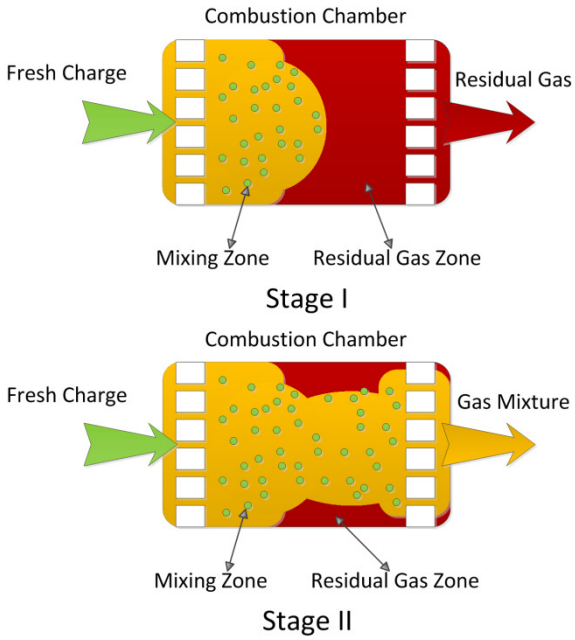

Fig. 2.2. Gas exchange phase diagram of the new Benson's model.

When the exhaust ports are uncovered by the inner piston pair, residual gas is exhausted from the combustion chamber. Similarly, when the outer piston pair uncovers the intake ports, fresh charge is drawn into the combustion chamber. Since the FPE is a two stroke engine, the two processes mentioned above will occur simultaneously (scavenging), instead of two dedicated strokes for each process in a four stroke engine. The OPOC design of the engine enables the uniflow scavenging, during which the fresh charge moves in the same direction with the exhaust residuals resulting in a more efficient scavenging process. Reed valves are mounted on the intake ports to enhance the uniflow pattern. (Fresh charge can only enter through the intake ports).

The fact that intake and exhaust occur simultaneously throughout the scavenging process makes it difficult to compute the gas mixing outcome. In order to simulate the process accurately, we employ the new Benson's model [43] where the scavenging is divided into a two-zone, two-stage process as shown in Fig. 2.2.

At stage I, the fresh charge enters the chamber and mixes with the residual gas to form a mixing zone. The residual flow to the mixing zone is assumed to be proportional to the fresh charge flow to the chamber from the intake ports. Meanwhile, the residual gas is being pushed by the fresh charge and exits from the exhaust ports. At stage II, gas in the mixing zone reaches the exhaust ports and is pumped out of the chamber. The model is based on the following assumptions [44]:

- Uniform pressure across the combustion chamber
- Temperature in each zone is uniform and two zones can have distinct temperature
- No heat transfer between the zones
- Molecular weight and the specific heat of the gas are identical

The mass flow across the intake and exhaust ports are calculated based on steady state compressible isentropic flow equations [45]. When $P_T/P_o \leq (2/(\gamma+1))^{\gamma/(\gamma-1)}$ (choked flow)

$$\dot{m} = \frac{C_d \cdot A_R \cdot P_o}{\sqrt{R \cdot T_o}} \sqrt{\gamma} \left(\frac{2}{\gamma+1} \right)^{\frac{\gamma+1}{2(\gamma-1)}} \tag{2.5}$$

When $P_T/P_o > (2/(\gamma+1))^{\gamma/(\gamma-1)}$ (subsonic flow)

$$\dot{m} = \frac{C_d \cdot A_R \cdot P_o}{\sqrt{RT_o}} \left(\frac{P_T}{P_o} \right)^{1/\gamma} \sqrt{\frac{2\gamma}{\gamma-1} \left(1 - \left(\frac{P_T}{P_o} \right)^{\frac{\gamma-1}{\gamma}} \right)} \tag{2.6}$$

where C_d is the discharge coefficient, P_T is the pressure of downstream, A_R is the port opening area, P_o and T_o are the pressure and temperature of upstream.

2.2.3 Combustion

The hydraulic FPE is designed to operate on HCCI combustion given its ability to realize variable compression ratio operation. The gas mixture in HCCI combustion, which has high air-to-fuel ratio (lean) and is diluted with high exhaust gas recirculation (EGR), is compressed to autoignition. This process produces a more efficient and cleaner combustion cycle.

To ensure the autoignition and low peak temperature for NOx reduction, certain amount of residuals from previous cycle is retained within the combustion chamber to mix with the fresh charge. The Arrhenius integral is used to predict the start of combustion (SOC) timing. SOC is defined at the moment when 1% of the fuel is burned. The combustion duration is defined as the time duration between 1% and 90% fuel is burned, and it is dependent on the air-to-fuel ratio and the SOC temperature. The equations of SOC and combustion duration calculation can be found in [46].

Since HCCI generally operates on lean mixtures, the residual gas contains both air and burned gas. Thus, air-to-fuel ratio of the current cycle *k* is a function of fuel, air, residual gas and burned gas fraction of the previous cycle *k-1*:

$$AFR_{c,k} = \frac{m_{air,k} + \left(1 - b_{p,k-1}\right) m_{res,k}}{m_{fuel,k}} \tag{2.7}$$

where $b_{p,k-1}$ is the burned gas fraction of the residual gas from the previous cycle, $m_{res,k}$, $m_{fuel,k}$ and $m_{air,k}$ are the mass of residual gas retained, injected fuel mass and mass of intake air of the current cycle, respectively. Prior to combustion, the burned gas fraction $b_{c,k}$ can be calculated as

$$b_{c,k} = \frac{m_{res,k}}{m_{res,k} + m_{air,k} + m_{fuel,k}} \cdot b_{p,k-1} \tag{2.8}$$

After the combustion, the burned gas faction becomes

$$b_{p,k} = \frac{AFR_s + 1}{AFR_{c,k} + 1}\left(1 - b_{c,k}\right) + b_{c,k} \tag{2.9}$$

where AFR_s is the stoichiometric air-to-fuel ratio. And this value $b_{p,k}$ will be used in (2.7) for calculating $AFR_{c,k+1}$. Equation (2.7) to (2.9) imply a cycle-to-cycle dynamic coupling of the engine operation.

To simplify the combustion model, heat release from the combustion is assumed to be instantaneous at the end of the combustion duration [46]. So the temperature after combustion is given by

$$\begin{aligned} T_{ac} &= T_{bc} + \left(1 - b_{c,k}\right) \cdot \Delta T, \\ \Delta T &= \frac{Q_{LHV}}{C_v (1 + AFR_{c,k})} \end{aligned} \tag{2.10}$$

where T_{bc} and T_{ac} are the temperature before and after combustion, ΔT is the temperature rise, C_v is the constant volume specific heat and Q_{LHV} is the lower heating value of the fuel. And the pressure after combustion P_{ac} is a function of the pressure and temperature before combustion P_{bc} and T_{bc}:

$$P_{ac} = P_{bc} \cdot \frac{T_{ac}}{T_{bc}} \tag{2.11}$$

2.2.4 Hydraulic system

As described in the previous section, the left chambers of the hydraulic pumps are connected to the accumulators through the check valves and the servo valve, whereas the right chambers serve as the synchronization mechanism. Therefore, the rate of pressure change inside the left chambers of the hydraulic pumps is determined by flow from the check valves Q_{checks}, flow from the servo valve Q_{servo} and flow caused by the piston motion Q_{piston} :

$$\dot{P}_{LH} = \frac{\beta}{V_h}\left(Q_{checks} + Q_{servo} + Q_{piston} \right) \tag{2.12}$$

where P_{LH} is the pressure of the left chambers, β is the bulk modulus of the fluid and V_h is the left chamber volume. The rate of pressure change inside the synchronizing volume is determined by flow from the synchronization valve Q_{syn} and the chamber volume change that is caused by the relative motion between the inner and outer piston ΔQ_{piston}:

$$\dot{P}_S = \frac{\beta}{V_S}\left(Q_{syn} + \Delta Q_{piston} \right) \tag{2.13}$$

where P_S is the pressure of the synchronizing volume, the chamber volume V_S is varying with the piston position x. And flow caused by the piston motion Q_{piston} is given by

$$Q_{piston} = A_h \dot{x} \tag{2.14}$$

where A_h is the plunger area, and flow through the valves are modeled by the orifice equation as follows:

$$Q_{checks} = C_{checks} A_{checks} \sqrt{\frac{2(P_{LH} - P_{acc})}{\rho_{fluid}}} \tag{2.15}$$

$$Q_{syn} = C_{syn} A_{syn} \sqrt{\frac{2(P_s - P_{acc})}{\rho_{fluid}}} \tag{2.16}$$

$$Q_{servo} = C_{servo} A_{servo} \sqrt{\frac{2(P_{LH} - P_{acc})}{\rho_{fluid}}} \tag{2.17}$$

where C_{checks} A_{checks}, C_{syn} A_{syn} and C_{servo} A_{servo} are the discharge coefficients and orifice areas of the check valves, the synchronization valves and the servo valve, respectively. Fluid density is denoted by ρ_{fluid} , and accumulator pressure by P_{acc}. Value of the effective area of the servo valve ($C_{servo} \cdot A_{servo}$) is determined by the voltage signal sent to the valve, and here we assume the valve is a first order system with time constant τ:

$$\begin{aligned} &\frac{K(s)}{V_{signal}(s)} = \frac{K_{\max}}{V_{\max}(\tau s + 1)} \\ &K = C_{servo} \cdot A_{servo} \end{aligned} \tag{2.18}$$

where V_{signal} is the input voltage amplitude, V_{max} is the maximum voltage input, K is the effective orifice area and K_{max} is the maximum effective area given by the valve manual. Since the servo valve is a four-way-three-position valve, the sign of the input determines the position of the spool and thus determines which accumulator the hydraulic chambers are connected to. In other words, P_{acc} in (2.17) varies between high pressure and low pressure with the sign of the input voltage.

2.2.5 Piston dynamics

Piston dynamics of the FPE is a function of the combustion chamber pressure, hydraulic chamber pressure and friction force. The free body diagram of the piston pairs is shown in Fig. 2.3, and the governing equation is outlined in (2.19):

$$\ddot{x} = \frac{1}{M}\left(F_{left}\,(x,\dot{x}) - F_{right}\,(x,\dot{x}) - F_{f}\,(\dot{x}) + F_{hyd}\,(x,\dot{x}) \right) \tag{2.19}$$

where M is the piston mass. F_{left}, F_{right}, F_f and F_{hyd} denote the forces from left combustion chamber, right combustion chamber, friction and hydraulic chamber, respectively.

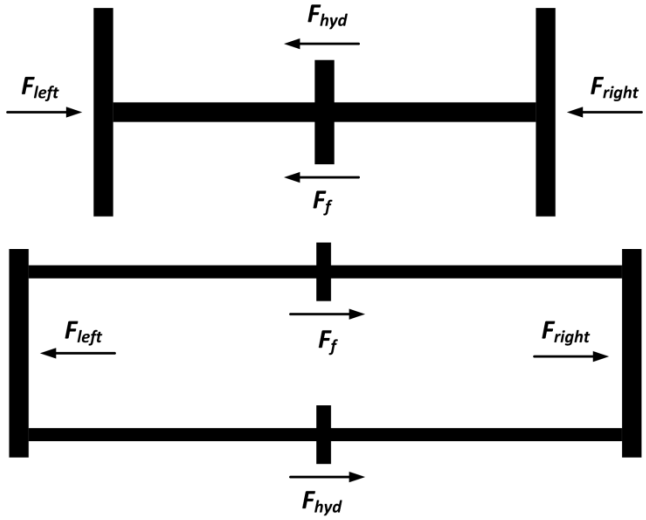

Fig. 2.3. Free body diagram of inner piston pair (top) and outer piston pair (bottom).

For our case, the friction force is assumed to be proportional to the piston velocity ($F_f = K_v \cdot \dot{x}$) which is obtained by integrating (2.19). And by taking the integral of the velocity, we will have the piston position.

2.2.6 Simulation results and discussion

The developed model is validated using engine motoring testing results, in which case the intake and exhaust manifold are at room temperature. A sinusoidal signal is sent to the servo valve, the simulated and measured data are shown in Fig. 2.4. A good match is observed between the model and the real system under engine motoring. Dynamic study is then conducted by simulating the validated system model.

Based on the simulation studies, the engine is found to be unstable at various operation points. That's because the engine operation is relatively complex in a way that the dynamics of the subsystems are heavily coupled as shown in Fig. 2.5. Specifically, the piston motion affects the hydraulic dynamics, the mixing of the gas mixture and the combustion process. Combustion chamber pressure and hydraulic chamber pressure further determine the piston dynamics. The intrinsic feedback nature of the engine implies that piston motion control is essential to ensure stable operations. A calibration-based piston motion control [47] is designed and implemented in the simulation program. The open and close timing of the servo valve is calibrated at each operating point, and the controller adjusts the valve opening area and duration to regulate the piston velocity. The calibration-based control leads to stable engine operations within a certain range of operation conditions.

The piston dynamics of the free piston engine is shown in Fig. 2.6. The displacement measures how far the piston is from a reference position (x = 0 m) which is at the center of the combustion chamber. Fig. 2.6 also compares the FPE piston dynamics with a conventional ICE of the same specifications operating at the same compression ratio and

frequency. A much higher acceleration is found around TDC and BDC of the FPE. The high acceleration is desirable because it provides shorter combustion duration, better mixing of in-cylinder gas and less time for heat transfer loss.

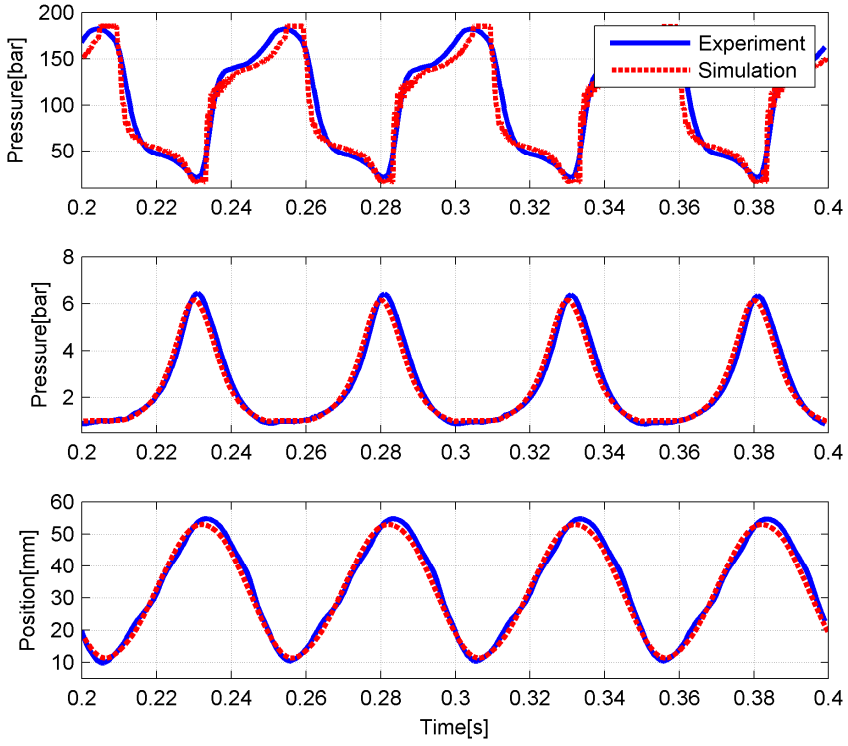

Fig. 2.4. Simulated and measured hydraulic pressure, combustion chamber pressure and piston position (from top to bottom).

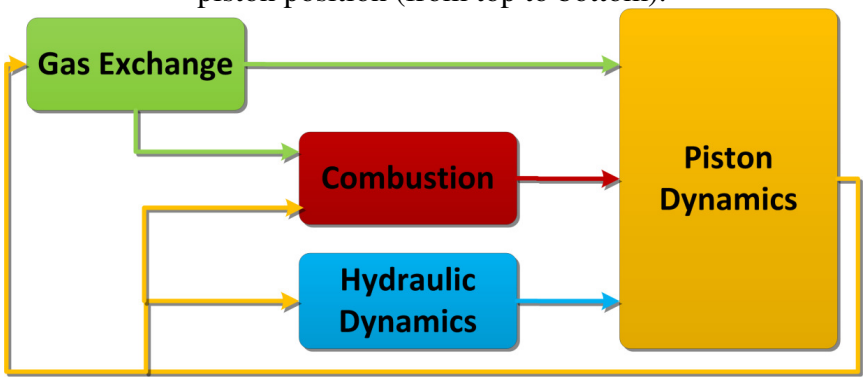

Fig. 2.5. Block diagram of dynamic couplings of the hydraulic FPE.

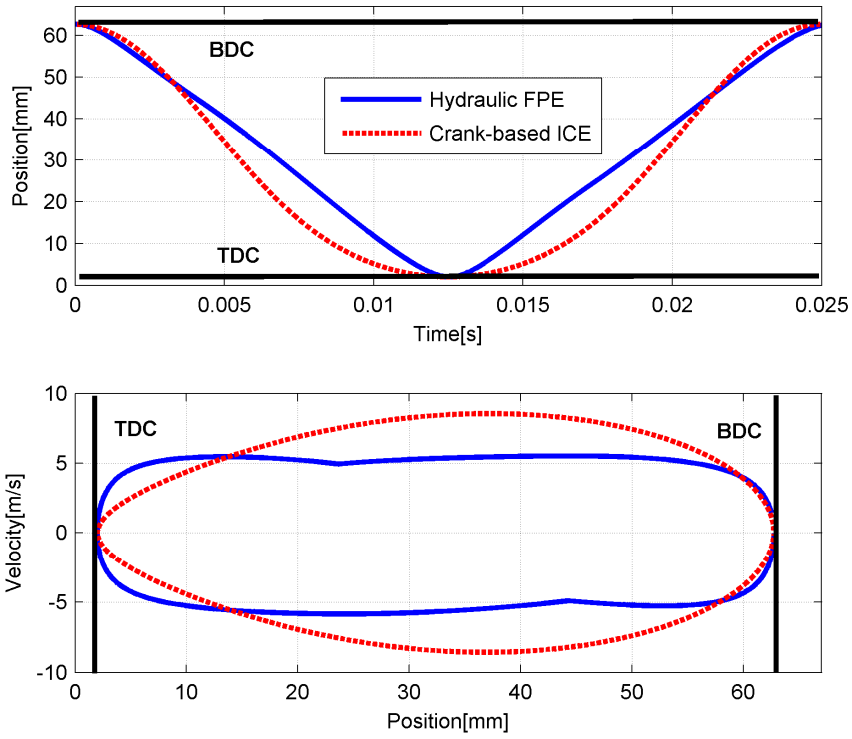

Fig.2.6. FPE piston dynamics and conventional ICE piston dynamics.

Fig. 2.7 shows the steady state combustion chamber pressure, hydraulic chamber pressure and piston position at two operating points. It is shown that engine operating frequency is slightly higher at high pressure load 345 bar (5000 psi) than low pressure load 193 bar (2800 psi). And the combustion timing in each case varies as well. An early combustion is observed at high pressure load and a late combustion is observed at low pressure load. That's because at high load, the in-cylinder gas mixture is richer, which advances the SOC and shortens the combustion duration. On the other hand, at light load, lean gas mixture retards the SOC and lengthens the combustion duration. Fig. 2.8 shows the engine transient after a sudden decrease of the loading pressure (from 345 bar to 193 bar). The transition occurs at 0.6 s on the plot, misfire is observed after the load change,

and the controller is not able to recover the operation from the misfire because of its calibration-based nature.

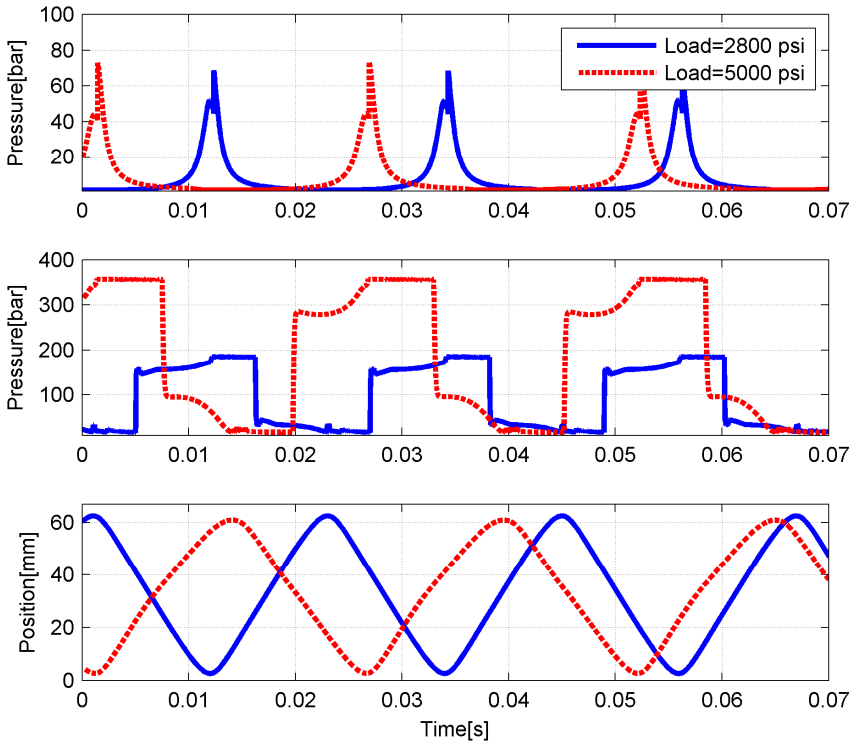

Fig. 2.7. Steady state combustion chamber pressure, hydraulic chamber pressure and piston position (from top to bottom) at two operating points.

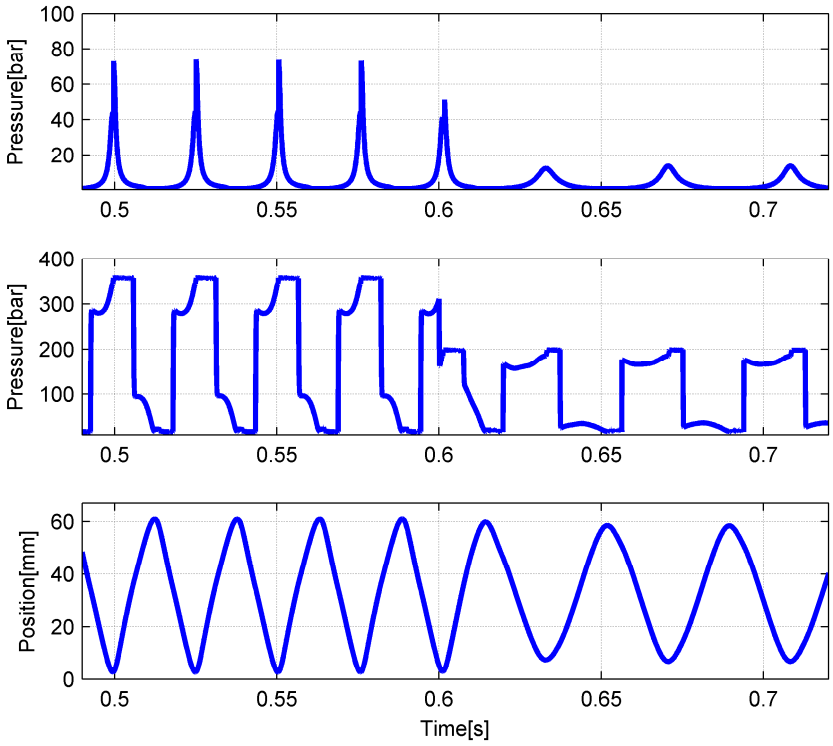

Fig. 2.8. Transient combustion chamber pressure, hydraulic chamber pressure and piston position (from top to bottom) after a sudden decrease of load.

In summary, the system model captures the FPE operating dynamics and it demonstrates the importance of piston motion control. The model also reveals the limitation of calibration-based control in terms of load change handling and disturbance rejection. The simulation results lead to the development of a systematic method of designing an active control in the following section.

Values of the parameters of the system model can be found in Table 2.2. The model outlines the main characteristics of the engine operation and offers great insights into the development of the control strategy in Chapter 3.

TABLE 2.2
PARAMETER VALUES FOR SYSTEM MODEL

Symbol	Definition	Value
γ	Specific heat ratio	1.31
R	Gas constant	296.25 J/Kg·K
C_d	Discharge coefficient	0.6
P_i	Intake manifold pressure	1 bar
T_i	Intake manifold temperature	350 K
x_i	Intake port location	51 mm
A_i	Intake port area	2000 mm^2
x_e	Exhaust port location	50 mm
A_e	Exhaust port area	2200 mm^2
P_e	Exhaust manifold pressure	1 bar
T_e	Exhaust manifold temperature	500 K
T_{wall}	Engine wall temperature	550 K
β	Bulk Modulus	1.2 GPa
ρ_{fluid}	Fluid density	875 Kg/m^3
$C_{checks}A_{checks}$	Check valve effective area	55 mm^2
$C_{syn}A_{syn}$	Synchronization valve effective area	0.5 mm^2
K_{max}	Maximum servo valve effective area	19 mm^2
V_{max}	Maximum servo valve input voltage	1 Volt
τ	Servo valve time constant	5 ms
K_v	Friction coefficient	200 N·s/m
P_{LP}	Low pressure accumulator pressure	14 bar

2.3 Stability Analysis

In the previous section, a high order nonlinear model of the engine was developed. The model includes a detailed two-zone-two-phase scavenging model, the hydraulic circuit model and the combustion model. Based on the simulation results, the engine stability is very sensitive to the operation conditions. In order to better understand the engine operation, a simplified discrete cycle-to-cycle model is developed. As mentioned above, the dynamics of FPE and HCCI are very sophisticated due to their feedback

nature. Now the complexity is magnified since we incorporate them in one system. The model is described in the next section and stability analysis is conducted and the result is compared with the high order nonlinear model simulation. The proposed stability analysis method offers insight for the dynamic behavior and guidance for control strategies synthesis.

2.3.1 Modeling approach

The opposed chamber design of the hydraulic FPE implies that not only each chamber would have its own feedback dynamic, but the dynamics of the two chambers are connected and affected by each other. The inputs to the engine are the hydraulic load and fuel mass. Since the engine utilizes uniflow scavenging pattern, we do not have control over valve timing. The discrete model is derived by analyzing the cyclic events of the engine. The engine cycle is divided into four stages: gas mixing, compression, combustion and expansion. The dynamic equation of the stages results in a model with 6 states and 2 inputs.

Gas Mixing

The gas mixing process relates the steady state exhaust port open (EPO) temperature T_{epo} and pressure P_{epo} to intake port close (IPC) temperature T_{ipc} and pressure P_{ipc}. The scavenging of a two stroke engine is a very complex process. In our model, several assumptions were made to simplify the dynamics.

1) The scavenging is perfect displaced
2) No heat transfer
3) Ideal gas

The mixture temperature at IPC is approximated by the mass average temperature of the intake charge and residual inside the chamber, and the pressure at IPC is assumed to be very close to the intake pressure, which is a reasonable assumption based on the gas dynamics simulation results,

$$T_{ipc} = \frac{T_{in} \cdot m_{fresh} + T_{epo} \cdot m_{res}}{m_{ipc}} \tag{2.20}$$

Apply ideal gas law at EPO to yield the total mass of in-cylinder mixture,

$$T_{epo} = \frac{P_{epo} \cdot V_{epo}}{R \cdot m_{epo}} \tag{2.21}$$

The exhaust gas is assumed to leave the combustion chamber instantaneously at EPO. That is, the volume and temperature remain the same, but the pressure drops instantaneously from EPO pressure to the exhaust pressure. And the total mass of in-cylinder mixture does not vary much at EPO and at IPC based on previous simulation data. Mass of the fresh charge gas and mass of the residual gas retained can then be calculated,

$$m_{epo} - m_{res} = \frac{\left(P_{epo} - P_{ex} \right) \cdot V_{epo}}{R \cdot T_{epo}} \tag{2.22}$$

$$m_{fresh} = m_{ipc} - m_{res} \tag{2.23}$$

The total mass at IPC is calculated based on mass conservation, which is the sum of mass of the fresh charge and mass of the residual

$$m_{ipc} = \frac{P_{ipc} \cdot V_{ipc}}{R \cdot T_{ipc}} \tag{2.24}$$

By substituting (2.21) – (2.24) into (2.20),we obtain P_{ipc} ,T_{ipc}, m_{ipc}, m_{fresh}, m_{epo} and m_{res} as functions of P_{epo} ,T_{epo}.

The residual gas fraction is defined as the ratio between mass of residual and the total mass.

$$x_r = \frac{m_{res}}{m_{res} + m_{fresh} + m_{fuel}} \tag{2.25}$$

Since HCCI operates on lean mixtures, the residual gas contains both air and burned gas. The in-cylinder burned gas fraction is defined as:

$$b_{c,k} = x_{r,k} \cdot b_{p,k-1} \tag{2.26}$$

And the in-cylinder air to fuel ratio is:

$$AFR_{c,k} = \frac{m_{fresh,k} + \left(1 - b_{p,k-1}\right) \cdot m_{res,k}}{m_{fuel,k}} \tag{2.27}$$

After combustion the in-cylinder burned gas fraction becomes:

$$b_{p,k} = \frac{AFR_s + 1}{AFR_{c,k} + 1} \cdot \left(1 - b_{c,k}\right) + b_{c,k} \tag{2.28}$$

By inspecting (2.27) – (2.30), we can see that the current cycle air fuel ratio and burned gas fraction depend on the air fuel ratio and burned gas fraction from previous cycle, and they can be derived as:

$$b_{c,k} = \frac{m_{res}(-AFR_s + AFR_S b_{c,k-1} - 1 - b_{c,k-1} AFR_{c,k-1}) + 1}{(AFR_{c,k-1} + 1)(m_{res,k} + m_{fresh,k} + m_{fuel,k})} \cdot \tag{2.29}$$

$$AFR_{c,k} = \frac{m_{res,k} \cdot AFR_s \cdot b_{c,k-1} - m_{res,k} \cdot b_{c,k-1} \cdot AFR_{c,k-1}}{m_{fuel,k}\left(AFR_{c,k-1}+1\right)} + \frac{AFR_{c,k-1} \cdot m_{fresh,k} + AFR_{c,k-1} \cdot m_{res,k} + m_{fresh,k} - m_{res,k} AFR_s}{m_{fuel,k}\left(AFR_{c,k-1}+1\right)} \tag{2.30}$$

Compression and Combustion

As mentioned in the previous section, the timing of the autoignition depends on the pressure and temperature of the in-cylinder mixture. Since the compression process is isentropic, we are able to obtain the temperature and pressure based on the piston position and IPC temperature and pressure. The combustion model in [46] is used, though the variable "t" in the equation is converted to displacement. Note in (2.31) and (2.34), coefficient *A* and *k* are functions of the piston velocity. The combustion duration Δx is the piston travelling during the combustion. Figure 2.9 shows the piston velocity versus displacement diagram. A rectangle-shape trajectory is observed. Therefore, it is reasonable to assume that the piston velocity does not vary much during the cycle and an average piston velocity is assigned for each cycle.

$$\int_{x_{ipc}}^{x_{soc}} A \cdot P_{ipc}^{\,r} \left(\frac{x_{ipc}}{x}\right)^{r \cdot n} \exp\left(-\frac{E_a\left(\frac{x_{ipc}}{x}\right)^{1-r}}{R \cdot T_{ipc}}\right) dx \tag{2.31}$$

$$T_m = T_{soc} + e(1 - b_c)\Delta T \tag{2.32}$$

$$\Delta T = \frac{Q_{LHV}}{C_v(1 + AFR_c)} \tag{2.33}$$

$$\Delta x = k \cdot (T_{soc})^{-2/3} (T_m)^{1/3} \exp\left(\frac{E_c}{3R_u T_m}\right) \tag{2.34}$$

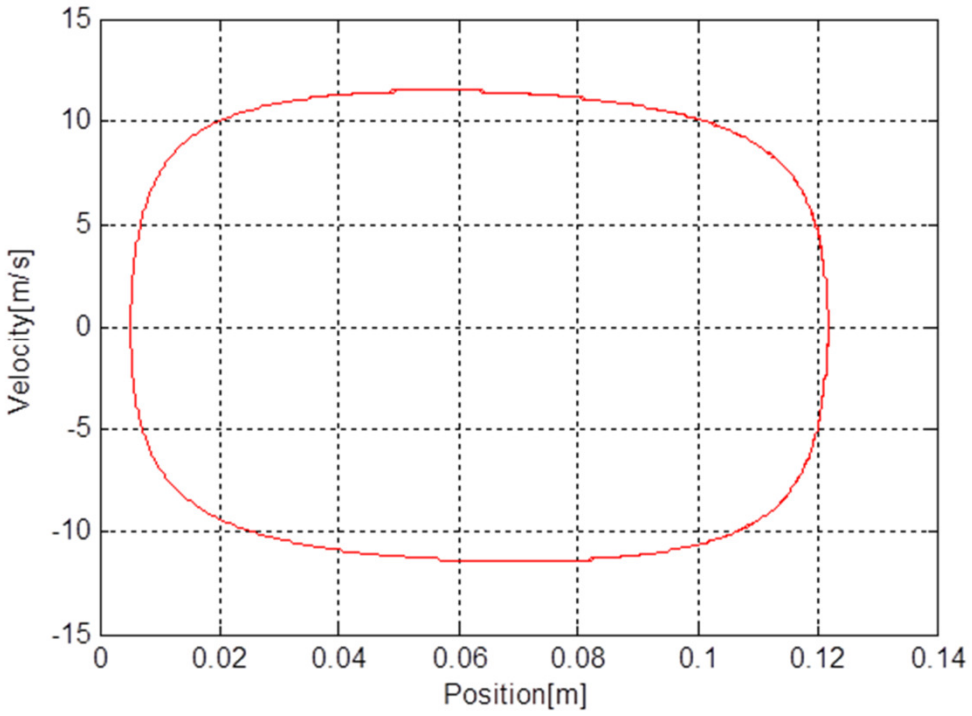

Fig. 2.9. Hydraulic FPE piston velocity versus position diagram

In order to solve for start of combustion (SOC) position, we need to solve the Arrhenius integral. The symbolic manipulation results in a complex solution which is not desirable. The author of [48] proposed a simplified solution by only taking into account the integrand value at TDC, and solve for the duration between SOC and TDC. In this case, the TDC position of the chamber at current cycle is determined by the combustion pressure and combustion position of the other chamber rather than a fixed value as in the

crankshaft engine. However, we can still choose a position which is at the lower bound of the TDC range for the combustion timing estimation purpose. Figure 3 shows the typical integrand value versus the piston displacement. We can see that the integrand value does not increase until the chamber volume is fairly small. And a small piston position x_l would give us a reasonable approximation of the Arrhenius integral.

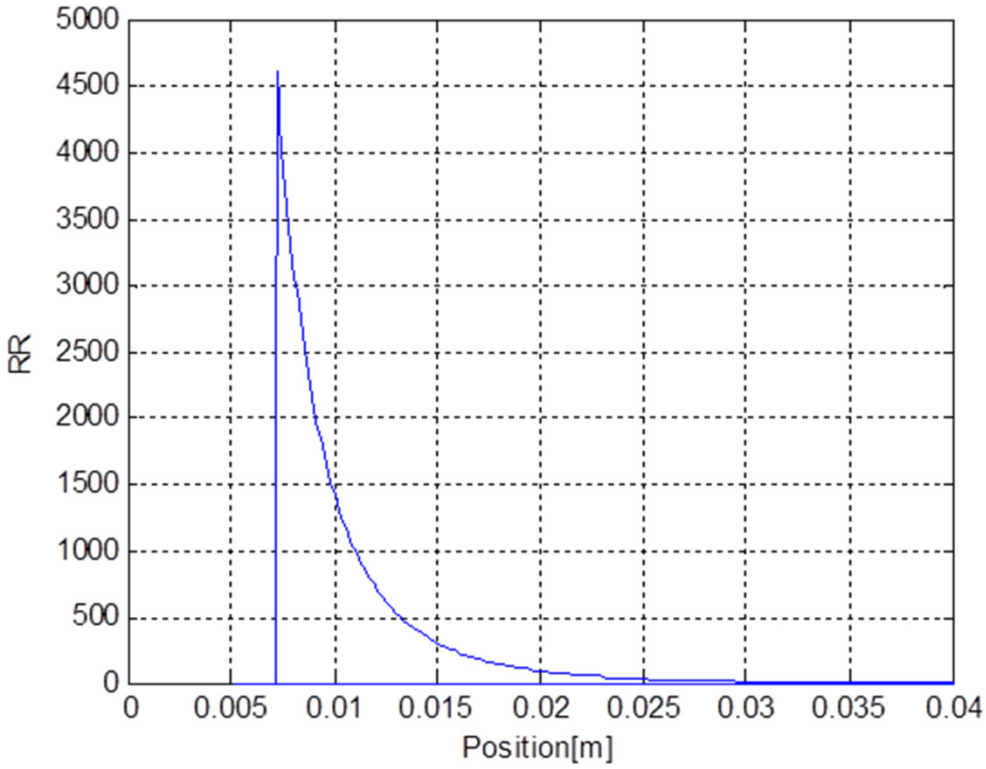

Fig. 2.10. Arrhenius integrand value versus the piston position

The integral approximation is shown in (2.35). Solve for x_{soc} at the given x_l would give us the piston position at start of combustion.

Our objective is to solve for the end of combustion position as a function of T_{ipc} and P_{ipc} since heat is assumed to be released instantaneously at that moment. By solving (2.31) – (2.34), we are able to derive x_{soc} and Δx as functions of T_{ipc} and P_{ipc}. And the

combustion position will be determined based on values of $x_{soc,}$ Δx and x_{tdc} .Note here that the end of combustion position x_c depends on the top dead center position x_{tdc} which is the key difference between free piston engine and crankshaft engine.

when x_{soc} - x_{tdc}> Δx *(combustion happens before TDC)*

$$x_c = x_{soc} - \Delta x$$

when x_{soc} - x_{tdc} < Δx *(combustion happens after TDC)*

$$x_c = 2x_{tdc} - x_{soc} + \Delta x$$

In this section, we only consider the case when heat release happens after piston has reached TDC, which is the case for medium and low load. Advanced combustion which is usually the case for high load, will be investigated in the future.

$$A \cdot P_{ipc}\left(\frac{x_{ipc}}{x_l}\right)^{r \cdot n} \exp\left(-\frac{E_a\left(\frac{x_{ipc}}{x_l}\right)^{1-r}}{R \cdot T_{ipc}}\right)\left(xl - x_{soc}\right) = 1 \tag{2.35}$$

The temperature at the end of combustion is given by

$$T_c = T_{ipc}\left(\frac{x_{ipc}}{x_c}\right)^{r-1} + \left(1 - b_c\right) \cdot \Delta T \tag{2.36}$$

Pressure at the end of combustion can then be calculated

$$P_c = \frac{P_{ipc}\left(\frac{x_{ipc}}{x_c}\right)^{r} T_c}{T_{ipc}\left(\frac{x_{ipc}}{x_c}\right)^{r-1}} \tag{2.37}$$

Expansion

The expansion is assumed to be an isentropic process, which means that we can obtain the pressure and temperature at EPO as a function of pressure and temperature at the end of combustion. And the pressure at EPO is given by

$$P_{epo} = P_c\left(\frac{x_c}{x_{epo}}\right)^r \tag{2.38}$$

$$T_{epo} = T_c\left(\frac{x_c}{x_{epo}}\right)^{r-1} \tag{2.39}$$

2.3.2 Dual Chamber Coupling

The compression, combustion, gas mixing and expansion are closely related to the two chamber dynamic coupling. Specifically, the combustion condition from one chamber determines the top dead center of the other chamber. The equation of piston dynamics is a second order ODE governing by the force balance. Through the derivation for the cyclic events, we are able to calculate the force from the two chambers as a function of piston displacement. We know that the hydraulic system is very stiff based on the simulation results of the high order nonlinear model. That is, if the hydraulic load is kept constant, the hydraulic chamber pressure will also stay at constant with small fluctuations that can be neglected. Assume the piston is currently located at the end of combustion position of the right chamber. In order to obtain the TDC position for the left chamber, the piston dynamic equation is rewritten as:

$$m\ddot{x} = -P_c\left(\frac{x_c}{S-x}\right)^r + P_{ipc}\left(\frac{x_{ipc}}{x}\right)^r - P_{hyd}\cdot A_{hyd} \tag{2.40}$$

Again, the symbolic manipulation gives out a very complex solution for the second order ODE. Alternative method is investigated for simpler but also accurate solutions. By inspecting (2.40), we know that the TDC position is a function of $P_{c,R}$, $x_{c,R}$ and load. The variation of TDC position is expected to be relatively small. If we know a reference TDC position at a reference $P_{c,R}$, $x_{c,R}$ and P_{hyd} , the deviation of TDC position from the reference value can be assumed to be a linear relation with the deviation of $P_{c,R}$, $x_{c,R}$ and P_{hyd} from their reference values., the relation is shown in (2.41). Data points were taken from the previous simulation results to calibrate the derivative term associate with each variable. This reduces the complexity of the solution significantly but with the same accuracy.

$$\delta x_{tdc} = \frac{\partial x_{tdc}}{\partial P_c}\cdot\delta P_c + \frac{\partial x_{tdc}}{\partial x_c}\cdot\delta x_c + \frac{\partial x_{tdc}}{\partial P_{hyd}}\cdot\delta P_{hyd} \tag{2.41}$$

2.3.3 Cyclic states

The start of a cycle is set to be at the instant when left chamber undergoes the instantaneous heat release while the right chamber undergoes the scavenging process. Thus, the initial states of left chamber are $x_{c,L}(k)$, $P_{c,L}(k)$ and $T_{c,L}(k)$. Initial states of right chamber are $AFR_R(k)$, $T_{ipc,R}(k)$ and $b_{c,R}(k)$. Next, left chamber undergoes expansion and then gas exchange process, the states are $P_{epo,L}(k)$, $T_{epo,L}(k)$ → $AFR_L(k)$, $T_{ipc,L}(k)$ and $b_{c,L}(k)$. While right chamber undergoes compression and then combustion, and the states

are $x_{soc,R}(k)$ and $T_{soc,R}(k) \rightarrow P_{c,R}(k)$, $x_{c,R}(k)$ and $T_{c,R}(k)$. Left chamber closes the cycle with compression and combustion, $x_{soc,L}(k)$ and $T_{soc,L}(k) \rightarrow P_{c,L}(k+1)$, $x_{c,L}(k+1)$ and $T_{c,L}(k+1)$, while right chamber finishes up with expansion and gas exchange process, $P_{epo,R}(k)$, $T_{epo,R}(k) \rightarrow AFR_R(k+1)$, $T_{ipc,R}(k+1)$ and $b_{c,R}(k+1)$. The states of the FPE operation are similar to what has been identified in [49-52], however, the coupling between the two combustion chambers (the TDC of a combustion chamber is determined by the condition from the other chamber) adds the complexity into the engine operation. This analysis shows that the engine cycle can be comprehended by 6 states : $x_{c,L}(k)$, $P_{c,L}(k)$, $T_{c,L}(k)$, $AFR_R(k)$, $T_{ipc,R}(k)$ and $b_{c,R}(k)$. Combine (2.20) – (2.41), we can obtain the dynamic equations of the states:

$$\begin{bmatrix} P_{c,L}(k+1) \\ T_{c,L}(k+1) \\ x_{c,L}(k+1) \\ AFR_R(k+1) \\ b_{c,R}(k+1) \\ T_{ipc,R}(k+1) \end{bmatrix} = \begin{bmatrix} f_1\left(x_{c,L}(k), P_{c,L}(k), T_{c,L}(k), AFR_R(k), b_{c,R}(k), T_{ipc,R}(k), m_{fuel}(k), P_{hyd}(k)\right) \\ f_{21}\left(x_{c,L}(k), P_{c,L}(k), T_{c,L}(k), AFR_R(k), b_{c,R}(k), T_{ipc,R}(k), m_{fuel}(k), P_{hyd}(k)\right) \\ f_3\left(x_{c,L}(k), P_{c,L}(k), T_{c,L}(k), AFR_R(k), b_{c,R}(k), T_{ipc,R}(k), m_{fuel}(k), P_{hyd}(k)\right) \\ f_4\left(x_{c,L}(k), P_{c,L}(k), T_{c,L}(k), AFR_R(k), b_{c,R}(k), T_{ipc,R}(k), m_{fuel}(k), P_{hyd}(k)\right) \\ f_5\left(x_{c,L}(k), P_{c,L}(k), T_{c,L}(k), AFR_R(k), b_{c,R}(k), T_{ipc,R}(k), m_{fuel}(k), P_{hyd}(k)\right) \\ f_6\left(x_{c,L}(k), P_{c,L}(k), T_{c,L}(k), AFR_R(k), b_{c,R}(k), T_{ipc,R}(k), m_{fuel}(k), P_{hyd}(k)\right) \end{bmatrix} \quad (2.42)$$

2.3.4 Stability Analysis

The model consists of 6 states and 2 inputs. The dynamic equations of the model can be linearized about an equilibrium point with a given input $(\overline{m_{fuel}}, \overline{P_{hyd}})$, and put in the state-space matrix as shown in the next page. The equilibrium point is calculated using the nonlinear dynamic equations described in the previous sections. The matrix gives us a clear picture of the engine dynamic couplings. Eigenvalues of the A matrix are calculated, and their location determines the stability of the engine operation with the corresponding inputs. For validation purpose, equilibrium was found at:

$$\left(\overline{P_{c,L}} = 17650000\ Pa, \overline{x_{c,L}} = 0.0028\ m, \overline{T_{c,L}} = 1541\ K,\ \ \overline{AFR_R} = 100, \overline{b_{c,R}} = 0.473, \overline{T_{ivc,R}} = 462.7\ K\right)$$

$$\begin{bmatrix} P_{c,L}(k+1) \\ T_{c,L}(k+1) \\ x_{c,L}(k+1) \\ AFR_R(k+1) \\ b_{c,R}(k+1) \\ T_{ipc,R}(k+1) \end{bmatrix} = \begin{bmatrix} G11 & G12 & G13 & G14 & G15 & G16 \\ G21 & G22 & G23 & G24 & G25 & G26 \\ G31 & G32 & G33 & G34 & G35 & G36 \\ G41 & G42 & G43 & G44 & G45 & G46 \\ G51 & G52 & G53 & G54 & G55 & G56 \\ G61 & G62 & G63 & G64 & G65 & G66 \end{bmatrix} \begin{bmatrix} P_{c,L}(k) \\ T_{c,L}(k) \\ x_{c,L}(k) \\ AFR_R(k) \\ b_{c,R}(k) \\ T_{ipc,R}(k) \end{bmatrix} + \begin{bmatrix} C11 & C12 \\ C21 & C22 \\ C31 & C32 \\ C41 & C42 \\ C51 & C52 \\ C61 & C62 \end{bmatrix} \begin{bmatrix} m_{fuel}(k) \\ P_{hyd}(k) \end{bmatrix} \tag{2.43}$$

The linearized matrix was then calculated. And the eigenvalues of the A matrix were found to be outside the unit disc, so the system is unstable with the given inputs $\overline{m_{fuel}} = 5.57 \frac{mg}{cycle}, \overline{P_{hyd}} = 10700000\ Pa$

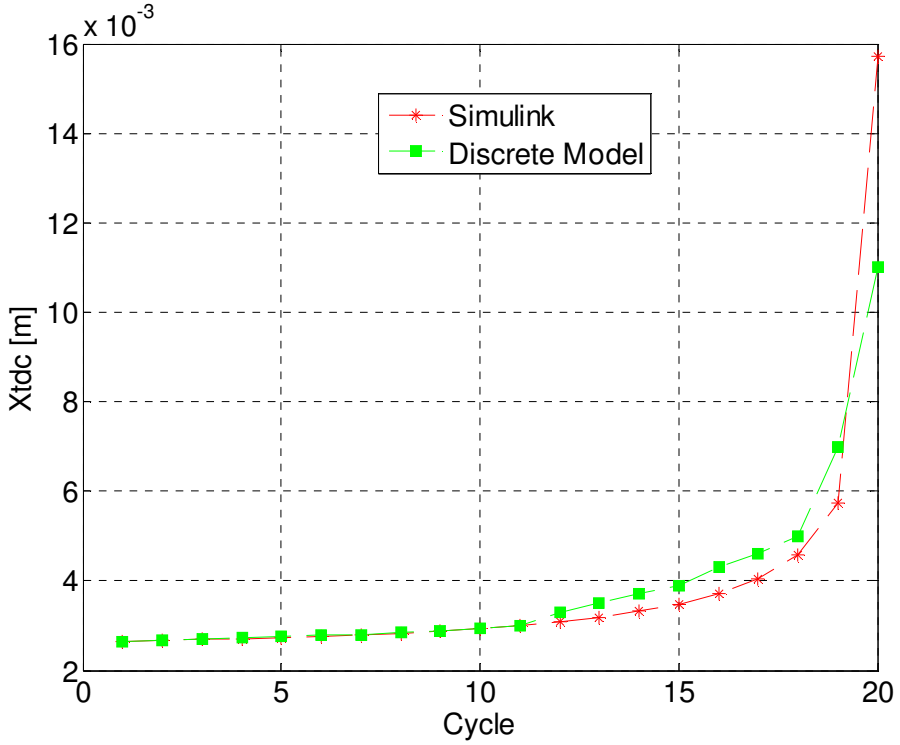

Fig. 2.11. TDC position of the left chamber with a small perturbation from the discrete and continuous model

Figure 2.11 shows the transient response of the left chamber TDC position during the unstable operation from the discrete model and the continuous model developed earlier. The discrete model is able to capture the dynamics of the engine operation, and both model reveal that a small deviation of the initial condition from the equilibrium point would result in an unstable engine operation. As shown in Fig. 2.11, the TDC position is increased cycle by cycle, which eventually leads to engine stall. Thus, a feedback controller is required in order to operate the engine at steady state; the discrete model can then be used to guide the design and evaluation of the controllers.

2.4 Conclusions

In this chapter, a comprehensive model of the hydraulic FPE system is developed. The piston dynamics of the FPE is compared with the conventional ICE. A calibration-based piston motion control is investigated using the model, and simulation results demonstrate the limitation of the calibration-based control when operating condition changes. Stability analysis of the engine operation is also investigated in this chapter. A discrete cycle to cycle model of a hydraulic free piston engine with HCCI is described in this section. The model is developed to be simple but still be able the capture the complex dynamic coupling among the engine subsystems. The discrete model is derived by analyzing the cyclic events of the engine. The engine cycle is divided into four stages: gas mixing, compression, combustion and expansion. Additionally, assumptions are made to simplify the model and sort out the main states. The dynamic equations of the stages result in a model with 6 states and 2 inputs. The transient results of the model are validated through numerical simulation of the high-order model under a specified set of

input values. The dynamic equations of the model can then be linearized about an operating point. Eigenvalues of the system matrix are calculated, and their location determines the stability of the engine operation. The stability analysis explores the complex dynamic coupling among the engine subsystems and it offers guidance for control strategies synthesis.

Chapter 3

Design of Active Piston Motion Control

Based on the analysis in Chapter 2, a robust and effective piston motion control is indispensable for the FPE operation. Besides the limitation of being applicable to only a specific FPE architecture, many of the existing control strategies rely on calibration to be effective. However, the complex interactions between the gas dynamics and the load in real time make the calibration a tedious task, and the resulting controllers are sensitive to variation of the operating conditions and disturbances. This imposes a huge challenge on the engine operation control and calls for systematic active controls that can precisely regulate the piston motion. Therefore, in this chapter, a novel FPE control strategy is designed [26, 53]. The controller acts as a virtual crankshaft which utilizes the energy in the storage element to regulate the piston position. Due to the repetitive piston motion, the robust repetitive control is employed in the controller design.

The ability to alter trajectory in real time opens up a new research frontier: the optimal trajectory design. Not just the TDC position but also the piston travel pattern within can affect the combustion process, so we can design distinct trajectories for various operating conditions for optimized efficiency and reduced emissions. However, in order to realize this advantage, precise tracking is needed. Therefore, a linear and nonlinear feedforward controller are designed to assist the repetitive control to further improve the tracking performance [54].

In this chapter, the control of an alternative hydraulic FPE structure, that utilizes digital hydraulic valves in place of the current servo valve plus check valves design to reduce cost and improve efficiency, is investigated as well. The simulation results demonstrate the feasibility of such a design with the proposed control structure.

3.1 Control of Hydraulic and Piston Assembly

The hydraulic subsystem was first separated from the engine housing (Fig. 3.1). System dynamics can be very complex once combustion chamber gas dynamics is involved. Therefore, it is desirable to have a platform which would enable us to investigate the effectiveness of the virtual crankshaft in the presence of disturbances, exerted by combustion chambers on hydraulic pistons, before conducting actual motoring and firing tests.

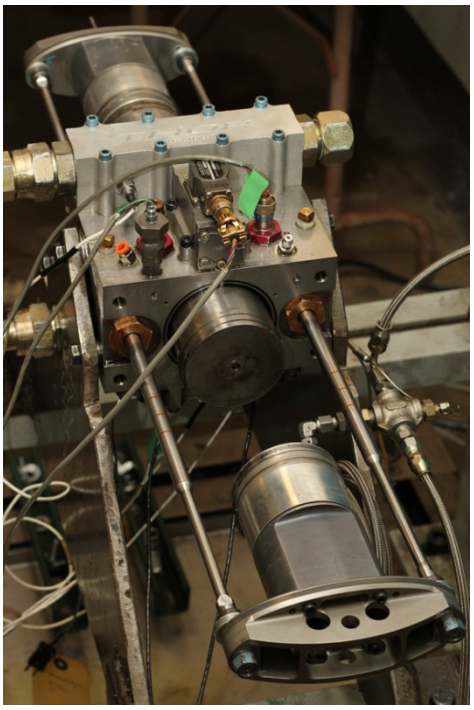

Fig. 3.1.Hydraulic subsystem and piston assembly

To precisely track the reference signal in real-time, high bandwidth response of the system is required. The ability to achieve high bandwidth response depends on a number of factors which include the dynamic response of the hydraulic system, mass of the piston pair, sampling rate and the unmodeled dynamics of the plant.

System identification of the hydraulic system based on frequency response is conducted. To do this, first the open-loop hydraulic system was stabilized by a proportional feedback controller. A large control gain is chosen, as it gives faster response time and smaller steady state error. The hydraulic system has static friction, when the system is tracking a signal with small amplitude, the steady state error would be fairly large. However, a large proportional gain would help the system overcome the friction and thus reduce tracking error.

The frequency response of the hydraulic system was obtained using the swept sine method, where a series of sinusoidal signals from 1 to 100 Hz are sent to the system and the response is recorded. The system is assumed to be linear as the nonlinear effect is lumped into the unmodeled dynamics. The discrete-time transfer function developed for the stabilized hydraulic system based on frequency response is :

$$\frac{B(q^{-1})}{A(q^{-1})} = \frac{2.781e^{-5}q^{-4} - 5.737e^{-4}q^{-5}}{1 - 6.247q^{-1} + 17.71q^{-2} - 29.92q^{-3}} \\ \frac{+\,4.307e^{-4}q^{-6} - 9.087e^{-5}q^{-7}}{-\,24.51q^{-5} + 11.96q^{-6} - 3.512q^{-7} + 0.4744q^{-8}} \tag{3.1}$$

where q^{-1} is the one step delay operator.

Despite its success in stabilizing the hydraulic system, the proportional feedback controller is incapable of tracking periodic reference signals with high frequency. This

necessitates the employing of a more advanced controller. The controller used here is repetitive control [55-57] which is capable of tracking any periodic reference signal with known period. A key feature of repetitive control is its extremely fast convergence rate of the tracking error due to its high feedback gains at the desired frequency locations.

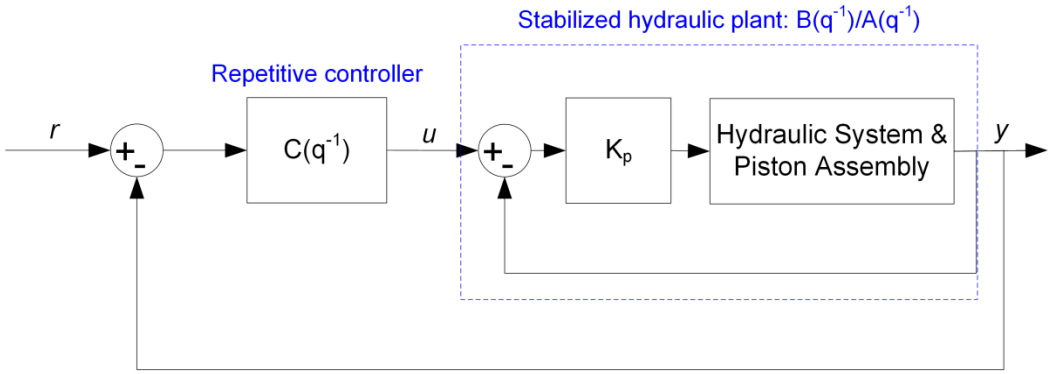

Fig. 3.2 Control system configuration.

The repetitive close-loop control system is shown in Fig. 3.2 and can be represented as follows:

$$y(k) = \frac{B(q^{-1})}{A(q^{-1})}u(k) \tag{3.2}$$

$$u(k) = C(q^{-1})[r(k) - y(k)] \tag{3.3}$$

where k is the discrete step index, $u(k)$ and $y(k)$ are the input and output of the stabilized hydraulic system, $r(k)$ is the desired motion profile and $C(q^{-1})$ is the robust repetitive controller which can be described as:

$$C(q^{-1}) = \frac{R(q^{-1})q^{-N}}{1-q^{-N}} \tag{3.4}$$

The repetitive controller designed based on the idea of zero phase compensation [56-57] is used to shape $R(q^{-1})$:

$$R(q^{-1}) = \frac{K_r A(q^{-1}) B^{-1}(q)}{B^{+}(q^{-1}) b}, 0 < K_r < 2,$$
$$b \geq \max \left| B^{-}(e^{-j\omega}) \right|^2 \tag{3.5}$$

where K_r is the repetitive control gain. $B(q^{-1}) = B^{+}(q^{-1})B^{-}(q^{-1})$, and $B^{-}(q^{-1})$ contains all the unstable plant zeros.

Large feedback gain at the repetitive signal frequency is imposed to achieve precise tracking. However, to accommodate the plant unmodeled dynamics, we need to compromise between tracking performance and system robustness to ensure stability. A low pass filter $Q(q^{-1})$ is therefore introduced in the controller [56]. The filter helps retain robust stability by maintaining the learning mechanism of the internal model at low frequencies while turning off the leaning at high frequencies.

The transient response is shown in Fig. 3.3. A sudden amplitude change of the reference occurs around 29.4 s, and the actual piston position is able to follow the command in the next cycle. The tracking error converges to less than 0.4 mm in 3 cycles. Fig. 3.4 shows the steady state tracking performance of tracking a 3 Hz signal with 55 mm amplitude, the steady state error is within ± 1 mm. Fig. 3.5 shows the velocity vs. position diagram of the system under three different reference amplitudes. The plot indicates that the hydraulic subsystem actuation is highly repeatable.

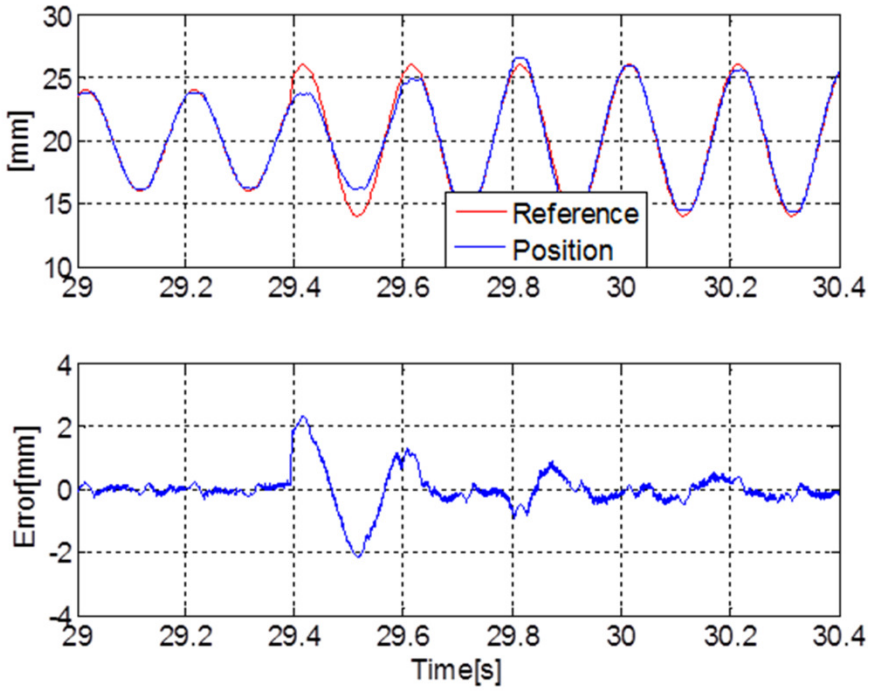

Fig. 3.3 Transient response of the robust repetitive controller.

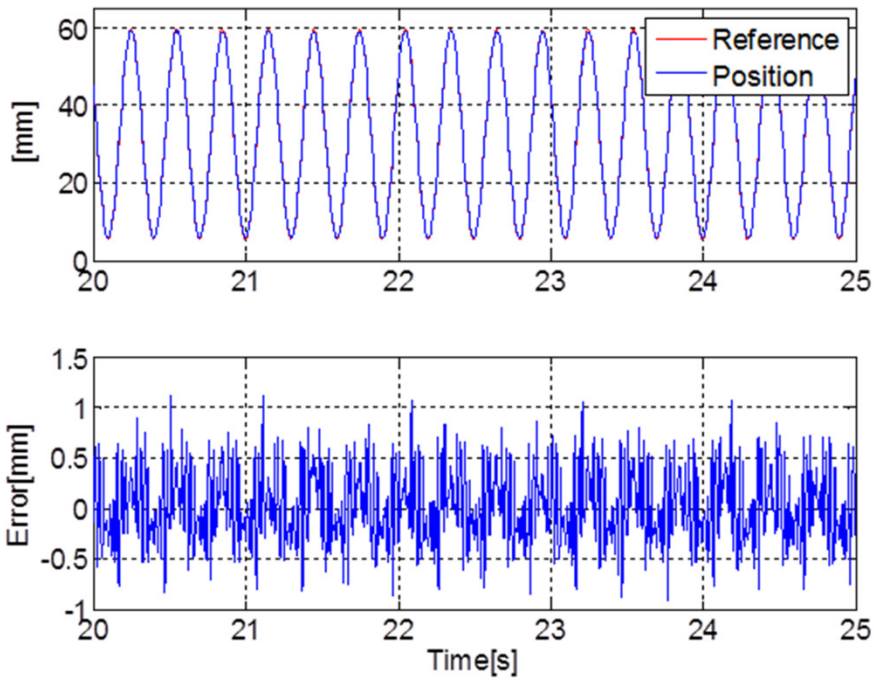

Fig. 3.4.Steady state response of the robust repetitive controller.

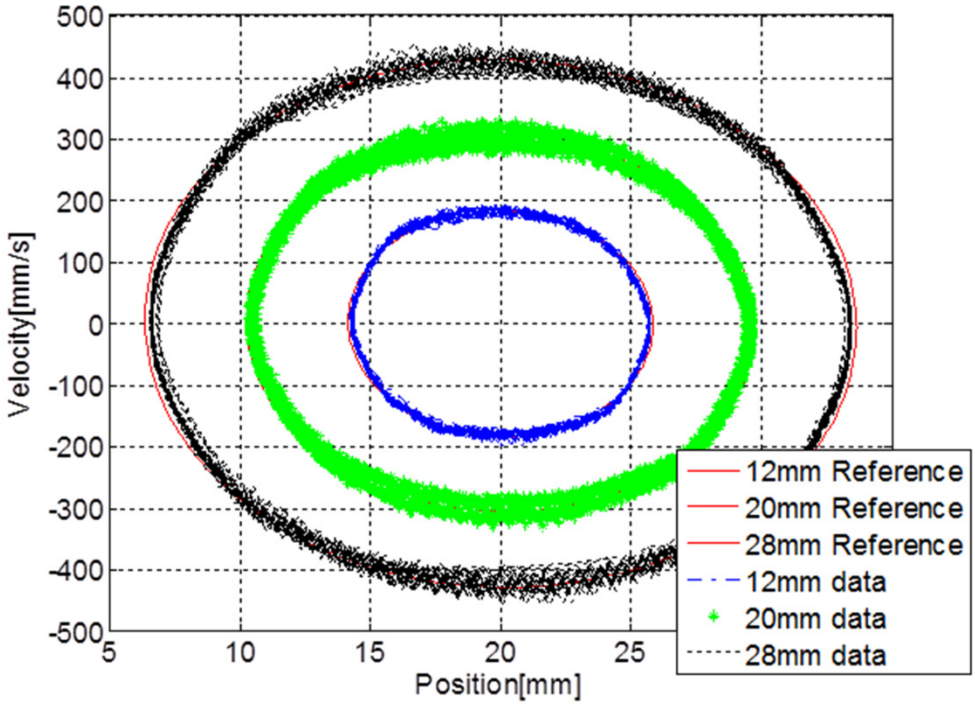

Fig. 3.5 Velocity vs. Position diagram of various stroke and speed.

A hardware-in-the-loop (HIL) control system is designed and implemented to investigate the effectiveness of the virtual crankshaft in the presence of disturbances, exerted by combustion chambers on hydraulic pistons, before conducting actual motoring and firing tests. The HIL successfully integrates the combustion chamber dynamics with the hydraulic system. Fig. 3.6 shows the HIL and control system configuration. The main idea is to use the combustion chamber model to perturb the actual shaft position and feed this perturbed value back to the control system. The combustion chamber model computes the pressure difference between left and right combustion chambers based on the actual piston position from the hydraulic system. By assuming that the combustion chamber pressure acts instantaneously on the pistons, the perturbed position can be found

through the fluid volume change based on the pressure difference and fluid compressibility.

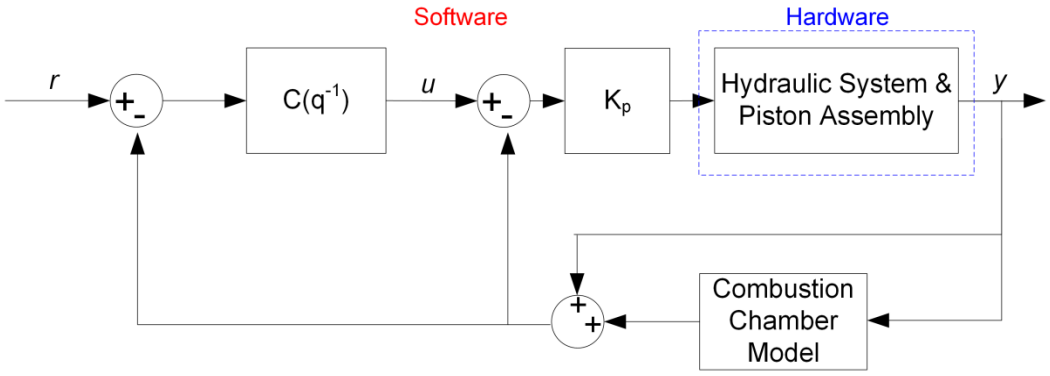

Fig. 3.6.Control and HIL system configuration.

Assume constant boundary conditions and polytropic process, the pressure and temperature at each piston position can be calculated as,

$$P_x = P_{in}(\frac{V_{in}}{V_x})^r \tag{3.6}$$

$$T_x = T_{in}(\frac{V_{in}}{V_x})^{r-1} \tag{3.7}$$

where x indicates the piston position, and sub-scrip *in* stands for intake. Equation 8- 10 derive the pressure difference equation with combustion, where the pressure rise caused by combustion $\Delta P_{combustion}$ is a function of temperature rise ΔT. And ΔT is determined by the residual gas fraction b and fuel air ratio λ. Sub-script BC stands for *before the combustion*. Q_{LHV}, C_v and σ are the lower heating value, specific heat and stoichiometric air-fuel ratio, respectively.

$$\Delta P = P_{left} - P_{right} + \Delta P_{combustion} \tag{3.8}$$

$$\Delta T = (1-b)\cdot(\frac{Q_{LHV}}{C_v(1+\lambda\cdot\sigma)}) \tag{3.9}$$

$$\Delta P_{combustion} = P_{BC}(\frac{T_{BC}+\Delta T}{T_{BC}} - 1) \tag{3.10}$$

Finally, the position perturbation Δx can be calculated based on pressure difference ΔP and fluid bulk modulus β,

$$\Delta x = \Delta P \frac{A_{piston}}{A_{Plunger}^2} \frac{V_{hydraulic}}{\beta} \tag{3.11}$$

Fig. 3.7 shows the tracking performance of the HIL system with the repetitive controller. In this particular case, we expect the piston to travel from 12 mm to 122 mm. In the combustion model, we assume ignition combustion, so combustion always occurs at certain position. However, to better emulate the real scenario, where the combustion may vary from cycle to cycle, a random perturbation is assigned to the temperature rise at every combustion event. Fig 3.7 (b) shows the net force from the combustion chamber that is acting on the piston during the HIL testing. And the tracking error remains very small during the HIL testing as shown in Fig. 3.7 (a).

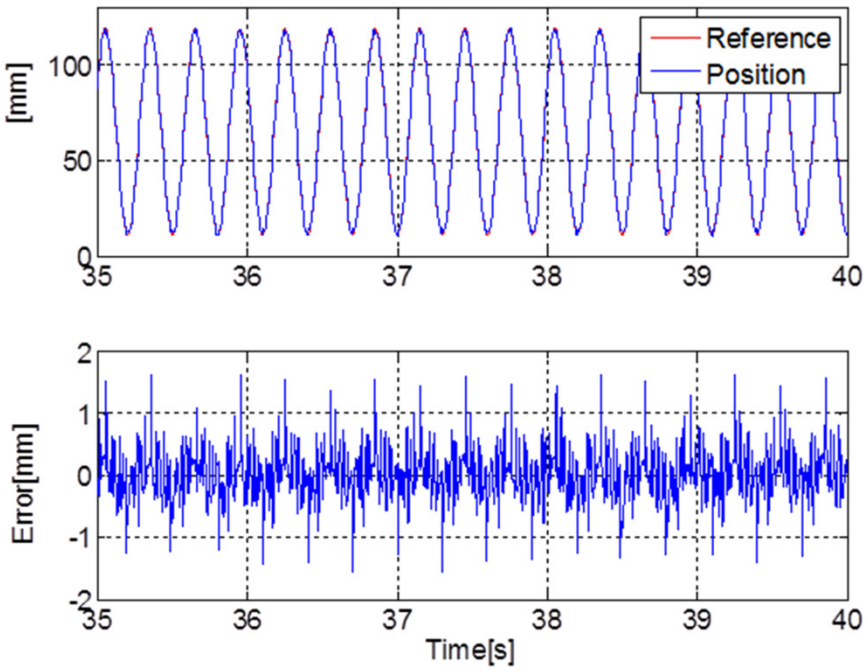

(a)

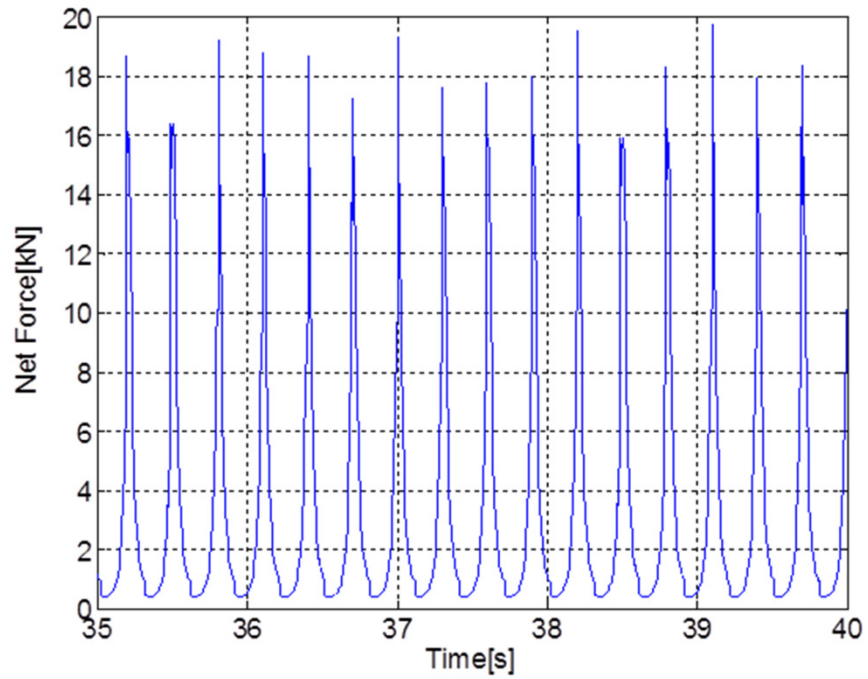

(b)

Fig. 3.7. a) HIL tracking performance. b) Calculated net force acts on the piston pair from combustion chambers

3.2 Repetitive Control Design of the Hydraulic FPE

After the effectiveness of the repetitive control being validated in section 3.1, the hydraulic system and piston assembly were combined with the combustion chambers for engine motoring tests. Since adding the combustion chamber increases the nonlinearity of the system significantly, new system identification needs to be conducted to yield a best-fit linear model with relatively low order of the assembled system. In order to render a model that best represents the engine during operation, the reference amplitude (piston traveling) should be within the same range of the nominal stroke length which is 60mm (single piston traveling distance, total length is 120 mm).

The frequency response is then recorded and processed. By utilizing Matlab system identification toolbox, a linear discrete model is estimated and its frequency response is plotted on the same figure with the experimental data as shown in Fig. 3.8. The transfer function of the linear discrete model of the engine is:

$$\begin{aligned} G(q^{-1}) &= \frac{q^{-d}B(q^{-1})}{A(q^{-1})} \\ &= \frac{q^{-4}(-0.006708 + 0.02038q^{-1} - 0.02099q^{-2} + 0.007379q^{-3})}{1 - 3.788q^{-1} + 5.4172q^{-2} - 3.4676q^{-3} + 0.8385q^{-4}} \end{aligned} \tag{3.12}$$

where q^{-1} is the one step delay operator. The model has no unstable poles but two unstable zeros at 1.145 (also note the system has 4 sample steps delay).

Fig. 3.8 also presents the nonlinearity of the engine and the discrepancy between the linear model and the engine. Major nonlinearity of the engine comes from the gas

chambers. During the engine operation, air in the combustion chambers are being compressed or expanded according to the ideal gas law. Therefore one can consider the engine as two moving masses attached to two nonlinear springs. And the discrepancy caused by nonlinearity is lumped into the unmodeled dynamics which will be taken into account in the design of the controller. To precisely track the reference signal in real time, high bandwidth response of the control system is required. This depends on a number of factors: sampling rate of the DAQ and control system, design of the piston and the hydraulic actuator, response time of the servo valve, actuation force etc. The repetitive control drastically improves the tracking performance of the system by placing high gains at the desired frequency locations.

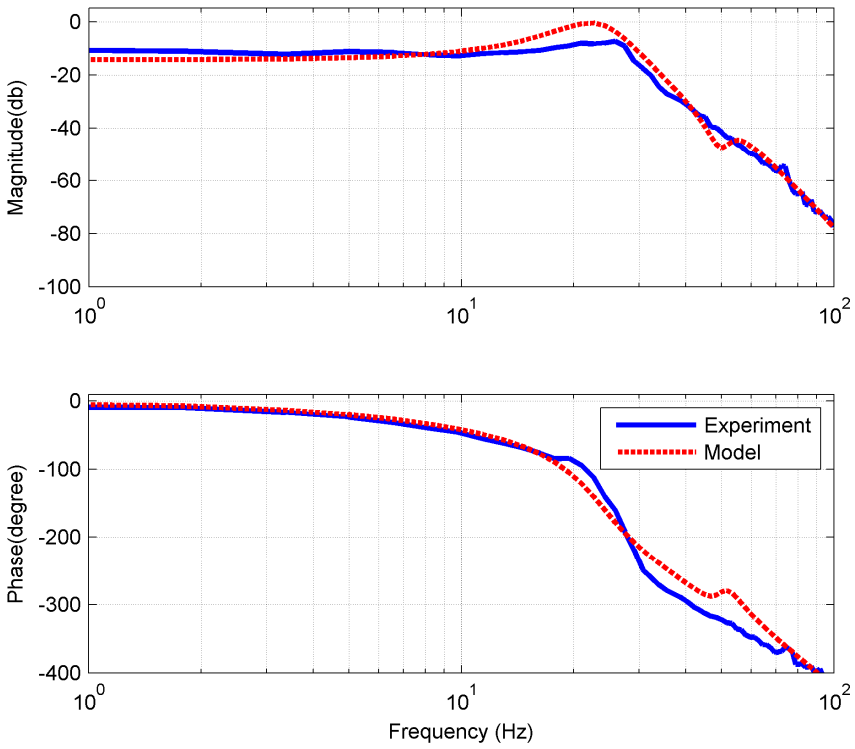

Fig. 3.8. Frequency response of the system and the estimated linear model.

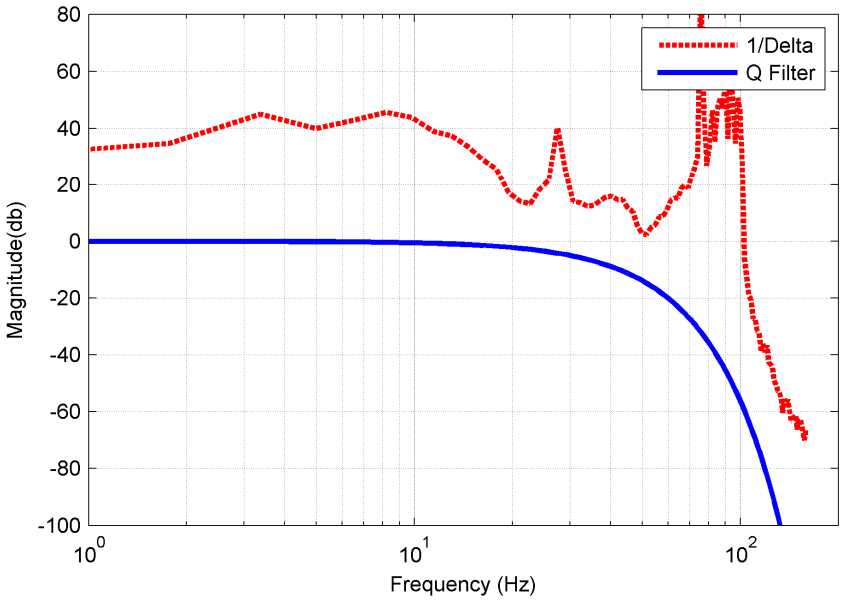

Fig. 3.9. Frequency response of Q filter and multiplicative uncertainty.

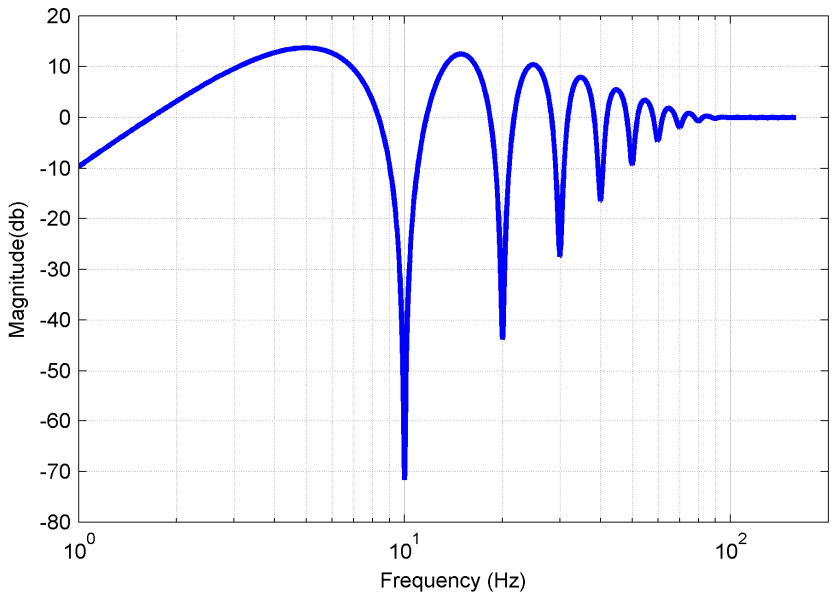

Fig. 3.10. Sensitivity function of the repetitive controller design.

To account for model uncertainties, a zero-phase-error low pass filter is introduced in the controller design. And robust stability is guaranteed if the following condition is satisfied:

$$\left|Q(e^{-j\omega})\right| \le \frac{1}{\left|\Delta(e^{-j\omega})\right|} \tag{3.13}$$

where Δ is the multiplicative uncertainty. The frequency response of the designed Q filter and the inverse of the model uncertainty are shown in Fig. 3.9, and it is seen that (3.13) is satisfied. Sensitivity function of the controller is plotted in Fig. 3.10 to evaluate performance of the control system. The controller is able to track references at low frequencies with small errors. However, the tracking accuracy degrades as the frequency increases because the high gains at the discrete high frequency points are reduced by the Q filter to accommodate the model uncertainty.

The designed motion controller is then implemented on a dSPACE system which has a 2.6 Ghz processor with 16-bit analog-to-digital (A/D) and 14-bit digital-to-analog (D/A). The inner and outer piston positions are measured by linear variable differential transducers (LVDT) with resolution of 0.1 mm that are embedded in the hydraulic block. Combustion chamber pressure is measured by two piezoelectric pressure transducers with Kistler Type 5010B charge amplifier, and hydraulic chamber pressure are measured by Silicon type pressure transducers with resolution of 2.5 psi. Based on the measured information, the control module sends actuation signals to the servo valve and synchronization valves to control the piston position and synchronization. Fuel injection and spark timing has been calibrated and are also controlled by the dSPACE system.

A picture of the test cell set-up is shown in Fig. 3.11. A more detailed schematic that shows the connection between the subsystems can be found in Fig. 3.12. Prior to engine start, the high pressure accumulator needs to be charged. And the high pressure fluid stored in the accumulator will be used for engine motoring later on. Once stable motoring is achieved, we initialize the fuel injection module, and the engine starts to produce positive power and pumps fluid into the high pressure accumulator. The loading valve is used to control the pressure in the high pressure accumulator. It throttles excessive fluid and the heat generated will be dissipated through the heat exchanger. The manual valves are used to shut off the accumulator flow/relief the accumulator pressure manually.

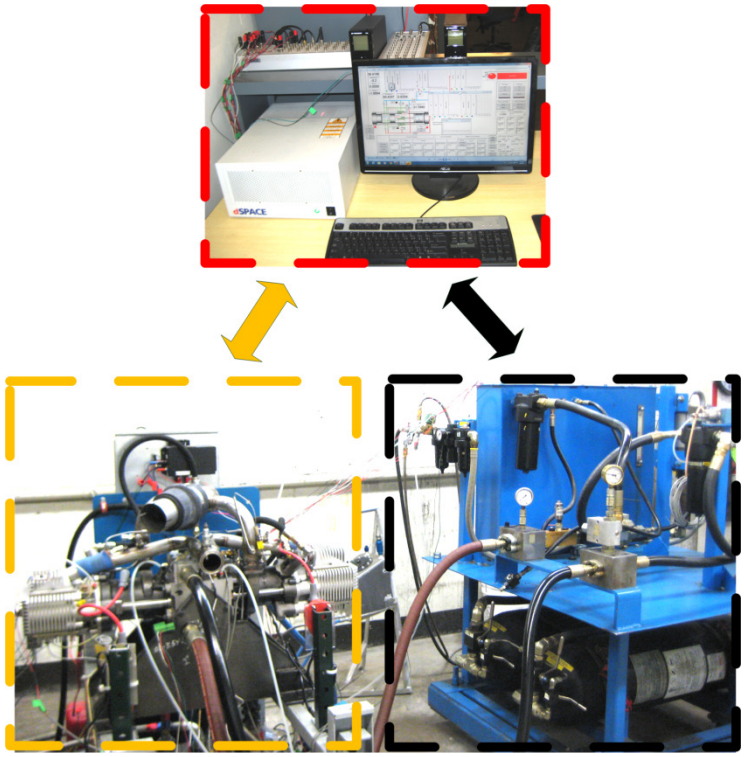

Fig.3.11. Experimental set-up in test cell: control system (top), free piston engine (left) and charging/loading system (right)

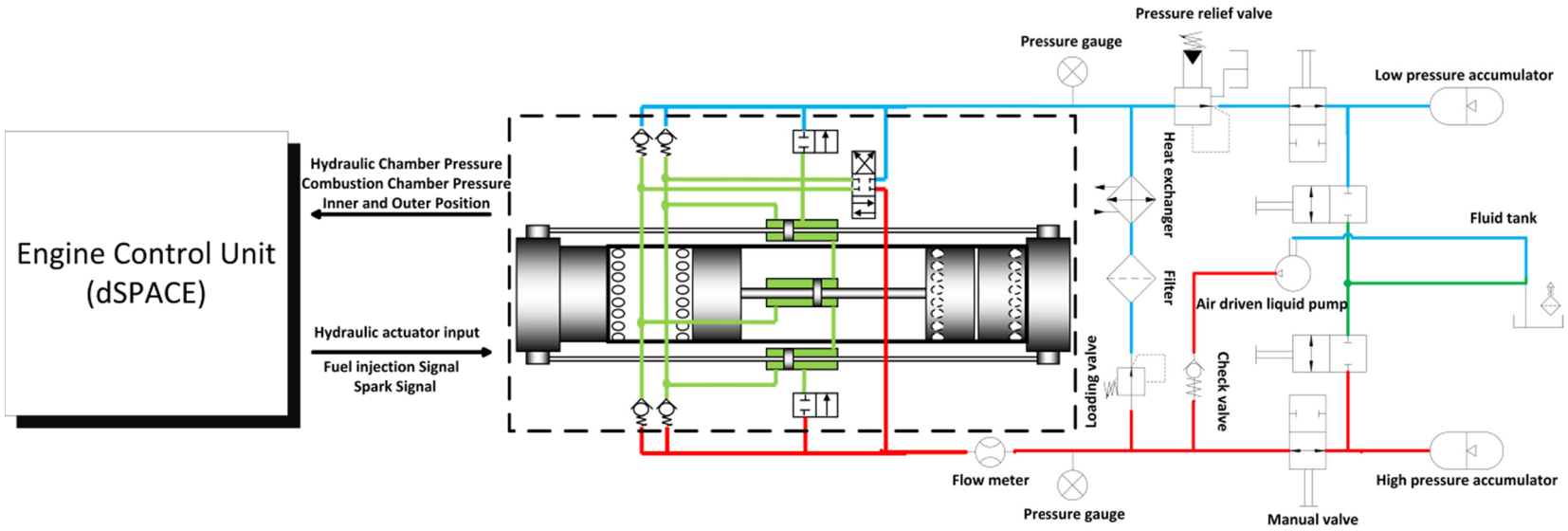

Fig.3.12. Detailed schematic of test cell set up.

Engine start is a challenging problem for FPE operation because the piston is not linked mechanically to a starter, and there have been no systematic methods of achieving rapid and reliable engine start in the literature. But the design of the virtual crankshaft addresses the problem naturally due to its ability of regulating the piston to follow any periodic signals with fast convergence rate and small tracking errors. The good repeatability of the cyclic piston motion offers more accurate estimation of injection and spark timing, and therefore produces a smoother engine start. Nevertheless, the design of the reference piston trajectories is itself a nontrivial task.

The hydraulic force required to maintain a piston trajectory can be back-calculated based on (2.5). The required hydraulic pressure to move the piston varies drastically as the operating frequency changes. Beside the frequency, trajectory shape also affects the amount of hydraulic pressure required. To find the optimal piston trajectory that minimizes the hydraulic energy consumption during engine motoring, we formulate the problem into a nonlinear programming framework. The piston position at each time interval is altered after each iteration to minimize the objective function, which is the hydraulic energy input to the system (integration of instantaneous power: hydraulic pressure multiplied by flow rate) In order to ensure convergence of the program, the piston dynamics in (2.5) is simplified to the dynamic equations shown in (3.14), where the compression and expansion of the in-cylinder gas are assumed to be adiabatic, and the pressure variation during gas exchange phase are neglected:

$$
\begin{aligned}
&\min I = \int_0^{t_f} u \cdot x_2 \cdot A_h dt \\
&\dot{x}_1 = x_2 \\
&\dot{x}_2 = \frac{1}{M}\left[P_i \cdot A_p \cdot \left(\frac{x_i}{x_1}\right)^r - P_i \cdot A_p \cdot \left(\frac{x_i}{L - x_1}\right)^r - K_v \cdot x_2 + u \cdot A_h \right] \\
&x_1(0) = x_{tdc}, x_1(t_f) = x_{bdc} \\
&x_2(0) = 0, x_2(t_f) = 0 \\
&x_{tdc} \le x_1(t) \le x_{bdc} \\
&u_{\min} \le u(t) \le u_{\max}
\end{aligned}
\tag{3.14}
$$

where u is the net hydraulic pressure required, x_1 and x_2 are the position and velocity respectively. Intake pressure is denoted by P_i, intake port opening position by x_i, piston area by A_p, maximum stroke length by L, friction coefficient by K_v and final time of one cycle by t_f. Values of the parameters can be found in Table I and Table II. Matlab optimization toolbox *fmincon* is used to solve the problem. Specifically, we specify boundary conditions (TDC x_{tdc} and BDC x_{bdc} positions etc.) as the linear equality constraints, and specify system dynamics as the nonlinear equality constraints. Upper and lower bounds for states and control are imposed in the problem formulation.

The calculated optimal piston trajectory at compression ratio 8 and its required net hydraulic pressure (the net pressure is the pressure difference across the piston plunger, e.g. P_{LH}-P_S) are shown in Fig. 3.13, where the optimal trajectory is compared with a sinusoid signal with the same amplitude and frequency. The optimal trajectory is a 25 Hz curve with sharper turning at TDC and BDC compared to the sinusoid signal. The energy saving of using the optimal trajectory instead of the sinusoid trajectory is found to be 19%. And peak net-hydraulic-pressure-required to maintain the sinusoid signal is 2 times

higher than the optimal trajectory (a piston trajectory optimization result with combustion is shown in Appendix 1).

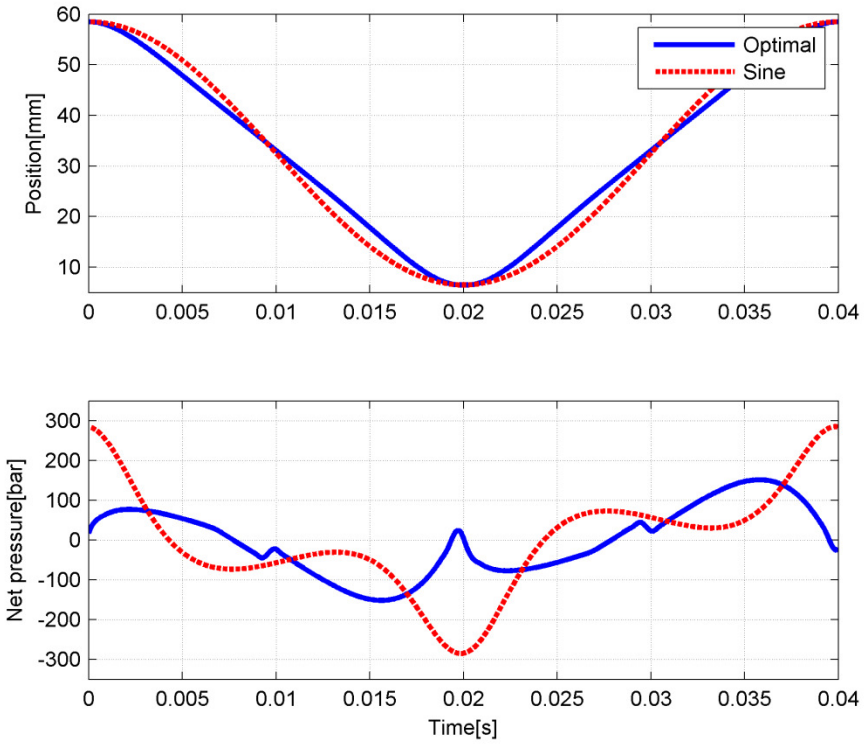

Fig. 3.13. Optimal trajectory and the corresponding hydraulic input.

When piston travels near TDC or BDC, it will be decelerated or accelerated rapidly. Therefore, to maintain a sinusoid trajectory that has a slower acceleration, the system requires more energy and larger force to overcome the chamber gas resisting force. Fig. 3.14 shows the experimental motoring results. The virtual crankshaft is able to produce a stable and repeatable motoring, and the piston tracking performance is excellent considering the fact that the moving mass and stroke length of the system is much larger compared to typical fluid power applications, whereas the actuation force (hydraulic force) is almost the same level as the resisting force.

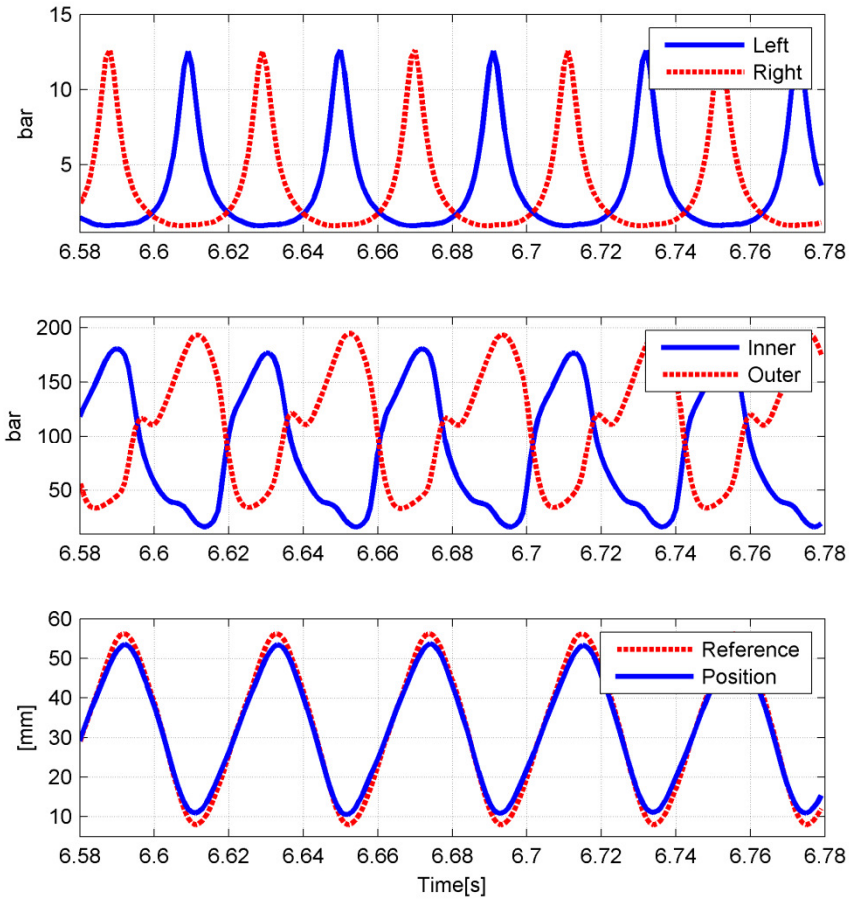

Fig. 3.14. Motoring: Gas pressure, hydraulic chamber pressure and piston tracking performance (from top to bottom).

3.3 Feedforward Control Design

It is obvious that precise motion control is necessary in order to control compression ratio and optimize engine operation in real time. While most of the electrohydraulic actuation systems are capable of tracking references less than 10 Hz with relatively small stroke length [58]-[61], the operating frequency of the FPE is 25 Hz with 50 mm piston displacement. The nonlinearity of the FPE system is more prominent compared to a

typical hydraulic system due to the nonlinear dynamics of the hydraulic system and the combustion chamber, which is caused by the compression and expansion of the in-cylinder gas mixture. Furthermore, to achieve precise tracking in most of the applications, the actuation force is generally much larger than the resisting force. However, in our case, the resisting force caused by piston inertia and combustion chamber pressure is on the same level with the hydraulic actuation force, which is limited by the maximum operating pressure of the hydraulic components. These combined factors mentioned above make the precise motion control of the FPE a challenging task even with the robust repetitive control. To assist the existing motion control and further improve the tracking performance, two feedforward control designs are proposed in this section. The first feedforward design involves the inversion of a linear model that describes the dynamic of the engine operation. The second design is based on the flatness approach, which involves the inversion of a nonlinear model of the hydraulic FPE system.

The most important procedure in a linear model inversion, besides inverting the stable poles and zeros, is the inversion of the unstable zeros. A number of techniques have been developed to minimize the effect of unstable zeros on the linear model inversion. Among these is the Zero Phase Error Tracking (ZPET) scheme [62]-[64] which is a noncausal feedforward compensation that has the effect of completely eliminating any phase error. However, with the plant model of the hydraulic FPE which has an unstable zero in the right half plane, employing the ZPET scheme induces high gains in the frequency range of the engine operation. Therefore, to ensure robust stability, another scheme which

utilizes series expansion for the model inversion is introduced [65]. The nonlinear feedforward control in this section is designed based on the flatness approach. The property of flatness of a system can be extremely useful when tracking trajectories: from the reference trajectories, states and control inputs can be calculated directly [66]. Therefore, flatness-based control is widely used from motion planning to stabilization of reference trajectories. A considerable amount of realistic models are flat, such as aircrafts [67], motors [68] and clutch systems [69]. A major property of differential flatness is that the state and input variables can be directly expressed, without integrating any differential equation, in terms of the flat output and a finite number of its derivatives.

The two feedforward controls are implemented on the hydraulic FPE together with the repetitive control. The tracking results of various piston trajectories are compared and discussed. Configuration of the control systems with the two feedforward controllers are shown in Fig. 3.15. The advantages of employing the feedforward controls here are the fast convergence rate, especially during transient caused by reference trajectory change. As mentioned in the previous section, a proportional feedback control is utilized first to stabilize the hydraulic FPE system, so that system identification can be conducted to render an estimated linear model. Signal from the linear feedforward control *u2* is added to signal from the repetitive control *u1* to form the input of the stabilized system (reference of the inner proportional control loop), due to that fact that the linear feedforward control is also designed based on the estimated linear model. However, the nonlinear feedforward control is designed based on a physical model of the hydraulic FPE system. Thus, signal from the nonlinear feedforward control *u3* is directly added to

the input of the hydraulic FPE as shown in Fig. 3.15.

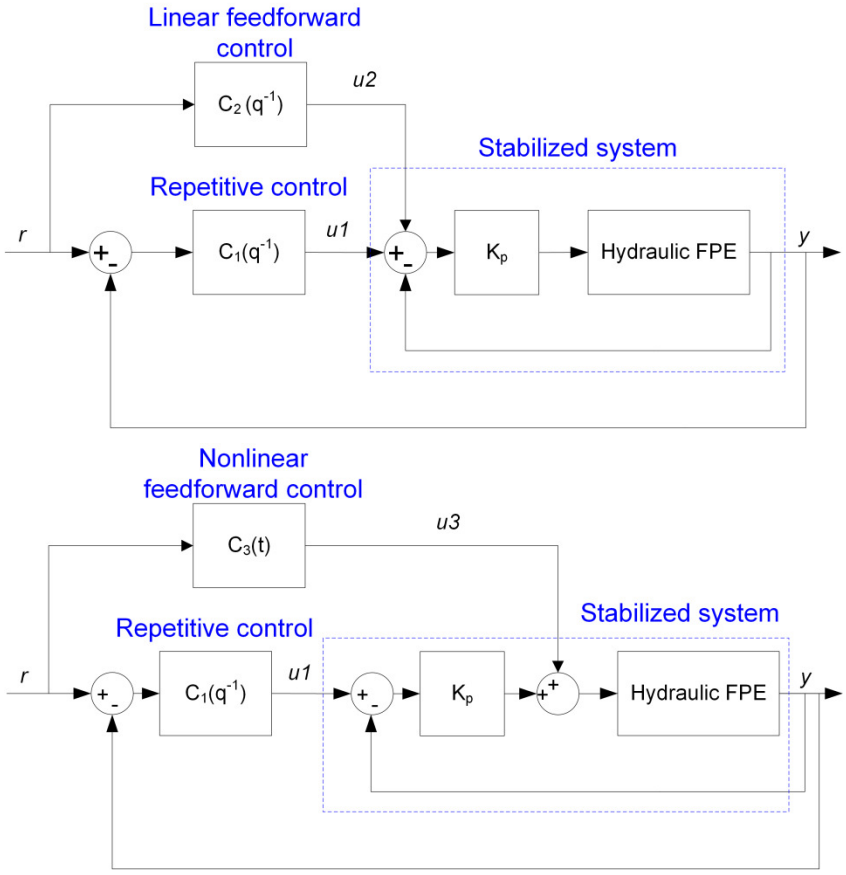

Fig. 3.15. Configuration of the control systems with linear and nonlinear feedforward control

3.3.1 Linear feedforward control design

The ZPET control scheme includes the inverse of stable poles and zeros of the system, as well as a noncausal compensator to approximate the inverse of unstable zeros, which eliminates the phase error completely. The resulting control is shown below:

$$C_{zpet}(q^{-1}) = Q(q^{-1})\frac{q^{d}B^{-}(q)A(q^{-1})}{B^{+}(q^{-1})} \tag{3.15}$$

where $B^{+}(q^{-1})$ is the stable zeros, $B^{-}(q^{-1})$ is the unstable zeros, and $Q(q^{-1})$ is a zero phase

error lowpass filter that reduces large control gain at high frequencies for robust stability. Note the controller is noncausal, therefore, it requires preview of the reference. For position tracking of the hydraulic FPE, the reference trajectory is pre-defined and repetitive, so the future reference is accessible. Transfer function of the feedforward control system after applying the ZPET scheme can thus be reduced to

$$L(q^{-1}) = C_{zpet}(q^{-1}) \cdot G(q^{-1}) = Q(q^{-1}) \cdot B^{-}(q^{-1}) \cdot B^{-}(q) \tag{3.16}$$

Bode plot of $B^{-}(q^{-1}) \cdot B^{-}(q)$ is shown in Fig. 3.16, magnitude of the transfer function starts to grow rapidly from 10 Hz. In order to ensure the robustness of the system, a high order Q filter with low cut-off frequency is required to suppress the high gain. Nevertheless, this will result in degradation on the tracking performance of the controller. An alternative method is thus considered in this case, which utilizes series expansion to cancel the unstable zeros:

$$\frac{1}{q-a} = -(\frac{1}{a} + \frac{1}{a^2}q + \frac{1}{a^3}q^2 + \frac{1}{a^4}q^3 ... + \frac{1}{a^n}q^{n-1}) \tag{3.17}$$

where a denotes the unstable zero, the resulting control is shown in (3.18).

$$C_2(q^{-1}) = -\frac{q^d A(q^{-1})}{B^{+}(q^{-1})}\left(\frac{1}{a} + \frac{1}{a^2}q + \frac{1}{a^3}q^2 \cdots + \frac{1}{a^n}q^{n-1}\right) \tag{3.18}$$

Transfer function of the feedforward control system becomes:

$$\begin{aligned} L(q^{-1}) &= C_2(q^{-1}) \cdot G(q^{-1}) \\ &= -B^{-}(q^{-1}) \cdot \left(\frac{1}{a} + \frac{1}{a^2}q + \frac{1}{a^3}q^2 \cdots + \frac{1}{a^n}q^{n-1}\right) \end{aligned} \tag{3.19}$$

The objective is to make $L(q^{-1})$ close to 1. The location of the unstable zero and the

number of terms used in the series determine how close the transfer function is to 1. Generally, the further the unstable zero lies from the unit circle, the fewer terms are required for the transfer function to approach 1. The unstable zero of the system model is 1.14, therefore, 16 terms are used to keep the peak gain below 2 dB as shown in Fig. 3.16. The series expansion approach is proven to be the optimal solution in a least squares sense for cancelling the effect of the unstable zeros in the model inversion [65].

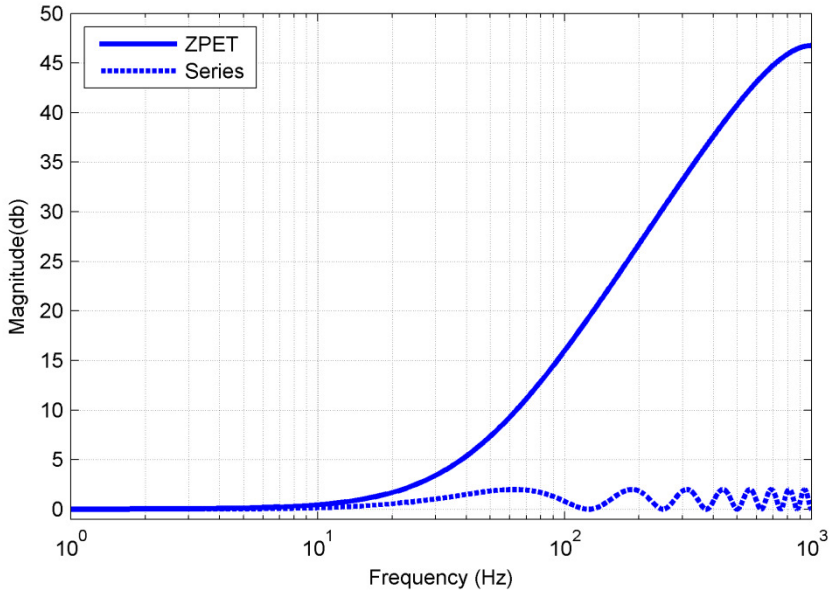

Fig. 3.16. Inversion of the unstable zero based on the ZPET and Series expansion schemes

3.3.2 Nonlinear Feedforward Control Design

During the operation, the engine is a highly nonlinear system, and majority of the nonlinearity arises from the gas dynamics of the combustion chambers. Therefore, a nonlinear feedforward control is investigated in this section, and the control design is based on the flatness approach. A nonlinear system is flat if the states and the inputs can be determined by the output and finite number of output derivatives [70], which is true

for the hydraulic FPE system.

The dynamics of the engine operation can be described by the piston motion, gas dynamics and hydraulic pressure dynamics. The piston motion can be determined by Newton's second law:

$$\ddot{x} = \frac{1}{M}(P_{hyd} \cdot A_{hyd} + P_{gas} \cdot A_{pis} - F_f) \tag{3.20}$$

where x is the piston position, M is the mass of the piston, P_{hyd} and A_{hyd} are the pressure and area of the hydraulic chamber, P_{gas} and A_{pis} are the pressure and area of the combustion chamber, and F_f is the friction force that is assumed to be proportional to the piston velocity. The gas pressure inside the combustion chamber is estimated by the ideal gas law:

$$P_{gas} = P_{in} \cdot (\frac{x_{in}}{x})^{\gamma} - P_{in} \cdot (\frac{x_{in}}{L-x})^{\gamma} \tag{3.21}$$

where P_{in} is the intake manifold pressure, x_{in} is the intake port location, γ is the specific heat ratio and L is the nominal stroke length. Notice P_{gas} is the net pressure acts on the piston from the two combustion chambers.

As shown in Fig. 2.1(b), the left chambers of the hydraulic pumps are connected to the accumulators through the check valves and the servo valve, whereas the right chambers serve as the synchronization mechanism. Therefore, the rate of pressure change inside the left chambers of the hydraulic pumps is determined by flow from the check valves Q_{checks}, flow from the servo valve Q_{servo} and piston motion:

$$\dot{P}_{LH} = \frac{\beta}{V_h}\left(Q_{checks} + Q_{servo} + A_{hyd} \cdot \dot{x}\right) \tag{3.22}$$

$$P_{hyd} = P_{syn} - P_{LH} \tag{3.23}$$

where P_{LH} is the pressure of the left chambers, P_{syn} is the pressure of the synchronization volume, β is the bulk modulus of the fluid and V_h is the left chamber volume. Based on the experimental results, the variation of the pressure in the synchronization chamber is relatively small compared to other hydraulic chambers during the engine operation. Therefore, it is assumed to be constant for simplification. And flows through the valves are modeled by the orifice equation as follows:

$$Q_{checks} = \begin{cases} -K_{checks} \cdot \sqrt{\dfrac{2 \cdot (P_{LH} - P_{HP})}{\rho_{fluid}}}, & P_{LH} - P_{HP} > 1400000 \\ K_{checks} \cdot \sqrt{\dfrac{2 \cdot (P_{LP} - P_{LH})}{\rho_{fluid}}}, & P_{LP} - P_{LH} > 700000 \\ 0, \quad otherwise \end{cases} \tag{3.24}$$

$$Q_{servo} = \begin{cases} K_{servo} \cdot u \cdot sign(P_{HP} - P_{LH}) \cdot \sqrt{\dfrac{2 \cdot abs(P_{HP} - P_{LH})}{\rho_{fluid}}}, u > 0 \\ K_{servo} \cdot u \cdot sign(P_{LH} - P_{LP}) \cdot \sqrt{\dfrac{2 \cdot abs(P_{LH} - P_{LP})}{\rho_{fluid}}}, u < 0 \\ 0, \quad u = 0 \end{cases} \tag{3.25}$$

where K_{checks} is the effective area of the check valves and K_{servo} is the maximum effective area of the servo valve. Fluid density is denoted by ρ_{fluid}, high pressure and low pressure accumulator are denoted by P_{HP} and P_{LP} respectively. Value of the effective area of the servo valve is determined by the voltage signal u ($-1 \leq u \leq 1$), and here the dynamics of the valve is neglected since it is much faster than the system dynamics.

To derive the feedforward control for the system, the reference trajectory x_d is

considered as the output of the system. Since the trajectory is pre-defined, the velocity, acceleration and derivative of the acceleration are known as well. From (3.22) and (3.23), we can then calculate the desired hydraulic pressure if we are to maintain a reference trajectory x_d.

$$P_{hyd\_d} = \frac{M \cdot \ddot{x}_d + k_v \cdot \dot{x}_d - P_{in} \cdot A_{pis} \cdot (\frac{x_{in}}{x_d})^{\gamma} + P_{in} \cdot A_{pis} \cdot (\frac{x_{in}}{L - x_d})^{\gamma}}{A_{hyd}} \tag{3.26}$$

By taking the derivative of P_{hyd_d} and plugging (3.24) – (3.25) into (3.26), we can obtain the desired servo valve flow rate Q_{servo_d}:

$$Q_{servo\_d} = -\frac{V_h \cdot \dot{P}_{hyd\_d}}{\beta} - A_{hyd} \cdot \dot{x}_d - Q_{checks} \tag{3.27}$$

Finally, plug (3.27) into (3.25) we arrive at the control signal of the nonlinear feedforward control to achieve the desired trajectory:

$$u_3 = \begin{cases} \dfrac{Q_{servo\_d}}{K_{servo} \cdot \sqrt{\dfrac{2 \cdot (P_{HP} - P_{LH})}{\rho_{fluid}}}}, & Q_{servo\_d} > 0 \,\&\, P_{HP} > P_{LH} \\ \dfrac{Q_{servo\_d}}{K_{servo} \cdot \sqrt{\dfrac{2 \cdot (P_{LH} - P_{LP})}{\rho_{fluid}}}}, & Q_{servo\_d} < 0 \,\&\, P_{LH} > P_{LP} \\ 0, \quad otherwise \end{cases} \tag{3.28}$$

The feedfoward control signal can be smoothed for implementation. Values of the parameters used in the derivation can be found in Table 3.1.

3.3.3 Experimental and simulation results

The two feedforward designs have been implemented on the hydraulic FPE to

complement the robust repetitive control for precise piston motion control. The controllers are developed in Matlab/Simulink program and then loaded into a dSPACE processor board. To study the influence of adding feedforward controller on both steady state and transient performance, the reference trajectory is a 25 Hz sinusoid signal with a sudden peak-to-peak value change from 30 mm to 44 mm. System performances of adding the two feedforward controls are benchmarked with tracking performance of the

TABLE 3.1
PARAMETER VALUES FOR FEEDFORWARD DERIVATION

Symbol	Definition	Value
γ	Specific heat ratio	1.31
M	Piston mass	4.5 kg
A_{pis}	Piston area	5000 mm^2
A_{hyd}	Hydraulic plunger area	141 mm^2
P_{in}	Intake manifold pressure	1 bar
x_{in}	Intake port location	51 mm
β	Bulk Modulus	1.2 GPa
ρ_{fluid}	Fluid density	875 Kg/m^3
K_{checks}	Check valve effective area	55 mm^2
K_{servo}	Maximum servo valve effective area	19 mm^2
K_v	Friction coefficient	200 N·s/m
P_{HP}	High pressure accumulator pressure	193 bar
P_{syn}	Synchronization chamber pressure	97 bar
P_{LP}	Low pressure accumulator pressure	14 bar

repetitive-control-only case. Fig. 3.17 shows the steady state tracking performance of the three controllers when the piston peak-to-peak displacement is 30 mm and 44 mm, and Fig. 3.18 presents the transient tracking errors of the three controllers. By adding both feedforward controls, the system demonstrates better tracking capability that significantly

reduces the tracking error. Specifically, in the 30 mm case, both the linear and nonlinear feedforward control manage to reduce the errors from ± 2 mm to ± 1 mm; in the 44 mm case, the tracking errors without adding the feedforward controls are ± 3 mm. And the linear feedforward control is able to keep the errors within ± 2 mm, whereas the nonlinear feedforward control is able to keep the errors within ± 1 mm. Also notice in Fig. 3.18, a sudden increase of the reference amplitude occurs at 4 s. Compared to the repetitive-control-only case, adding the feedforward controllers has reduced the magnitude and duration of the transient simultaneously.

To summarize the experimental results: By adding both forward controllers, the system is able to achieve equally significant improvement on tracking in small displacement range. However, in large displacement range, the nonlinear feedforward control is more effective in reducing the tracking errors. An obvious explanation for the experimental outcome is that as the piston displacement increases, nonlinearity of the system increases as well. Thus, in small displacement range, both of the feedforward controllers make equivalent contribution to the tracking performance. However, the linear feedforward control is not able to fully capture the dynamics of the system operation in large displacement range, and therefore can only achieve limited improvement. This can also be illustrated in Fig. 3.17 by comparing the control signals of the system in different piston displacement ranges. In small displacement range, control signals of the system to which the two feedforward controllers are added, resembles each other. However, in the high displacement case, the control input of system with the nonlinear feedforward control had its distinct nonlinear features compared to the other two control inputs.

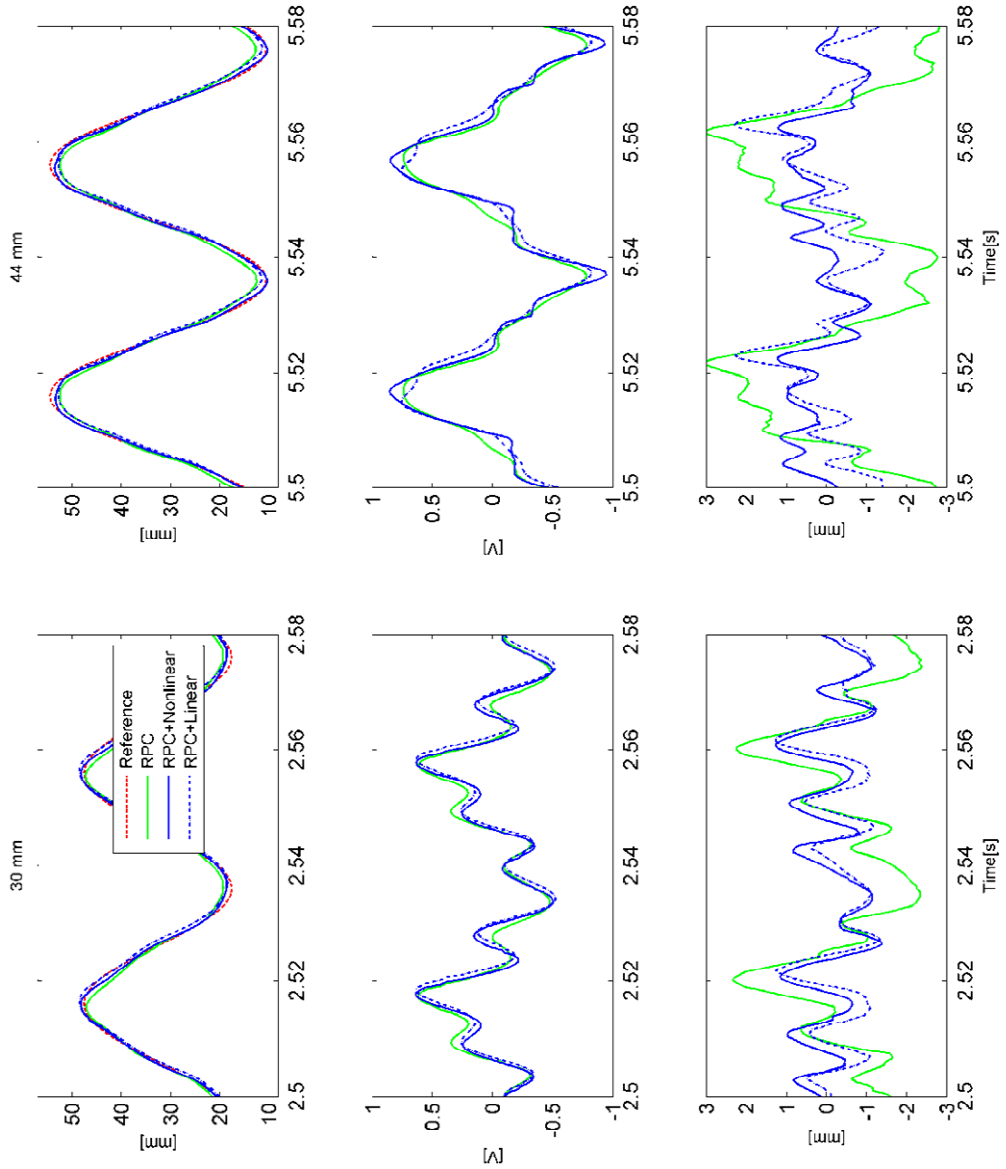

Fig. 3.17. Tracking performance of the three controllers at 30 mm and 44 mm displacement (from top to bottom: piston trajectory, control signal and tracking error)

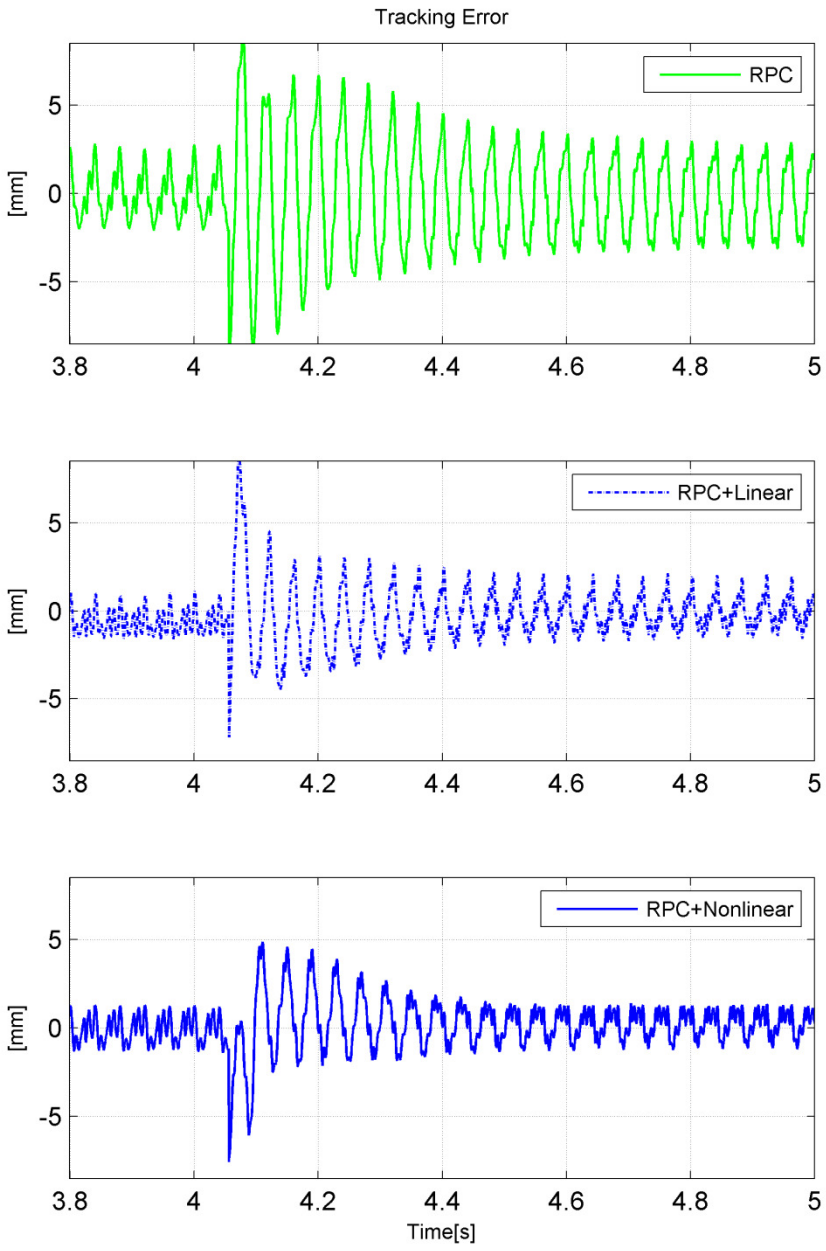

Fig. 3.18. Transient tracking errors of the three control systems.

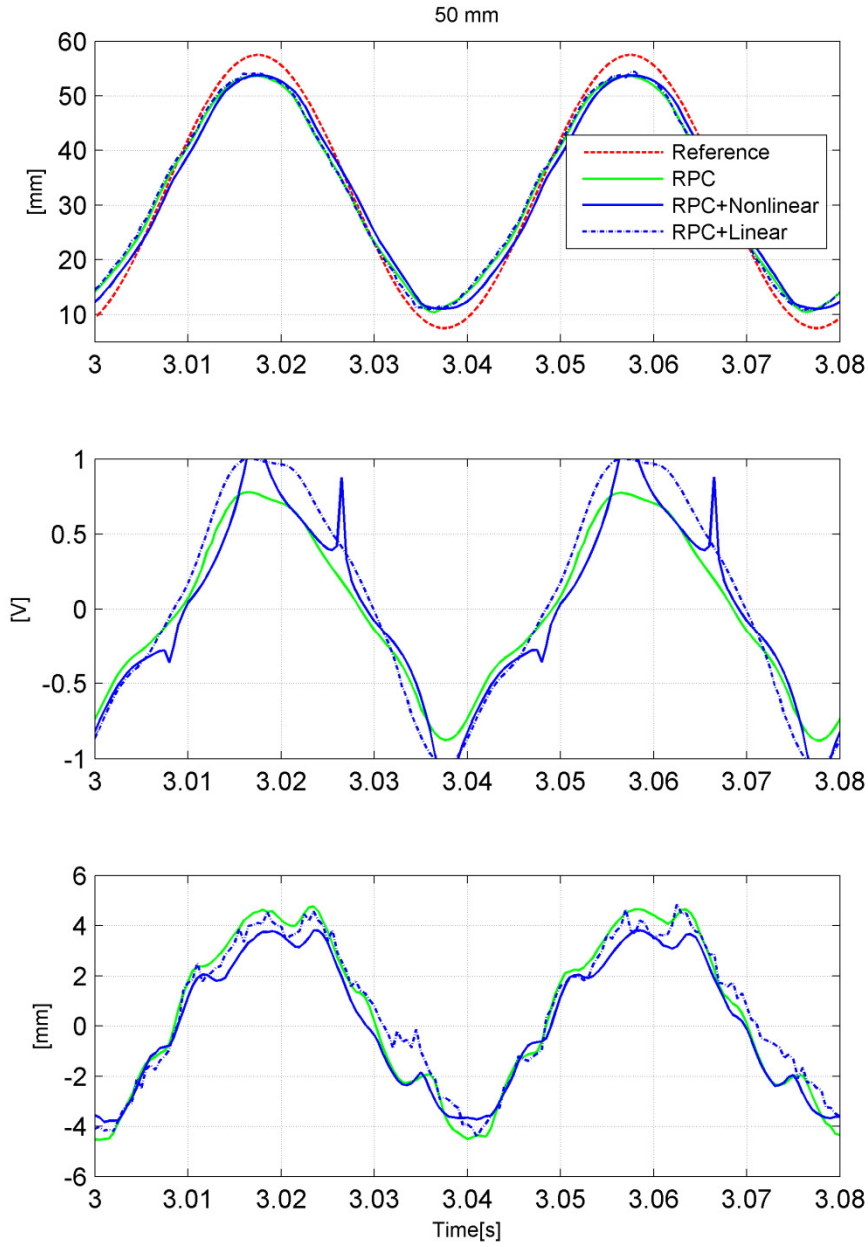

Fig. 3.19. Tracking performance of the three control systems at 50 mm piston displacement (from top to bottom: piston trajectory, control signal and tracking error)

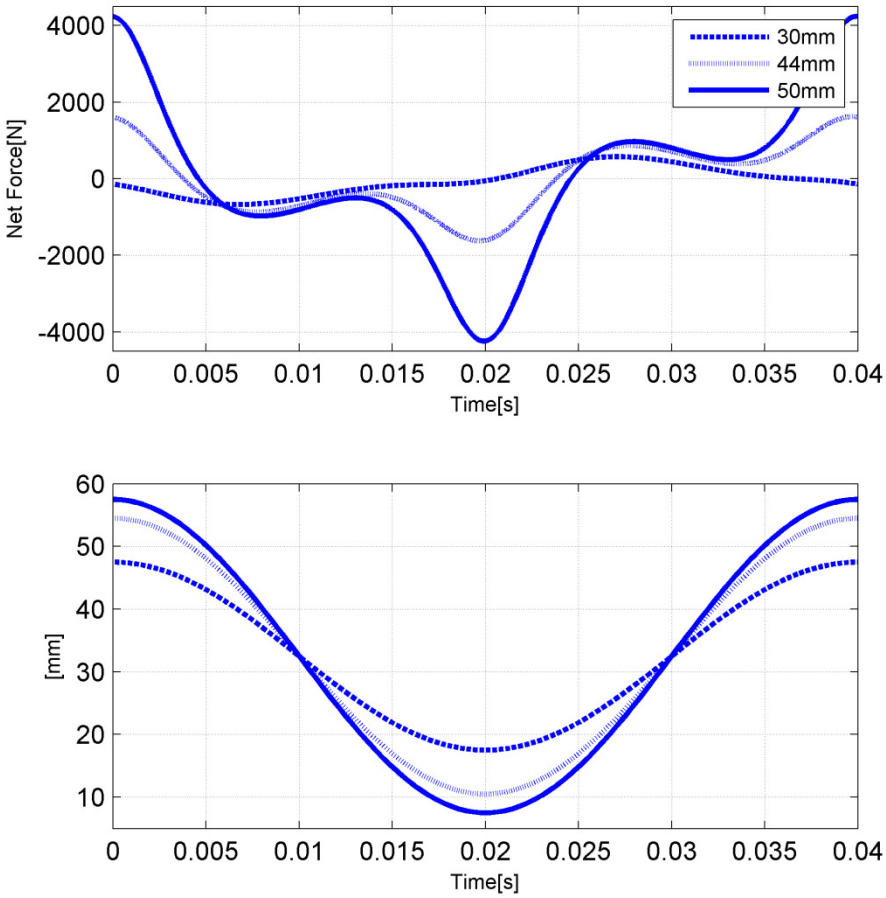

Fig. 3.20. Required net hydraulic force to track the references at three piston displacement ranges

Fig. 3.19 shows the performance of the three control systems of tracking a larger piston displacement (50 mm) trajectory. Even though the differences among the control signals are clearly shown, the improvement on position tracking of the feedforward controllers is limited. Notice the saturation of control inputs from systems with the feedforward controls, it indicates the actuation force is insufficient for tracking a reference with such high amplitude. And Fig. 3.20 shows the calculated net hydraulic force required to achieve the reference trajectories in three piston displacement ranges based on (3.20)-

(3.26). Positive force indicates an action of pulling the piston towards the BDC, whereas negative force indicates an action of pushing it towards the TDC. The peak net hydraulic force required in the 50 mm displacement case is 4000 N, which is nearly three times higher than the maximum net hydraulic force (1400 N) the supply pressure can provide in the experiments. And the reason for limited improvement on tracking performance of the feedforward controllers is readily revealed. Fig. 3.20 also shows that in order to precisely follow the reference trajectory from the BDC to TDC, the hydraulic force must resist the piston motion (0-0.005s) at first, and assist the motion (0.015-0.02s) at the end. Similarly when travel from the TDC to BDC, the hydraulic force shall decelerate and then accelerate the piston. Such hydraulic pressure profile as shown in Fig.3.20 is unlikely to be achieved by calibration-based control. This further emphasizes the significance of the proposed feedforward plus repetitive feedback control system on precise piston motion control.

Due to the hardware limitation of the prototype system, the maximum supply pressure of the operation is 193 bar. Therefore, to support the abovementioned explanation, we implement the three controllers in a high fidelity model of the hydraulic FPE, which was validated previously [70] with a supply pressure of 414 bar. And the simulation result of tracking the 50 mm displacement sinusoid trajectory is shown in Fig. 3.21. Compared to Fig. 3.19, the overall performance of the three controllers has been drastically improved with the high supply pressure. In particular, the linear and nonlinear feedforward control, whose effect on the control system is fairly similar in this case, are able to reduce the tracking error from ±1 mm in the repetitive-control-only case to less than ±0.5 mm.

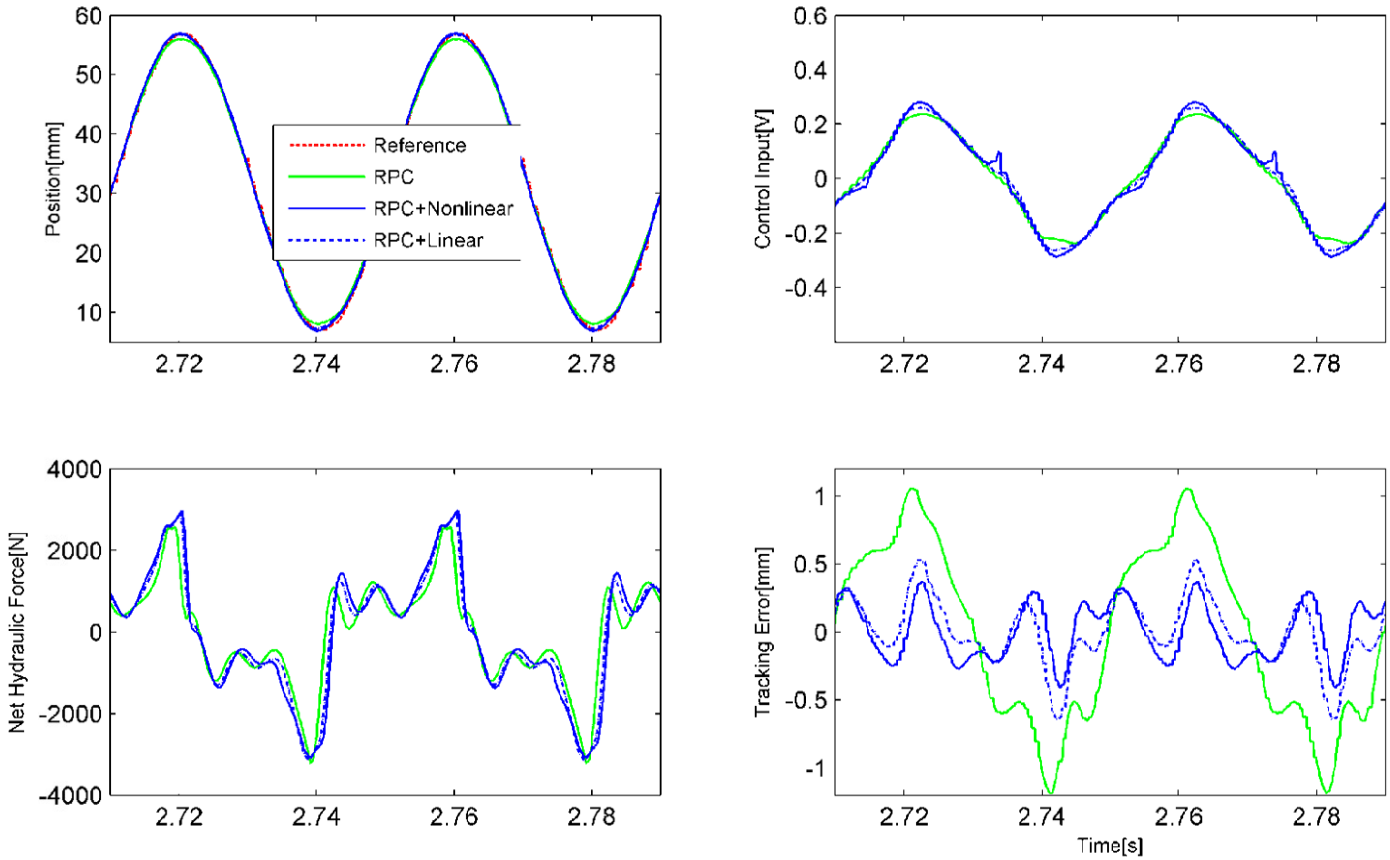

Fig. 3.21. Simulated tracking performance of the three controllers at 50 mm sinusoid piston

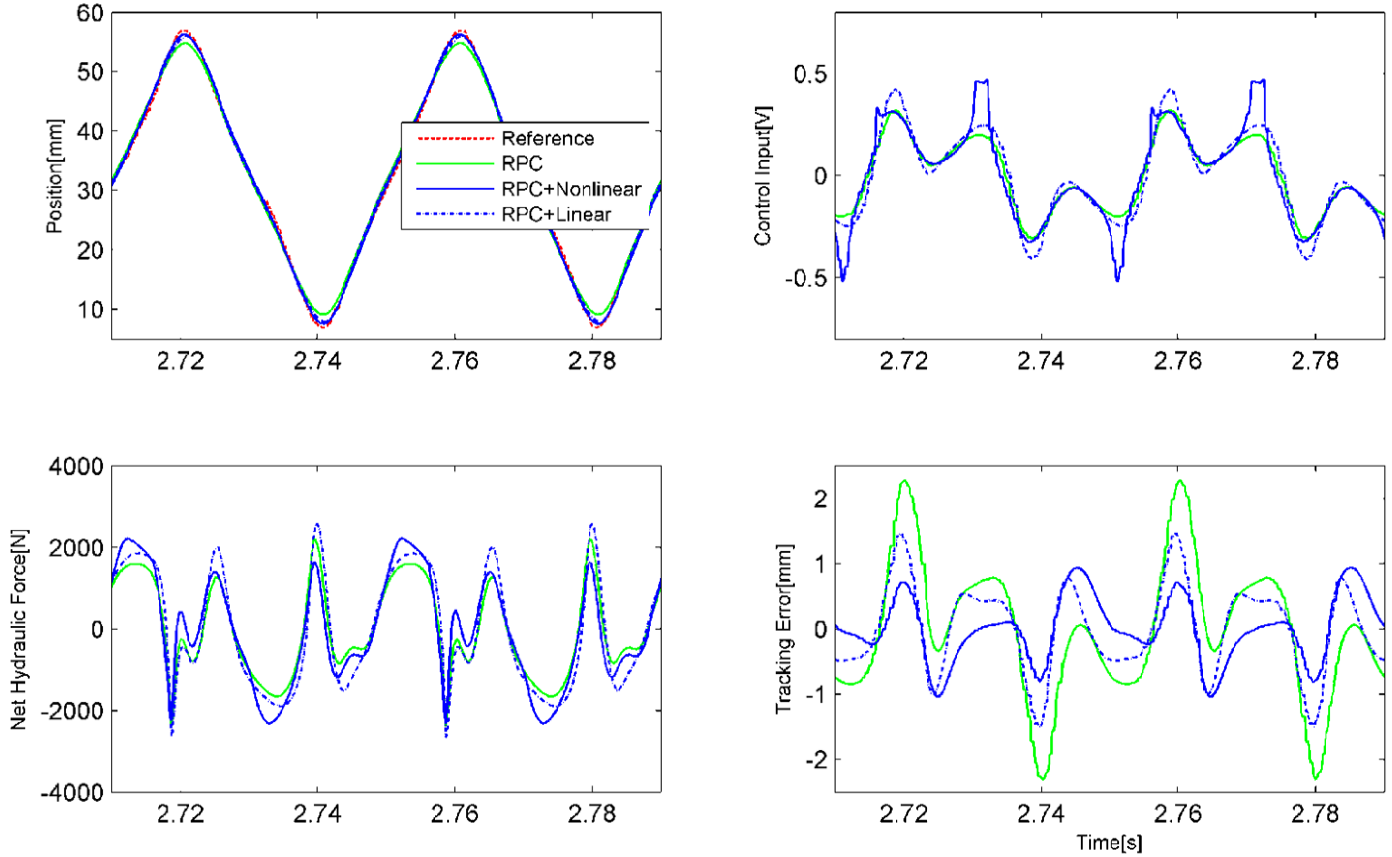

Fig. 3.22. Simulated tracking performance of the three controllers with a modified sinusoid piston trajectory (Top left: piston trajectory, top right: control signal; Bottom left: net hydraulic force, bottom right: tracking error)

To further explore how the two feedforward controls complement the repetitive control to achieve precise tracking of variant piston trajectories, simulation results of tracking a modified sinusoid signal at 50 mm displacement are shown in Fig. 3.22. Compared to a regular sinusoid trajectory with the same frequency, the modified sinusoid trajectory has sharper returns, which means the piston will spend less time at the TDCs and BDCs.

The tracking error of the repetitive-control-only system in this case is ±2 mm. However, the linear feedforward control reduces the error to ±1.5 mm whereas the nonlinear feedforward control is able to maintain the error within ±1 mm. Notice the peak tracking errors occur around TDCs and BDCs, the nonlinear feedforward control manages to keep it lower than the other two controls. To understand the rationale, let's first zoom into the time interval when piston reaches its TDC at 2.74 s. In the repetitive-control-only and linear feedforward control cases, the hydraulic force pushes the piston towards the TDC at a relative late stage (see net hydraulic force at 2.73 s), based on which the piston is not able to reach the reference TDC, and therefore the large tracking error occurs. However, in the nonlinear feedforward control case, the hydraulic force accelerates the piston in an earlier stage, and thus the piston travels closer to the reference TDC, which reduces the peak tracking error. The differences of the hydraulic force can be reflected on the control signal plot as well. Notice the spike of the nonlinear feedforward control signal at 2.73 s, which corresponds to the sudden increase of its hydraulic force before the TDC.

3.4 Digital Hydraulics Control

To reduce system cost and improve efficiency, an alternative design of the HFPE is investigated. As shown in Figure 3.23, the check valves and the Moog valve have been replaced with digital valves. The pump flow can be routed to either the low pressure tank or the high pressure supply in real time. It can also be used as a control means for piston/pump motion by controlling the hydraulic chamber pressure using the digital valves. Compared to the current design with check valves and servo valve, the digital hydraulics design significant production cost reduction and offers more flexibility as well. The passive nature of the check valves determines that once the pressure drop across the check valves reaches the preloading condition, it is difficult to alter the piston motion via adjusting the chamber pressure. However, with the digital valves, such constraints can be removed, and active control can be enabled throughout the operating conditions. The digital valves can either be fully open or fully closed, therefore the throttling loss will be reduced as well. However, instead of controlling the flow by adjusting the opening of the valve, the digital valves control flow by the opening duration. This imposes challenges to the precise piston motion control, as model-based advance control cannot be directly applied. In this section, a repetitive control approach to the digital hydraulics system is explored.

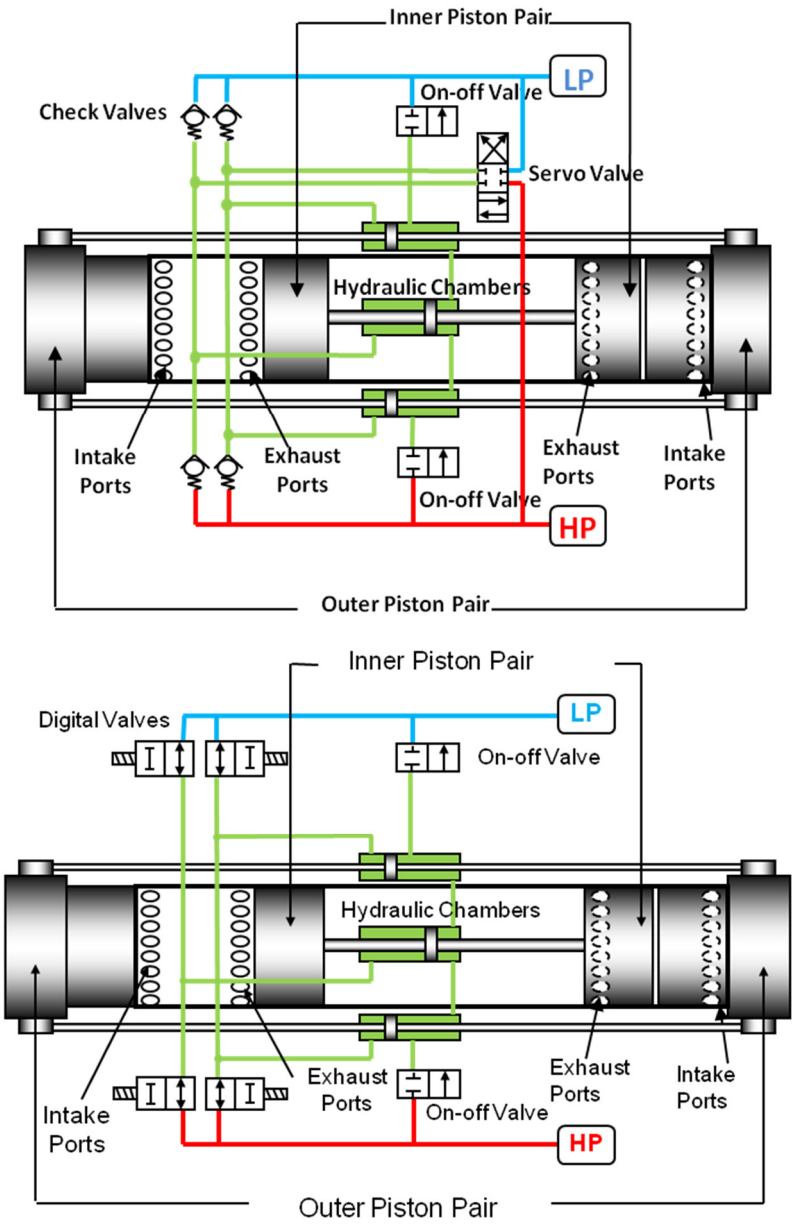

Fig. 3.23 Comparison of the configuration of the current design and the digital hydraulic design

There are four digital valves that can be used to control the flow between the hydraulic chambers and high pressure source, each of the four valves has two states. That means at a given time instance, the controller has a total of sixteen modes of the valves to choose

from. Table 3.2 summarizes the digital valves states at each mode , a 'O' indicates a particular valve is turned on, a 'F' indicated the valve is turned off (where d1, d2, d3 and d4 corresponds to the upper left, upper right, lower left and lower right valve in Figure 3.3, respectively). Upon careful inspection of the table, one can actually identify many 'redundant' modes. By applying general rules, the number of modes can be significantly reduced. For example, there is no need to open d1 and d3 (Mode 3,5,6,7) or d2 and d4 (Mode 4,5,11, 12) simultaneously.

Table 3.2 Sixteen Modes of the Digital Hydraulic Valves

Mode	*d1*	*d2*	*d3*	*d4*
1	O	F	F	F
2	O	O	F	F
3	O	O	O	F
4	O	O	F	O
5	O	O	O	O
6	O	F	O	F
7	O	F	O	O
8	O	F	F	O
9	F	O	F	F
10	F	O	O	F
11	F	O	F	O
12	F	O	O	O
13	F	F	O	F
14	F	F	O	O
15	F	F	F	O
16	F	F	F	F

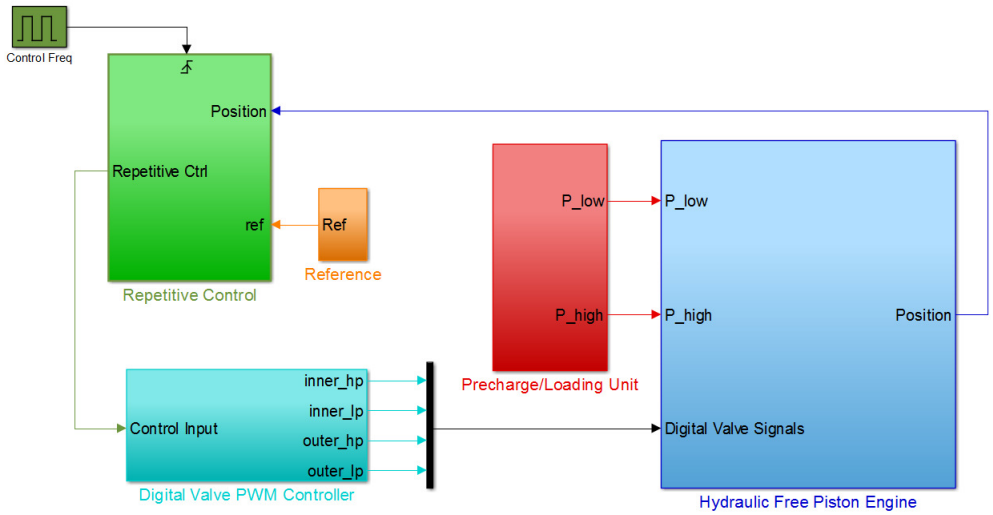

Fig. 3.24 Block diagram of the control system of the digital hydraulic design

Three modes remain after applying the redundancy eliminating rule: Mode 8, Mode 10 and Mode 16. Mode 8 connects the left chamber of the outer piston pump to high pressure, while draining pressure from the left side of the inner piston pump. Therefore, the outer piston moves to the right and inner piston to the left. Mode 10 connects the left side of the inner piston pump to the high pressure while draining the left sides of the outer piston pump. This causes the inner piston moving to the right and outer piston to the left. Mode 16 completely shuts the flow between the engine and the high pressure source and drain. This mode is useful especially in the case where piston is required to remain at a constant position. The incompressibility of the fluid enables the position to be held without wasting energy even when the resisting force from the combustion chamber is large. Assume $\tau 1$, $\tau 2$ and $\tau 3$ represents the duty cycle of Mode 8, 10 and 16, respectively (duty cycle represents the fraction of a normalized switch period that each mode is active). Therefore,

$$\tau 1 + \tau 2 + \tau 3 = 1 \tag{3.29}$$

Due to the constraint of (3.29), we now have $\tau 1$ and $\tau 2$ as the control inputs to the system. To simplify the problem, another constraint is imposed that when $\tau 1$ is active during a particular switching period, $\tau 2$ will be set to zero. Similarly, when $\tau 2$ is active, $\tau 1$ will be set to zero. In this way, the problem is reduced to the control of a single-input single-output system. The virtual crankshaft mechanism can be readily applied in this case where the four digital valves are functioning as a four-way three-position valve. A proportional control was designed first to stabilize the open loop system. When the piston position is larger than the reference (negative error), Mode 8 is activated to decelerate the piston. On the other hand, if piston position is smaller than the reference (positive error), Mode 10 is activated to accelerate the piston. Fig. 3.25 shows the duty cycles of Mode 8 and Mode 10 as a function of the calculated control signal.

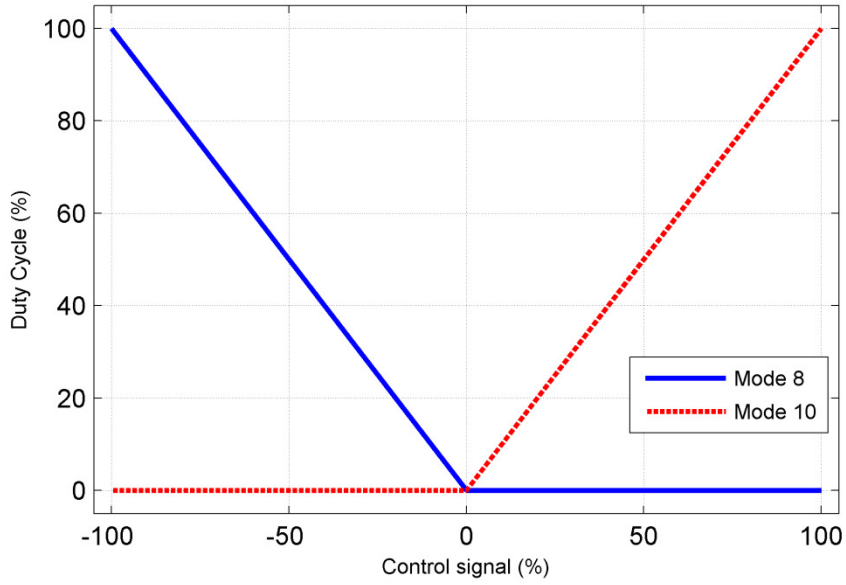

Fig. 3.25 Duty cycles of the two valve modes versus the control signal

A Model of the digital hydraulic system is developed based on the hydraulic FPE system in Chapter 2. The valves investigated in this case have a response time of 2.5 ms. The switch frequency of the valves is 200 Hz. Fig. 3.26 shows the simulated tracking performance of the proportional control with a 25 Hz sinusoid reference. The bottom plot in Fig. 3.26 is the duty cycles of Mode 8 and Mode 10. As shown in Fig. 3.26, the proportional control is not able to regulate the piston to follow the reference trajectory. Therefore, the robust repetitive control is applied. Similar to the virtual crankshaft design, a 'swept sine' system identification is performed on the digital hydraulic FPE model with the proportional control. A linear discrete model is obtained using the Matlab system identification toolbox. Note other method can also be utilized to render the linear model of the digital hydraulic FPE system for control design such as the averaged model [70-71]. A repetitive control is then designed with the linear model at 25 Hz. The tracking performance of the repetitive control with a 25 Hz sinusoid reference is shown in Fig. 3.27. The result demonstrates the effectiveness of the repetitive control. The control signal plot shows that when piston travels from BDC to TDC, the hydraulic force assists the motion at the beginning, and resist the motion at the end, similarly when piston travels from TDC to BDC. This observation is consistent with the findings from previous section, which further emphasizes the importance of the virtual crankshaft mechanism.

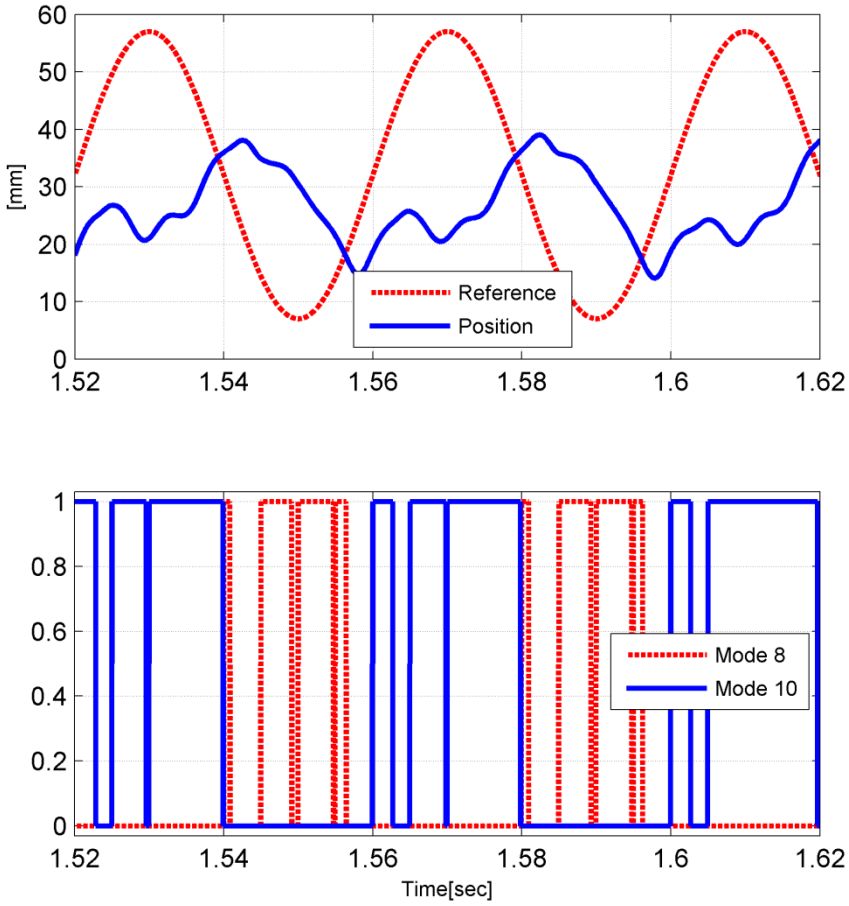

Fig. 3.26 Simulated tracking performance of the proportional control with a 25 Hz signal

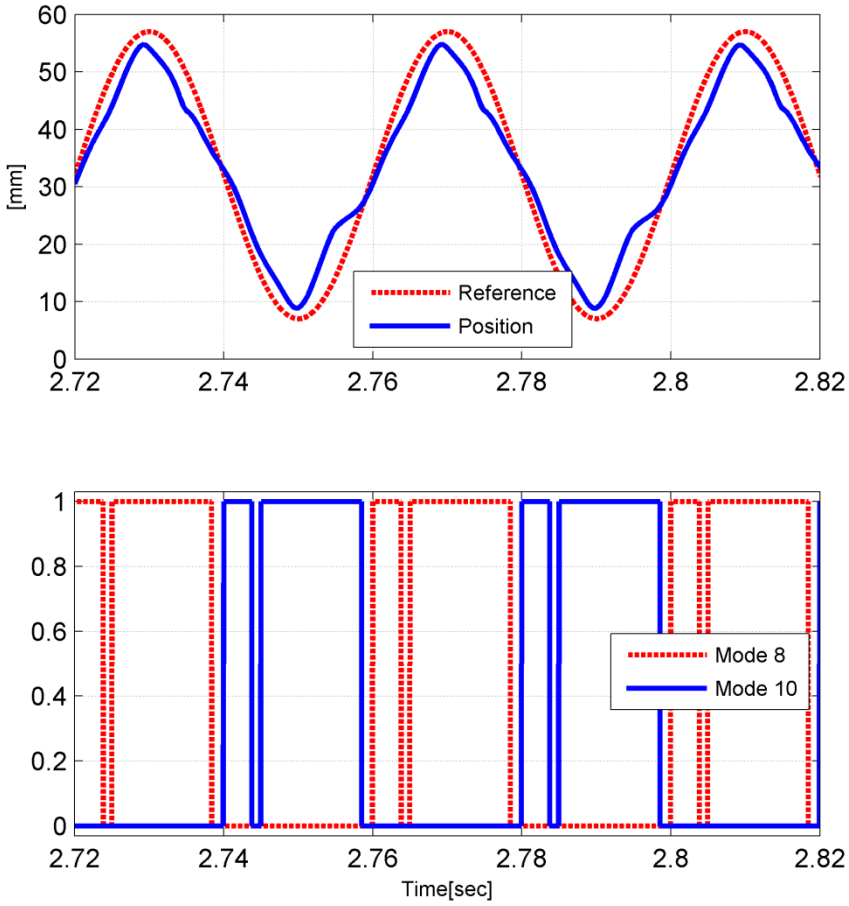

Fig. 3.27 Simulated tracking performance of the repetitive control with a 25 Hz signal

As mentioned previously in this section, for this simulation study, a constraint was added to simplify the digital hydraulic control. However, alternative methods [72-78] can be utilized as well, such as PWM valve pulsing schemes [79] shown in Fig. 3.28. Basically, it sets the duty cycle of Mode 16 to zero during a switch period. This scheme is proven to be more effective at reducing the deadband when required active time is smaller than the response time of the valves. The resulting flow of the new scheme is more linear when compared to the scheme shown in Fig. 3.25 as well. Another approach

is to formulate the problem into a multi-input multi-output control design, where individual valve can be controlled independently.

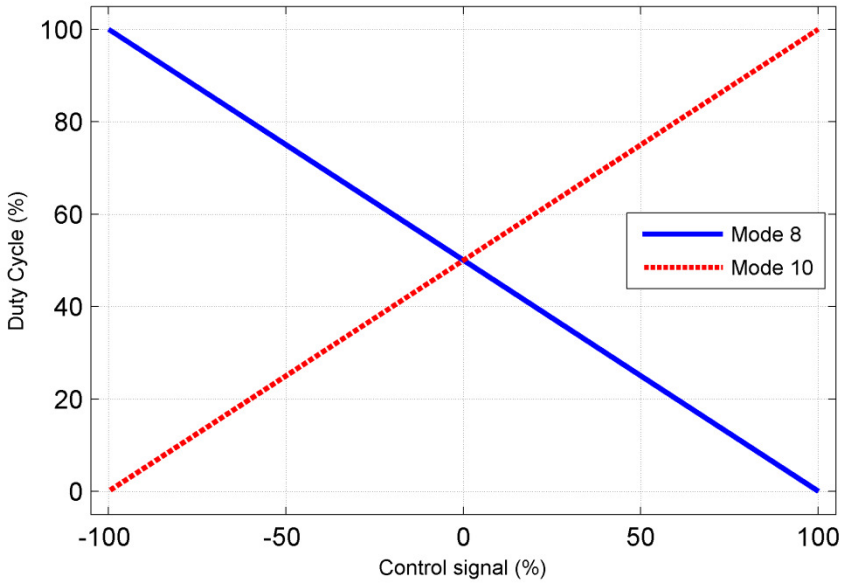

Fig. 3.28 An alternative PWM valve pulsing scheme

3.5 Conclusions

Despite the attractive features of FPE such as variable compression ratio, compact and modular design, less friction loss, etc., there has been a major technical barrier holding the technology back from being fully operational: precise motion control of the pistons in FPE. This arises from the fact that piston motion is not mechanically constrained and the dynamic couplings among the engine subsystems are sophisticated. The modeling and analysis in Chapter 2 reveals the importance of piston motion control for the FPE operation, and motivates the development of an active control. The controller acts as a virtual crankshaft that regulates the piston to follow a predefined reference trajectory using the energy from the storage element.

Optimal trajectory is designed for engine motoring and experimental results show that precise reference tracking of the system is made possible using the proposed control method. Two feedforward controls are designed to improve the tracking performance of a previously designed robust repetitive control system, which is utilized as the active motion control of a hydraulic FPE. The two feedforward designs have been implemented on the hydraulic free piston engine together with the robust repetitive control.

Steady state and transient performance of adding the proposed feedforward controls are benchmarked with the repetitive-control-only case. When the hydraulic supply pressure is limited to 193 bar, the linear feedforward control demonstrates significantly improved tracking results in the small piston displacement range, but limited improvement in the large displacement range. Whereas the nonlinear feedforward control shows consistent improvement over all displacement ranges. To further explore the influence of the feedforward control, simulation results of the tracking performance with a higher hydraulic supply pressure are presented and discussed in this section as well. The improvement of the tracking performance by adding the linear and nonlinear feedforward controller are again clearly shown, with the nonlinear control being more effective at reducing the peak tracking error around the TDCs and BDCs.

Additionally, the control of a digital hydraulic FPE design is also investigated in this chapter. The simulation results demonstrate the feasibility of piston motion control with fast response hydraulic on-off valves.

Chapter 4

Transient Control and Combustion Analysis

The focus of this chapter is on the combustion testing of the hydraulic FPE with the active motion control proposed in Chapter 3. The stable and repeatable piston motion during the engine motoring stage allows us to calibrate the fuel injection and spark timing with respect to the piston position for engine combustion tests. When switching from engine motoring to engine firing, the large combustion force will deviate the piston from the reference trajectory. Even though the engine operation will not cease as the motion control recovers the piston trajectory within few cycles, a transient period after the combustion cycle, especially when a strong combustion occurs, prevents the continuous engine operation. The transient period exists due to the fact that the coordination between the hydraulic force and piston motion, built up by the active motion control during engine motoring is interfered by the combustion force. Through a careful study of the couplings between the hydraulic force, combustion chamber force and control signals, a transient control algorithm is developed to eliminate the transient period after the combustion cycle[80]. The algorithm consists of two parts: combustion detection and shifting (control signal shifting, reference shifting and tracking error shifting). Essentially, the transient control modifies the control signal to alter the hydraulic force, and restore the coordination with the combustion chamber, so that piston motion will be maintained. The advantage of the transient control lies on the fact that it retains the repetitive learning

mechanism but can adjust intelligently to nonrepetitive disturbances such as motoring to firing transition, misfire and cycle-to-cycle combustion variations.

The transient control is implemented on the hydraulic FPE for combustion tests, and its effectiveness has been demonstrated by various combustion scenarios. With the transient control, continuous firing tests are conducted. However, the continuous firing results show that even with the similar fuel injection, spark timing and piston motion, the combustion outcomes are different. Therefore, a detailed analysis of the combustion with various operating conditions is conducted. The results identify the problem and give insights to the optimization of the engine operation.

4.1 Introduction

The overall control structure of the hydraulic FPE is shown in Fig. 4.1, which consists of fuel injection control, spark timing control and piston motion control. Specifically, the fuel injection timing, quantity and spark timing can be calibrated with respect to the position of the piston, at different operating points, to ensure the optimal engine performance. And the active motion control: the Virtual Crankshaft, regulates the piston to follow the designated piston trajectories. The virtual crankshaft mechanism not only maintains stable piston motion during the FPE operation, but also achieves precise position tracking which opens up the opportunity for specifying the in-cylinder gas pressure-temperature history via altering the piston trajectory.

The unique feature allows for the implementation of advanced combustion strategies such as HCCI and its variants: premixed charge compression ignition (PCCI) [81-82], low temperature combustion (LTC) [83-84], controlled auto-ignition (CAI) [85-86] etc.

The challenge of the technology is the lack of a robust and precise ignition mechanism in the conventional ICE. The primary control mechanisms in the conventional HCCI combustion have been limited to the fuel injection timing [87-88] and the trapping of residual gas to affect the charge temperature [89-90]. Unfortunately, none of these control schemes are able to moderate HCCI over the full range of operation demanded by vehicle applications and simultaneously maintain fuel efficiency and regulated emissions targets. The virtual crankshaft with FPE provides an additional and effective control mean to regulate the autoignition process under different loading conditions.

The effectiveness of the piston motion control was demonstrated by the engine motoring results [26, 53-54]. In order to conduct combustion tests, a direct fuel injection system and a multi-spark capacitor discharge ignition control box are installed. A picture of hydraulic FPE with all the subsystems is shown in Fig. 4.2 The combustion tests results shown in this thesis were conducted at a constant hydraulic load (loading pressure 2800 psi) with Grade 87 gasoline. Additionally, to simplify the engine operation and better evaluate the virtual crankshaft mechanism under the engine firing condition, the right combustion chamber is utilized as a bounce chamber (no combustion on the right chamber only air compression and expansion). The repeatable pistons motion of engine motoring makes the calibration process of the combustion system easy and straightforward.

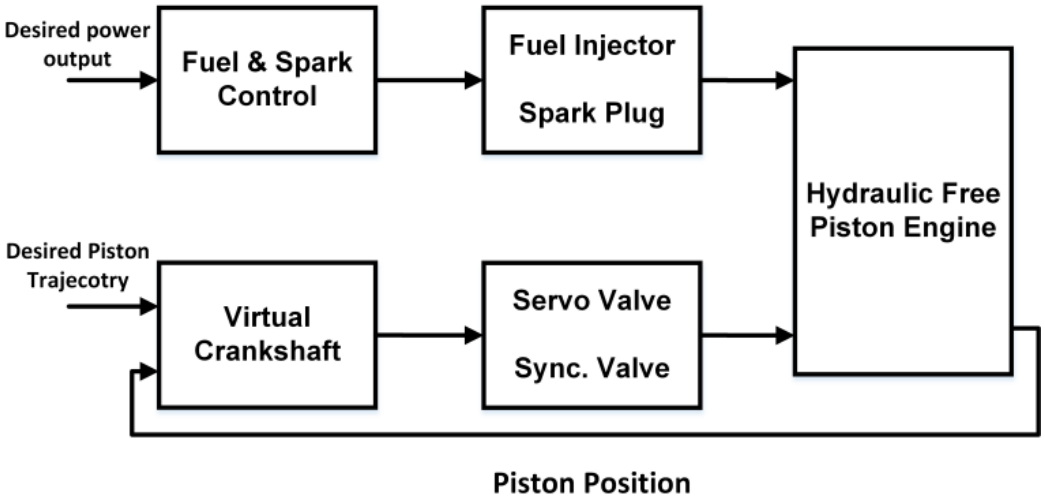

Fig. 4.1. Control structure of the HFPE

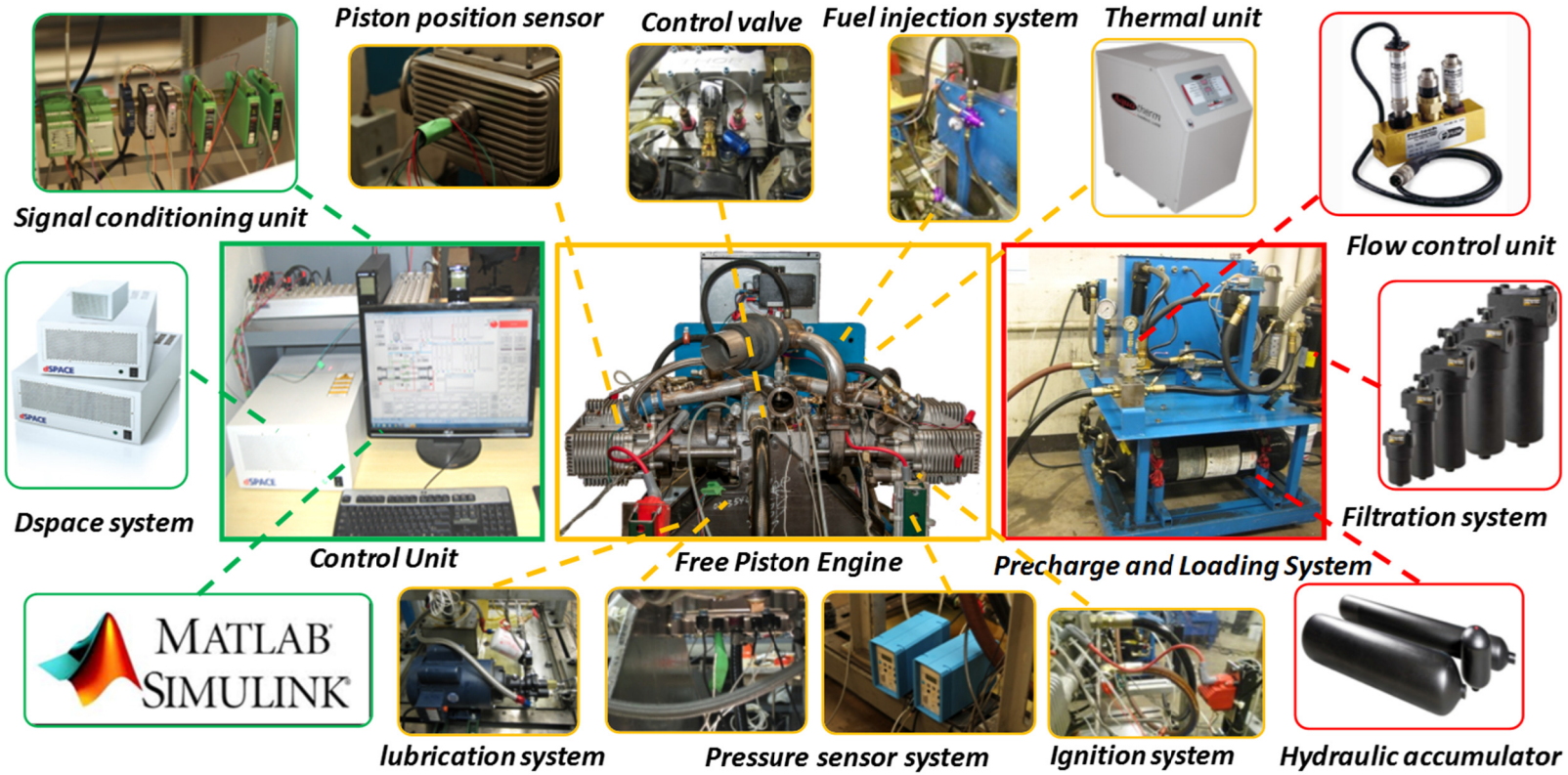

Fig. 4.2. Photograph of the experimental set-up

4.2 Combustion Transient

Fig. 4.3 shows the results of a single-injection combustion in which fuel was injected once to trigger a single combustion. Specifically, the piston motion, net hydraulic force acting on the piston, and control signals are plotted. A negative net force denotes the hydraulic force is pushing piston towards the TDC, and a positive means the opposite. However, a positive control signal sent to the servo valve is to add flow that increases the negative net force, and a negative control signal indicates the opposite.

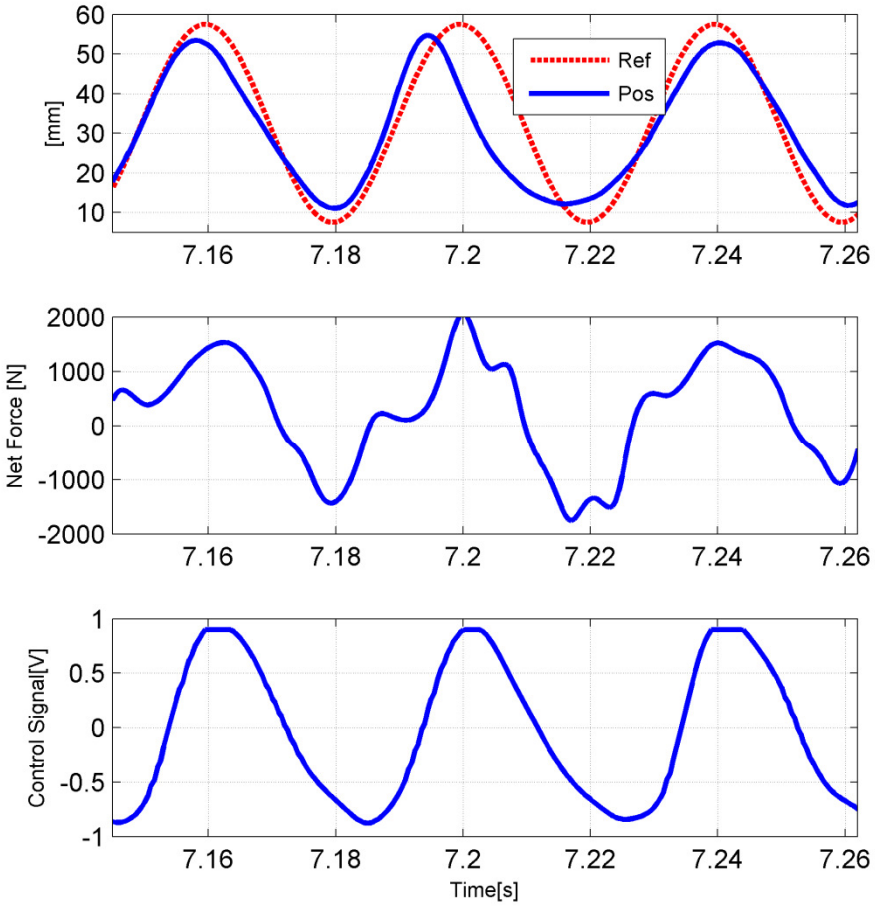

Fig. 4.3 Piston motion, net hydraulic force and control signals of a weak combustion

As we have learned from Chapter 3 and can be observed from Fig. 4.3 as well, when piston travels from TDC to BDC or vice versa, the control signal must adjust the hydraulic force to resist the motion and then assist it, in order to follow the reference trajectory. The combustion occurs at the TDC around 7.18s, and the combustion accelerates the piston motion so that it reaches the BDC at 7.195s instead of 7.20s as in the case of motoring. However, the repetitive control design of the piston motion control determines that the control signal will not change until the next cycle. Therefore, during the compression stroke from 7.195s to 7.215s, the hydraulic force resists the piston longer than assisting it. This slows down the piston at the TDC as shown in the figure. In this case, the 'unsynchronized' portion between the piston motion and control signal is small due to the weak combustion. Next, a strong combustion case is investigated.

Fig. 4.4 shows the piston motion, net hydraulic force and control signals of a strong combustion. The combustion occurs at the TDC around 6.412s, and the strong combustion creates a rapid piston motion that the BDC is reached at 6.422s. Because it is two times faster than the case of motoring, during the compression stroke that follows, the hydraulic force resists the piston motion completely. Therefore, the TDC around 6.44 s is higher than the other motoring cycles. Similarly, due to the large mismatch between the piston motion and control signal, the expansion stroke from 6.44 s starts with hydraulic force resisting the motion instead of assisting. That's why piston motion almost comes to a halt around 6.46s till the control signal finally changes direction and starts pushing piston towards the BDC. However, without inertia force that was built during the early stage of the expansion stroke, the hydraulic force alone cannot overcome large

compression force from the right combustion chamber. That's why the BDC position around 6.48s is lower than the ones in other motoring cycles. The high TDC position at 6.44s indicates a low compression ratio, and the low BDC position around 6.48s means small openings of the scavenging ports as well as a shorter mixing duration. These are undesirable for the combustion. Without proper compression and air fuel mixing, combustion will not even occur, not mentioning the optimization of it.

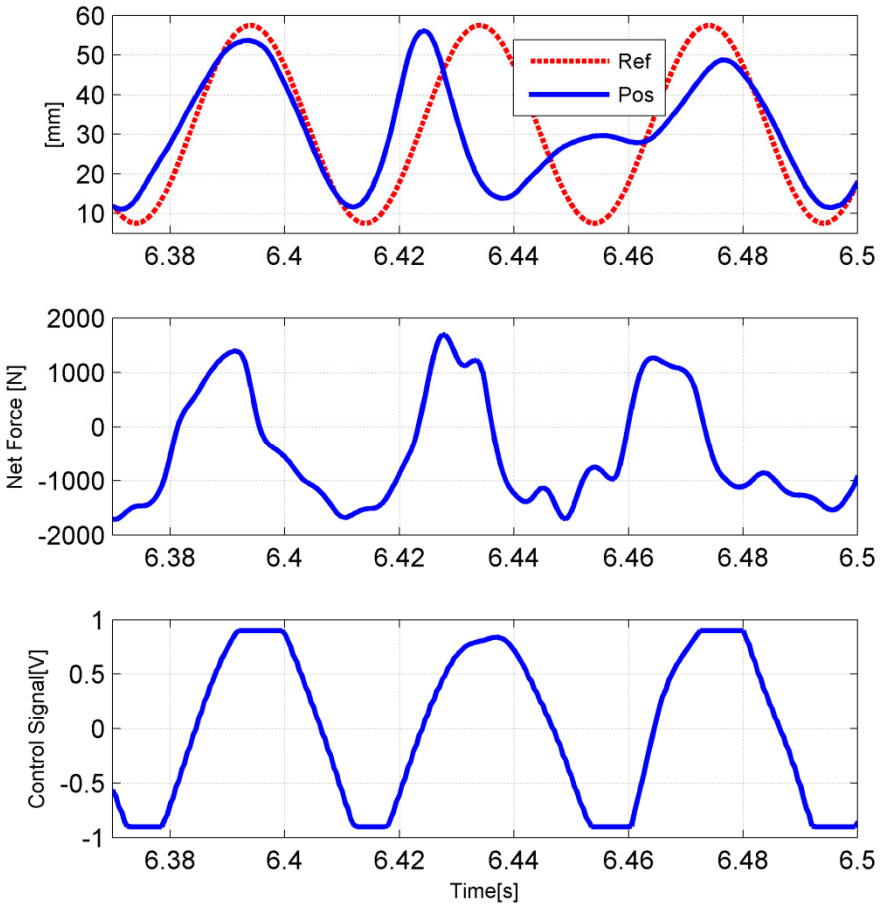

Fig. 4.4 Piston motion, net hydraulic force and control signals of a strong combustion

4.3 Transient Control

Based on the studies in section 4.2, the undesired transient is caused by a mismatch between the motion and the control signals. To better illustrate the phenomenon, a piston motion versus the control signal diagram is shown in Fig. 4.5.

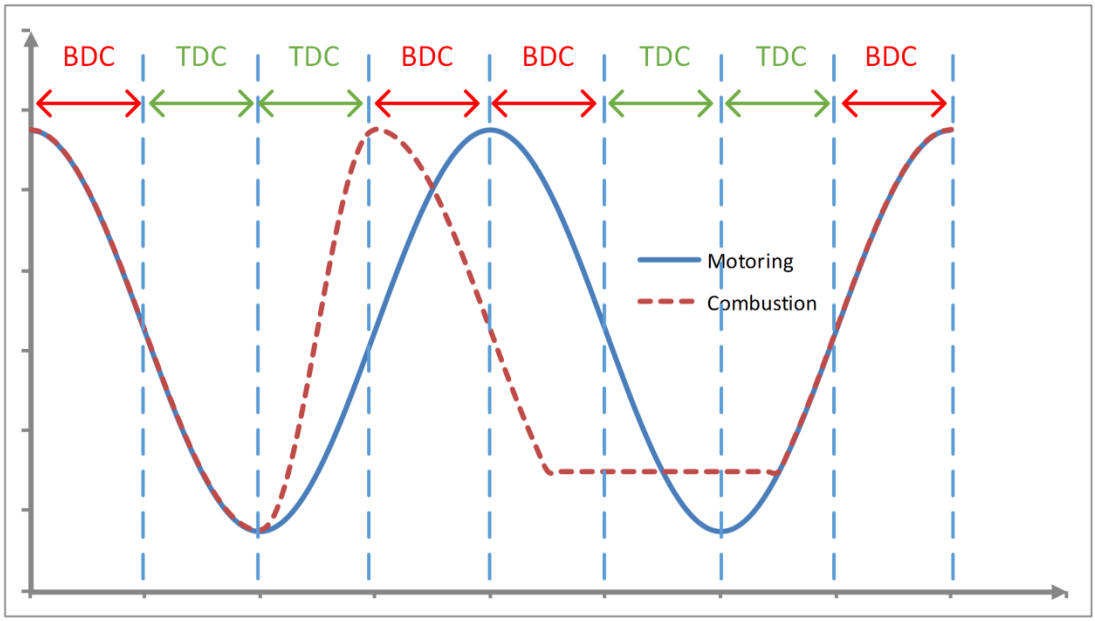

Fig. 4.5 Diagram of piston motion versus the direction of hydraulic force of in engine motoring and single combustion cases

The BDC and TDC intervals represent the intervals when the net hydraulic force is pushing the piston towards the BDC and TDC, respectively. In the motoring case, when the piston is at the BDC, the compression force from the right combustion chamber is pushing the piston towards its TDC, but the hydraulic force is resisting this motion until the middle of the compression stroke, when hydraulic force changes direction and assists the piston to reach the TDC. After the TDC, compression force of the left chamber is now pushing the piston towards the BDC, but the hydraulic force has not changed direction, it is still exerting force on the piston to retain it at the TDC until the middle of the

expansion stroke, when hydraulic force changes direction and assists the piston to reach the BDC. However, in the case of single-injection combustion, after the combustion starts, the piston is being pushed towards the BDC at a higher speed. The duration of the expansion stroke and location of the BDC are determined by the hydraulic load and heat release of the combustion. Since the servo valve control signal remains the same as the repetitive control updates its control output according to the tracking errors and control outputs from the previous cycle, the hydraulic force resists the piston motion during the entire expansion stroke. When the BDC is reached, the first interval of the resisting hydraulic force awaits. Note this interval of the hydraulic force was meant to assist the piston to reach the BDC in the case of a motoring cycle, but the piston is now at the BDC and is moving towards the TDC, therefore, it becomes the resisting force. Up to this point, the coordination between the hydraulic force and combustion chamber force is able to maintain a smooth piston motion. Even though the hydraulic force has been resisting the piston motion since the combustion occurs, it is desirable since the chemical energy from the combustion is converted to fluid power. In fact, extraction of the energy is necessary because it will otherwise be released to compress the gas in the right combustion chamber, which can cause collision of the piston heads (a common issue of the FPE operation with calibration-based control).

Nevertheless, it is what follows the first interval of the resisting hydraulic force that induces the transient period. Half way through the compression stroke, the second interval of hydraulic force acting towards the BDC direction begins. This further reduces the kinetic energy of the piston and it reaches a TDC position that is higher than the other

motoring cycles. Finally, the interval when hydraulic force is acting on the direction of the TDC arrives. But the hydraulic force is not able to push the piston further due to the fact that without inertia force, the hydraulic force alone cannot overcome the compression force from the left combustion chamber. This can be reflected on a simple calculation: the hydraulic supply pressure is 2800 psi, the synchronization chamber pressure can be assumed to be constant at 1400 psi, and the area of the hydraulic plunger is 141 mm^2. Therefore, the maximum net hydraulic force is calculated to be 1360 N. The piston has a diameter of 79.5 mm, so the maximum combustion chamber pressure the hydraulic force can overcome without the presence of inertia force is 2.7 bar, which corresponds to a compression ratio of 2:1. As a result, the piston is held at a high TDC location until the control signal switches the direction of the hydraulic force. Since the particular TDC location is higher than the other cycles, the stroke length available for building up the piston inertia is shortened during the expansion stroke, hydraulic force cannot overcome the compression force from the right combustion chamber, and therefore the BDC location is lower than the expected value. The high TDC and low BDC location result from the transient can significantly impact the combustion process of the next few cycles.

The analysis of Fig. 4.5 reveals the root cause of the engine transient when switch from motoring to firing, nevertheless, it also implies that piston motion can be maintained as long as the changing of directions of the inertia force and the hydraulic force are in the correct order. Specifically in Fig. 4.5, if the duration of the resisting hydraulic force can be reduced, the undesired TDC and BDC location can be eliminated. Therefore, a

transient control algorithm is developed for this task.

4.3.1 Combustion detection

In order to adjust the control signal accordingly, the algorithm must first know when and where the combustion starts. Therefore, accurate combustion detection is the key to the proposed transient control algorithm, and a combustion detection program is first developed within the control algorithm. Similar to the common practice of combustion analysis in the conventional ICE [91-95], the program detects combustion based on the instantaneous heat release rate which is calculated in real time via combustion chamber pressure and piston position:

$$\dot{Q} = \frac{\gamma}{\gamma - 1} \cdot P \cdot A_p \cdot \dot{x} + \frac{1}{\gamma - 1} \cdot A_p \cdot x \cdot \dot{P} + A_{wall} \cdot h \cdot (T - T_w) \tag{4.1}$$

where P is the combustion chamber pressure, x is the piston position, γ is the heat capacity ratio, A_{wall} is the surface area of the combustion chamber, h is the heat transfer coefficient, T is the gas temperature that can be derived based on the ideal gas law, and T_w is the mean engine wall temperature. Note the equation is derived based on first law of thermodynamics of a closed system. Therefore, it is only applicable when the piston head has sealed the exhaust and intake ports. Due to signal noises from the pressure sensors, high heat release rate may be calculated when a signal spike occurs instead of real combustion. Digital filters were designed and applied to smooth out the pressure signal, although a small delay was introduced as shown in Fig. 4.6.

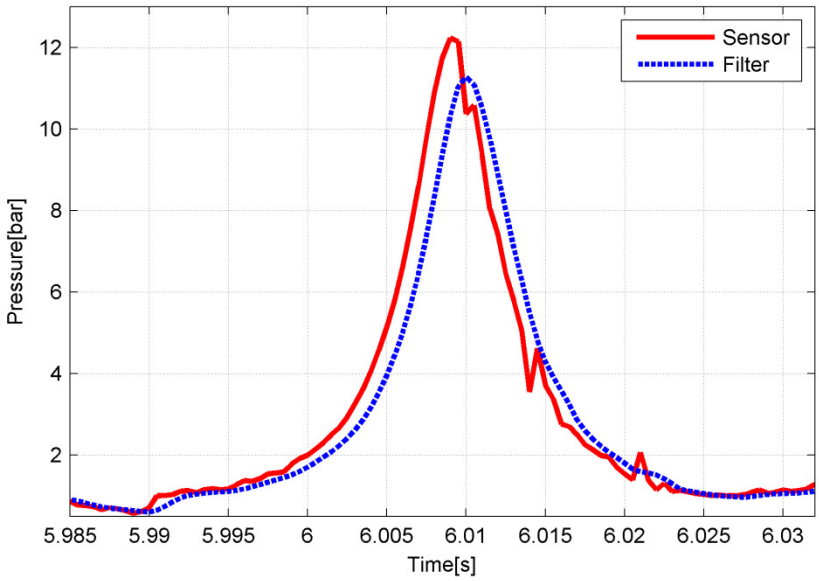

Fig. 4.6. Pressure sensor signal and filtered pressure signal

The calculated rate of heat release during the motoring and firing cases is shown in Fig. 4.7. The difference of the heat release rate between a motoring cycle and a combustion cycle is clearly shown. Therefore, the start of combustion is defined at the instance when the calculated heat release rate reaches a defined threshold. Another task of the combustion detection program is to determine the shifting duration for the next stage of the algorithm. The required shifting duration is linked to the start of combustion timing as well as the combustion strength. However, how to evaluate the combustion strength in real time so that the program can make actions in a timely fashion is a challenge. The research in this part of the thesis focuses on the study of relationship between combustion timing and the required shifting duration.

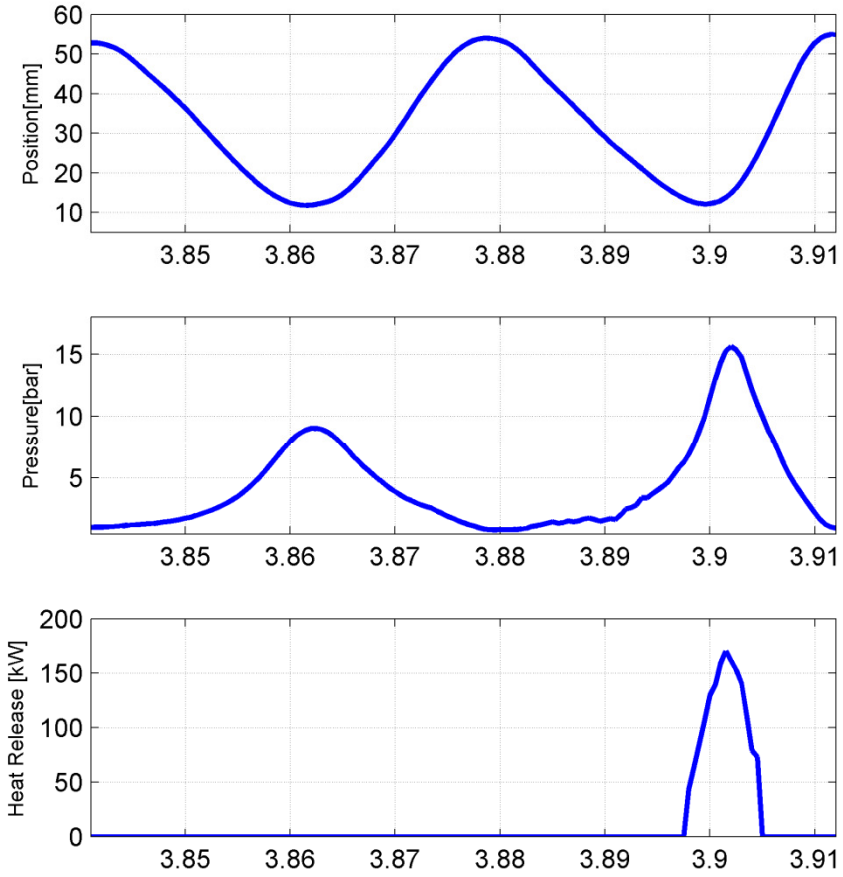

Fig. 4.7 Piston position, combustion chamber pressure and calculated rate of heat release from engine motoring to firing.

The timing of the start of combustion and the reference trajectory are used to determine the combustion timing and required shifting duration. Specifically, when a start of combustion is detected, the program first measures the sample steps between the particular instant and the time at which the TDC of the reference has arrived or will be arriving (depending on whether combustion starts before or after the TDC). Then, the required shifting duration is determined based on the measured sample steps. During a motoring cycle, the TDC timing of the piston position always aligns with the TDC timing

of the reference trajectory. For a combustion cycle, there are three possible scenarios for the start of combustion: before TDC of the reference, at TDC of the reference and after TDC of the reference. When combustion starts before the TDC of the reference, the combustion force prevents the piston from moving towards the TDC direction. Therefore, the deviation of the piston motion from the reference will be the largest in this case. When combustion starts at TDC of the reference, the combustion force will be the largest and the piston motion resembles the case shown in Fig. 4.4. About 1/4 of the control signal in a cycle should be shifted. When combustion starts after TDC, the deviation of the piston motion from the reference will be the smallest, so the required shifting duration should be the minimized as well. Based on this general rule, three different gains are assigned to the measured sample steps to render the required shifting duration. The same technique can be applied to combustion detection at BDC, so that the controller is capable of reducing the transient of combustion from both chambers.

4.3.2 Shifting

Based on the analysis at the beginning of the section, the elimination of the transient period lies on the fact that we can modify the future control input so that the mismatch between the piston motion and hydraulic force can be corrected. In order to do that, the structure of the repetitive control is first presented.

$$C(q^{-1}) = \frac{R(q^{-1})Q(q^{-1})q^{-N}}{1 - Q(q^{-1})q^{-N}} \tag{4.2}$$

Rearrange (4.2), we arrive at the formula for calculating the control signal *u(k)*:

$$u(k) = Q(q^{-1})[u(k-N) + R(q^{-1}) \cdot e(k-N)] \tag{4.3}$$

Equation (4.3) suggests that the current control signal *u(k)* is depended on the control signal and tracking error from the last cycle *u(k-N)* and *e(k-N)*, respectively. Because the control input and tracking error history are known, future control signals can also be calculated:

$$u(k+N) = Q(q^{-1})[u(k) + R(q^{-1}) \cdot e(k)] \tag{4.4}$$

Essentially, at each time step k, control signals of the following cycle are readily known. This makes the modification of the future control signals possible. To illustrate the idea of control signal shifting, a piston motion versus the hydraulic force diagram is shown in Fig. 4.8. At the start of combustion (here the combustion is assumed to start at TDC), the hydraulic force of the next cycle is shown on the top, which has been divided into four parts. In order to eliminate the transient period, future control signal corresponds to part 2 of the hydraulic force is removed, and signals that corresponds to part 3 and part 4 of the hydraulic force are now shifted to the left. However, control signal of part 4 of the hydraulic force is now empty, further information of the control signal is needed to fill part 4 which cannot be obtained at the current time step. Thanks to the repetitive nature of the engine operation, the control signal after part 4 should be very similar to part 1, therefore, control signal of part 1 is copied to fill the vacancy of part 4. The modified hydraulic force of the future cycle is shown underneath the original ones.

Another point worth mentioning here is that the control signal cannot be reflected on the hydraulic force immediately due to the response time of the servo valve and dynamics of the hydraulic system. For example, in order to change the direction of the hydraulic force to push the piston towards the BDC as shown in part 2, the corresponding control

signal must be sent to the servo valve during part 1. This is shown clearly in Fig. 4.4 where positive control signal corresponds the net hydraulic force in the direction of TDC (negative) , and negative control signal indicates net hydraulic force in the direction of BDC(positive). It takes about 8 ms for the control signal to be reflected on the net hydraulic force, which is 1/5 of the total period of a cycle. In other words, in order to remove part 2 of the hydraulic force, control signal sent to the servo valve during part 1 should be removed.

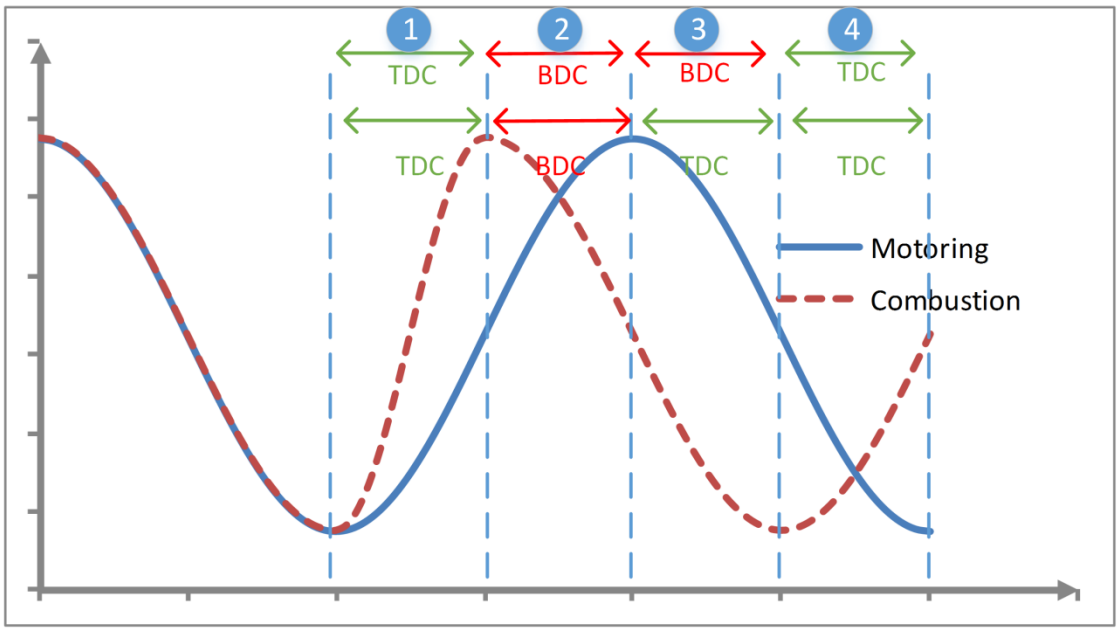

Fig. 4.8 Hydraulic force shifting diagram

Assume combustion is detected at time instant k, and the required shifting duration is j sample steps. Within the u(k) to u(k+N) future control signal array, u(k) to u(k+j) are first removed, and u(k+j+1) to u(k+N) are shifted to the left as shown in Fig. 4.9. The advantage of this control shifting algorithm is that not only does it correct the order of the future control signal with respect to the piston motion, but it also keeps the integrity of

the control information (the portion from u(k) to u(k+j) are not just removed, they are reattached to the back of the control array).

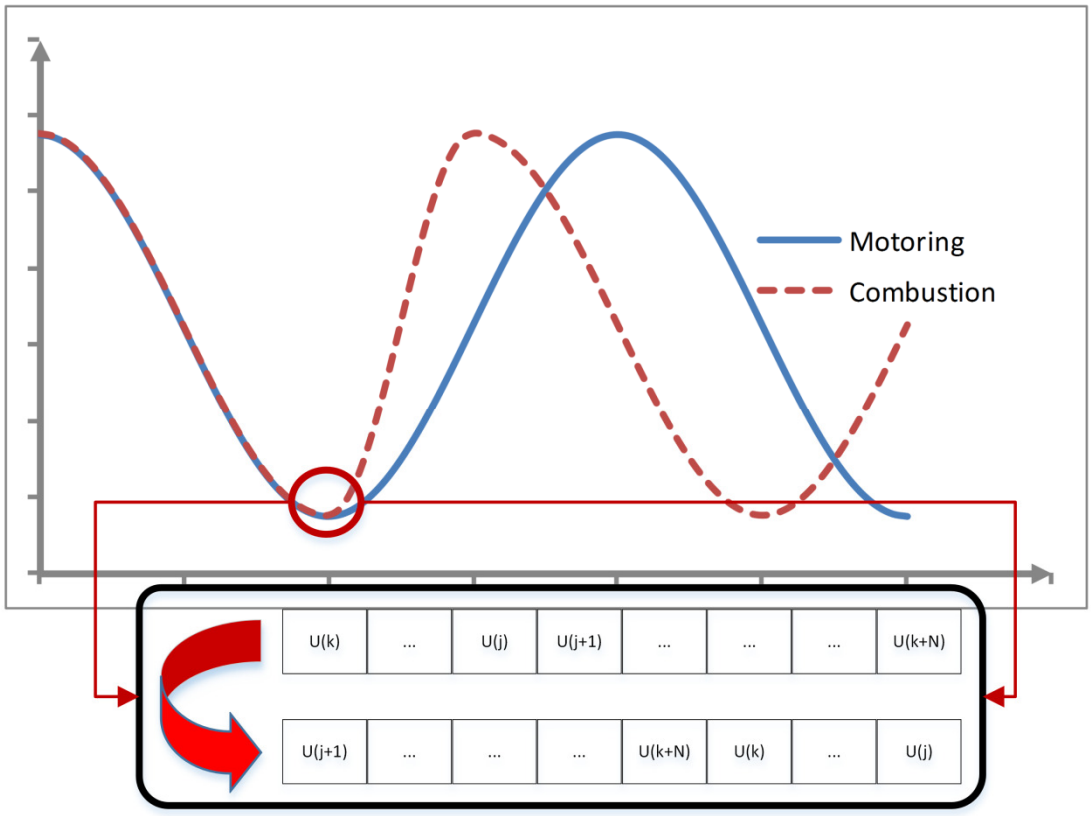

Fig. 4.9 Control signal shifting diagram

In order to ensure the consistency of the control calculation, two things need to be done after the future control signal array shifting: previous control signal and tracking error shifting. From equation (4.4), we know that the control signal from k+N is depended on the current and previous control signals, as well as the current and previous tracking errors. Therefore, in order to have a smooth control signal calculation after k+N, The past control signal array and tracking error array need to be shifted forward accordingly. For the past control signal array, the shifted future control signal u(k) to u(k+j) can be used to fill the vacancy. However, the information of future tracking errors is unavailable, so it

has to use the tracking errors from the previous cycle to fill up the vacancy caused by the shifting. The last step of the transient control algorithm is reference shifting, which is straightforward since future information of the reference trajectories is readily known at any time instant.

The configuration of the transient control algorithm with the hydraulic FPE system is shown in Fig. 4.10. The piston motion control starts the engine with motoring, after fuel is injected, it automatically detects combustion and adjust the control signal and reference accordingly to the combustion so that smooth piston motion can be ensured during the engine operation. A flow chart of the control algorithm is shown in Fig. 4.11.

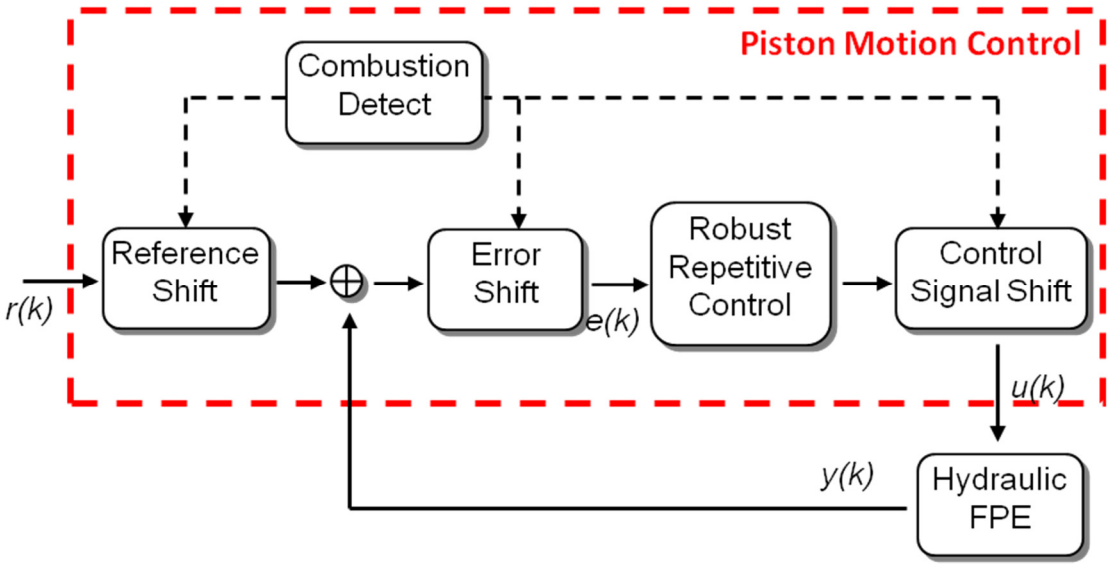

Fig. 4.10. Configuration of the hydraulic FPE motion control system.

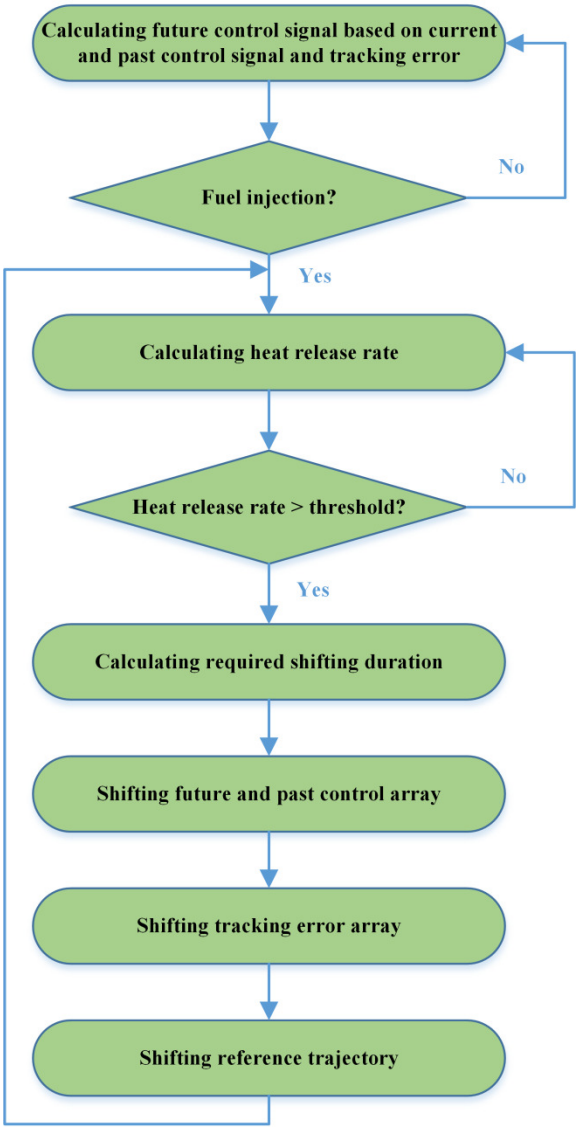

Fig. 4.11. Flow chart of the transient control algorithm

4.3.3 Experimental *results*

The transient control algorithm is first tested in a single-injection combustion test. Fig. 4.12 shows the piston motion, net hydraulic force and control signal of the particular test. The combustion occurs slightly before the TDC at 4.33s, and the transient control algorithm detects the combustion and shifts the control signal, tracking error and reference by 0.01 ms (20 sample steps). During the expansion stroke (from 4.335s to

4.345s), the direction of the net hydraulic force is towards TDC. During the following compression stroke (from 4.345s to 4.365s), the direction of the net hydraulic force changes from BDC to TDC. Finally, during the last expansion stroke (4.365s to 4.385s) in the figure, the net hydraulic force changes from TDC to BDC. The hydraulic force demonstrates the same pattern as discussed in Fig. 4.8, and smooth piston motion is observed. This is due to the factor that the transient control reduces the portion of the negative control signals at 4.33 when combustion was detected. The reduced control signal results in a reduced positive net hydraulic force period, which matches the resist-assist pattern between the hydraulic force and the deviated piston motion after combustion. Therefore, the effectiveness of the transient control algorithm is validated. Multiple-injection combustion can henceforth be tested. Fig. 4.13 shows the engine operation with four fuel injection events.

The transient control is able to detect and shift the control signal accordingly for all the combustion, so that piston motion is kept smooth during the test. However, from the rate of heat release plot, we can see the combustion is not very consistent. The first and third combustion are weak, the second combustion is fairly strong. Additionally, on the fourth fuel injection, no combustion occurs (misfire). Even though the piston motion resembles each other among these injection cycles, the combustion outcomes are different. The combustion process in a two stroke engine is complicated due to the scavenging process when air intake and gas exhaust are happening at the same time. The direct injection feature of the engine introduces more complexity into the system, which make it more difficult to identify the root causes.

Fig. 4.14 shows a zoomed-in portion of the continuous engine operation with the transient control. Fuel was injected every cycle, however, a pattern was observed: a strong combustion followed by a weak combustion. The combustion results will be explained with more details in the next section. Despite the combustion variation, the transient control is able to adjust the control signal accordingly to ensure a smooth piston motion, and this further proves the effectiveness of the proposed transient control design.

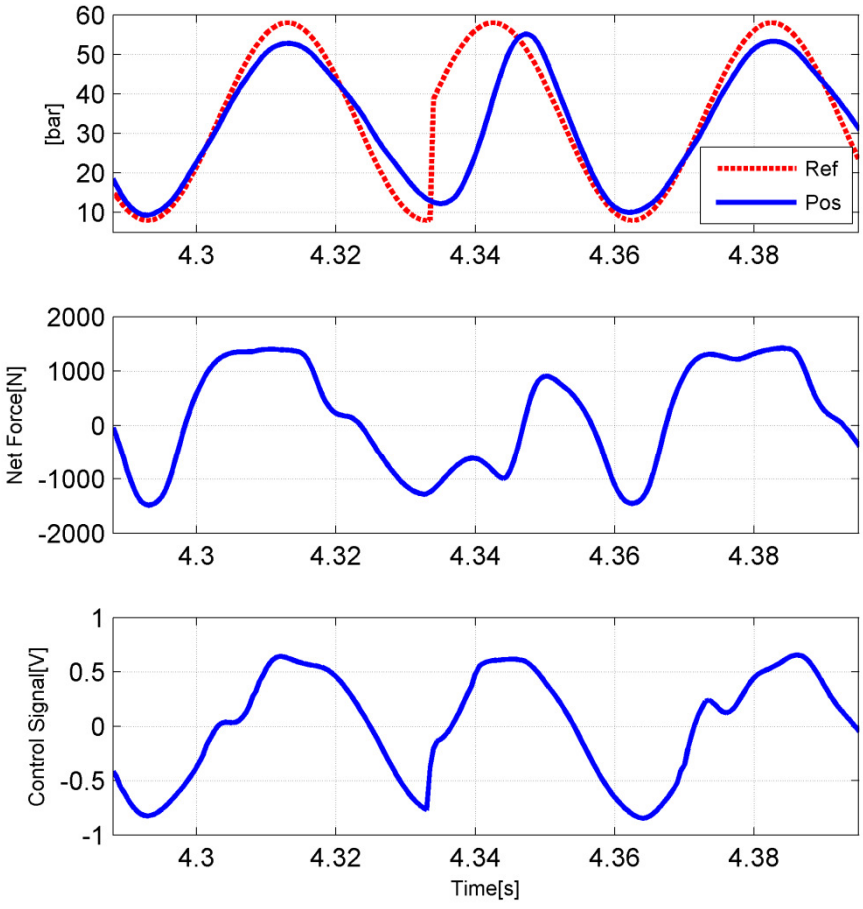

Fig. 4.12 Piston motion, net hydraulic force and control signals of a single-injection combustion with transient control

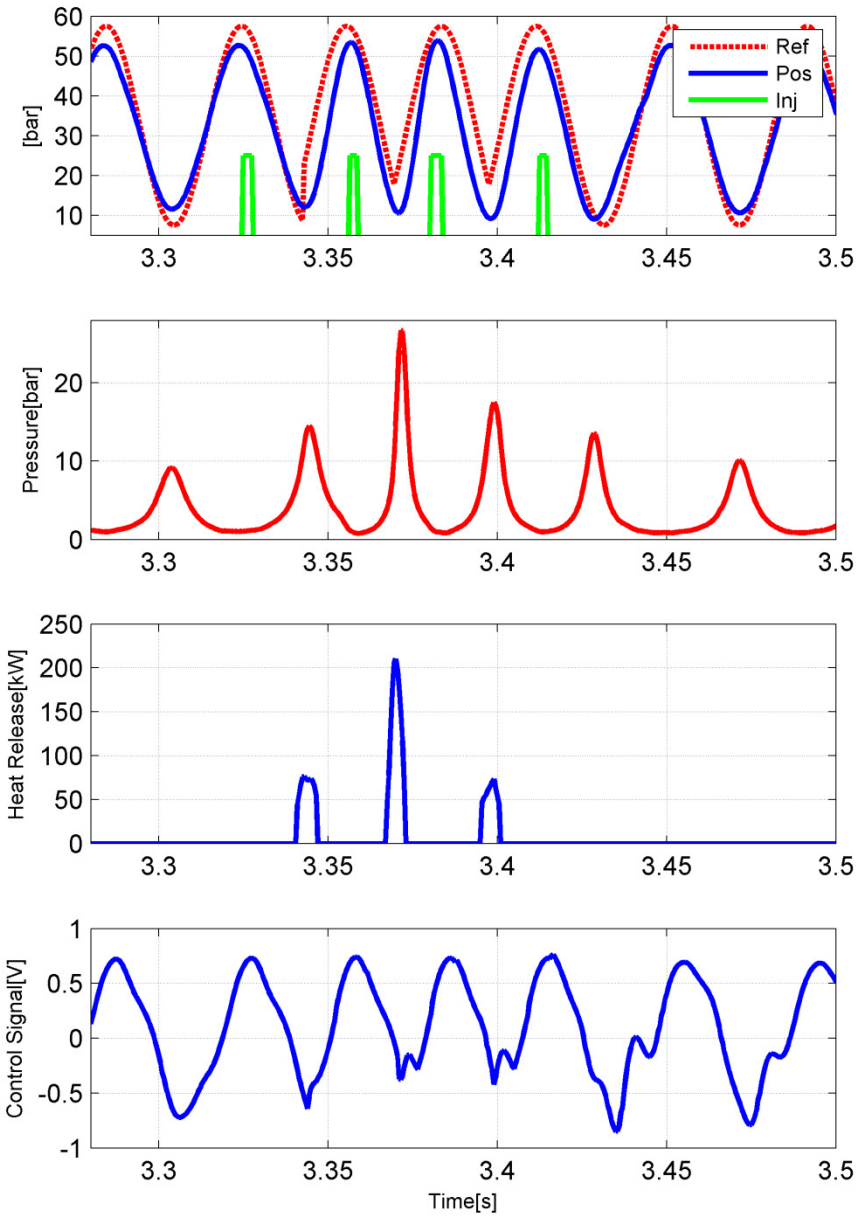

Fig. 4.13. Piston motion, pressure, heat release and control signals of a multiple-injection combustion with transient control.

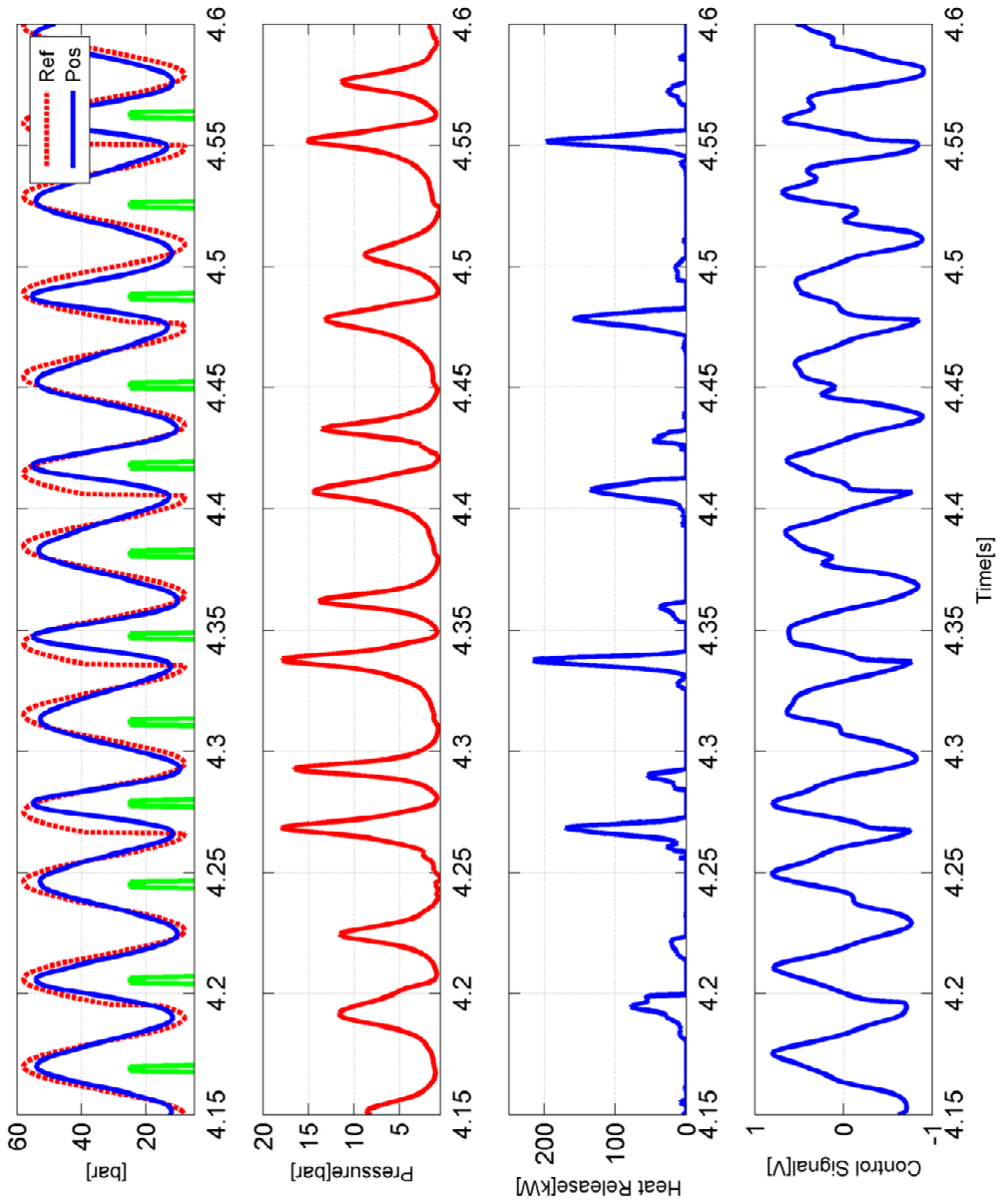

Fig. 4.14. Piston trajectory with the transient control in the case of continuous engine opeation

4.3.4 Discussions

As mentioned previously, besides the combustion timing, combustion strength can also be measured and used in the control signal updating. The motivation of utilizing combustion strength is to compensate for the non-repetitive behavior of the combustion. For instance, combustion has occurred in the previous cycle, since the current control input will be calculated based on the previous control signal and tracking error, if the same combustion occurs at the current cycle, tracking error of the current cycle will be reduced. However, combustion varies from cycle to cycle, and misfire may occur from time to time, which implies that we should not directly apply the control signal from previous cycle to the current cycle, instead, a strength compensation term can be added to modify the previous control signal. The compensation term compares the combustion strength of the current cycle to the previous cycle, and modifies the control signal accordingly. Combing the combustion timing and strength into the transient control allows for better tracking of the reference trajectory. Many variables can be used to represent the combustion strength, integration of the instantaneous heat release rate can be a good candidate.

4.4 Combustion Analysis

The combustion process in the engine is heavily related to the fuel injection and the scavenging process. The design of the combustion chamber, piston head and scavenging ports are important factors that determine the characteristic of the combustion. However, the operating conditions will have great impact on the combustion as well. In this section,

combustion under various operating conditions is analyzed. Specifically, Section 4.4.1 investigates the influence of fuel injection pressure on combustion, Section 4.4.2 analyzes the effect of fuel injection timing on combustion, Section 4.4.3 is on the influence of centerline position, and the combustion results from the continuous engine operation are analyzed in detail.

4.4.1 Fuel injection pressure

The hydraulic FPE is designed for direct fuel injection. The fuel used in the combustion test is 87 gasoline. Initially, a low pressure fuel pump that can provide up to 120 psi pressure, was utilized for fuel injection. Due to the location of the fuel injector, fuel injection must occur during the scavenging process when piston heads uncover the intake and exhaust port. The operating frequency of the engine is 25 Hz (0.04 s per cycle), and the injection window available is about 10 ms. However, based on experimental results, the range of the fuel injection duration that will allow combustion to occur is from 8 to 12 ms (which corresponds to 54 mg and 64 mg fuel mass injected). That means fuel injection timing cannot really be adjusted with the low pressure fuel injection system. Fig. 4.15 shows the pressure and calculated heat release rate after a 10 ms fuel injection, with respect to the piston displacement. Note here zero denotes the TDC position. A small amount of heat release is detected before the piston reaches TDC, majority of the fuel is burnt after TDC until the middle of the expansion stroke which indicates slow flame propagation. This can be attributed to the insufficient mixing of the air and fuel. When fuel injection pressure is low, poor atomization allows the fuel attaching to the engine wall, and few mixing with the fresh charge. Even though the spark is able to

create a flame at its rich local mixture, it propagates slowly due to the poor mixing condition, and the pressure drop during the expansion stroke further slows down the propagation. In order for the combustion to occur, large quantity of fuel needs to be injected to maintain a rich fuel-air mixture. The indicated thermal efficiency in this case is 15%.

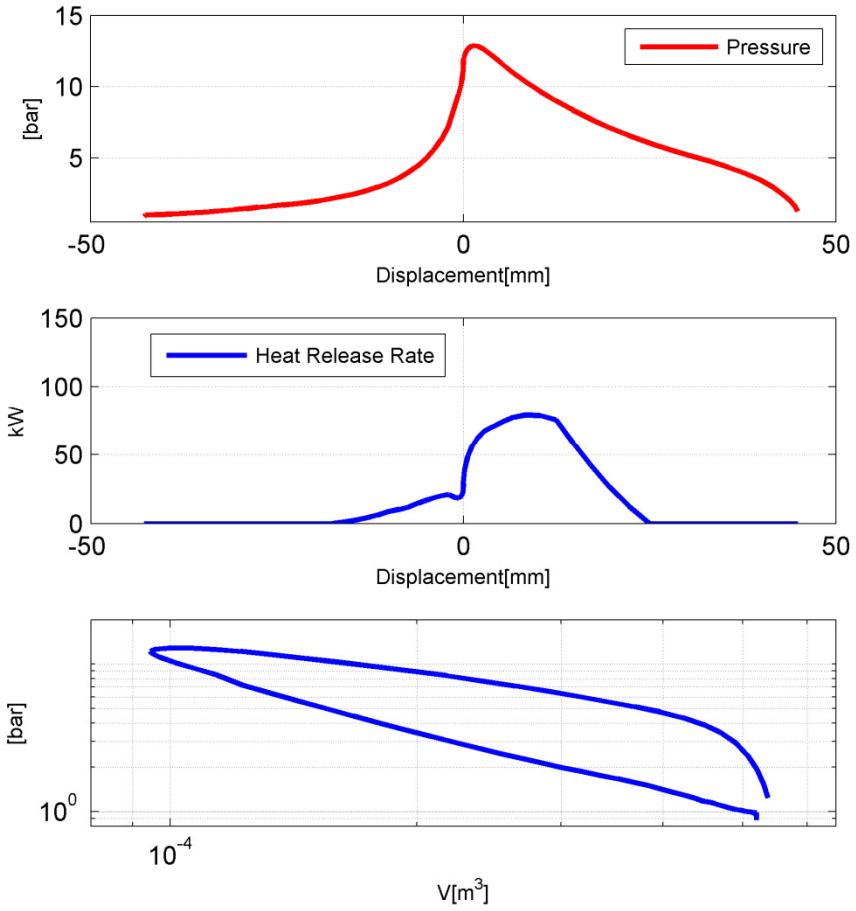

Fig. 4.15 Combustion data at 120 psi fuel injection pressure (from top to bottom: combustion chamber pressure versus displacement, heat release rate versus displacement, and pressure versus volume)

A high pressure gasoline direction injection (GDI) system is then installed to provide higher injection pressure (Fig. 4.16). The GDI fuel pump is mounted on a customized camshaft box where a 3-pole cam drives the pump plunger up and down to generate high pressure fuel. Torque is provided by an electric motor couples with the shaft of the cam box. The outlet pressure of the pump can be adjusted via a solenoid control valve. Higher injection pressure not only provides better atomization, but will also shorten the fuel injection duration which allows for injection timing adjustment. Based on experimental results, at 500 psi fuel injection pressure, range of the fuel injection duration that allows combustion to occur is from 4 ms (33 mg) to 6 ms (50 mg). The fuel quantity required has been reduced due to the fact that high pressure improves the atomization, so that less fuel remains on the engine wall after injection. Fig. 4.17 shows the combustion data of a 5 ms fuel injection at 500 psi. Compared to the low pressure case, it has a shorter but more intense heat release. This indicates a more complete combustion, and the indicated thermal efficiency in this case is 28 %.

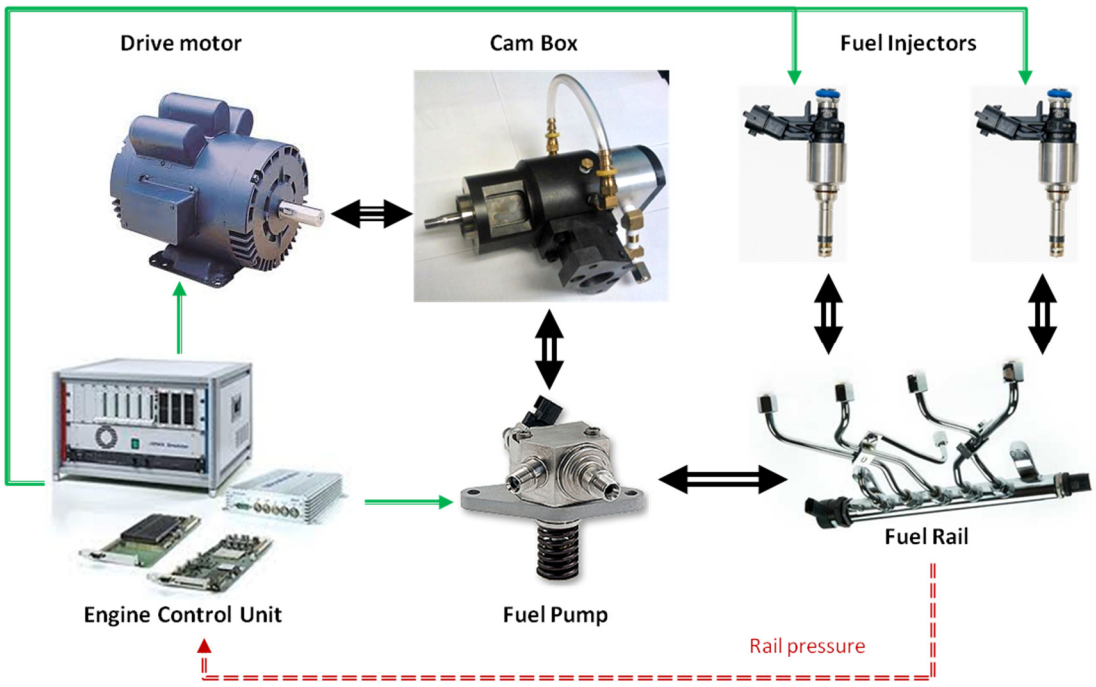

Fig. 4.16 Configuration of high pressure fuel injection system

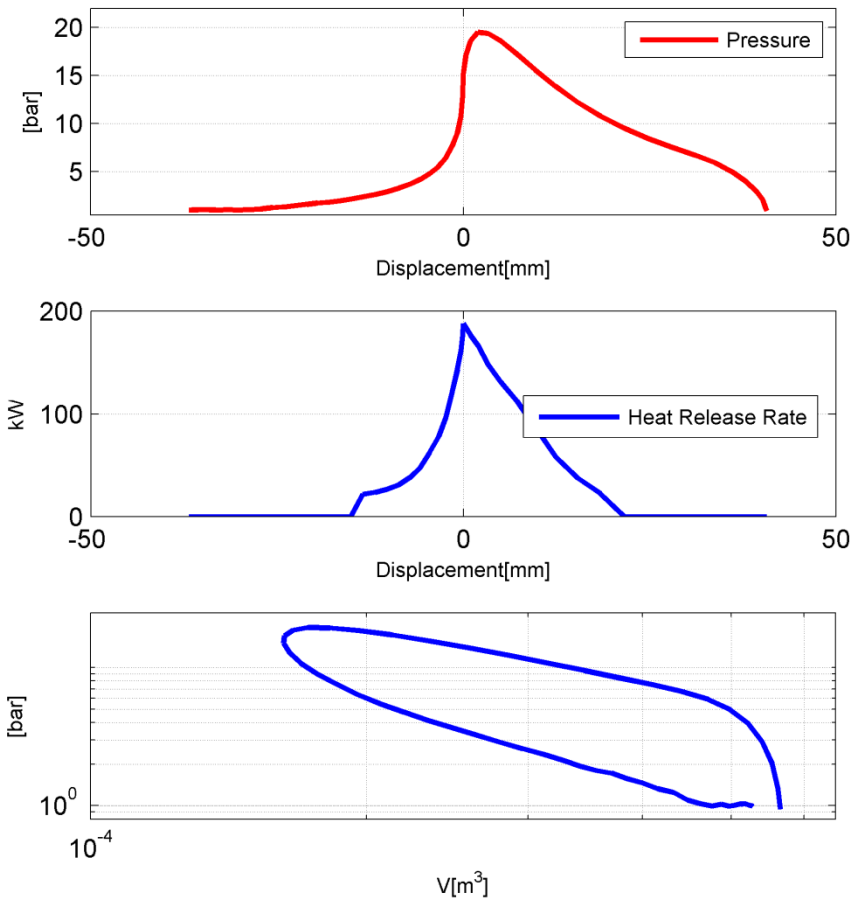

Fig. 4.17 Combustion data at 500 psi fuel injection pressure (from top to bottom: combustion chamber pressure versus displacement, heat release rate versus displacement, and pressure versus volume)

4.4.2 Fuel injection timing

The installation of the high pressure GDI system allows for fuel injection timing adjustment. The scavenging process of the FPE includes the blow down of exhaust and intake of the fresh charge. Therefore, fuel injection timing is an important factor as it is directly related to the mixing of the in-cylinder gas. The intake port of the engine is located at 50 mm from the centerline of the combustion chamber. In this section, the

effects of three fuel injection timings are investigated: - 46 mm (before BDC), 54 mm (around BDC), and 52 mm (after BDC). Fig. 4.18 shows the fuel injection signals with respect to the piston trajectory. With the same injection duration (5ms), the -46 mm injection denotes an injection event at the early stage of the scavenging process when momentum of the flow just starts to build. However, the early injection also means more fuel will be scavenged out through the exhaust port. The 54 mm injection starts slightly before the BDC, when the intake and exhaust port openings are at the maximum, and the uniflow scavenging pattern produces turbulent flow that promotes the air fuel mixing. Nevertheless, compared to the -46 mm injection, the 54 mm injection allows less time for the fuel to escape from the exhaust port. The 52 mm injection, on the other hand, represents injection events that occur at the late stage of the scavenging process, when the intake and exhaust ports are about to close. Mixing of the fuel and fresh air is mainly due to the piston motion during the compression stroke that follows.

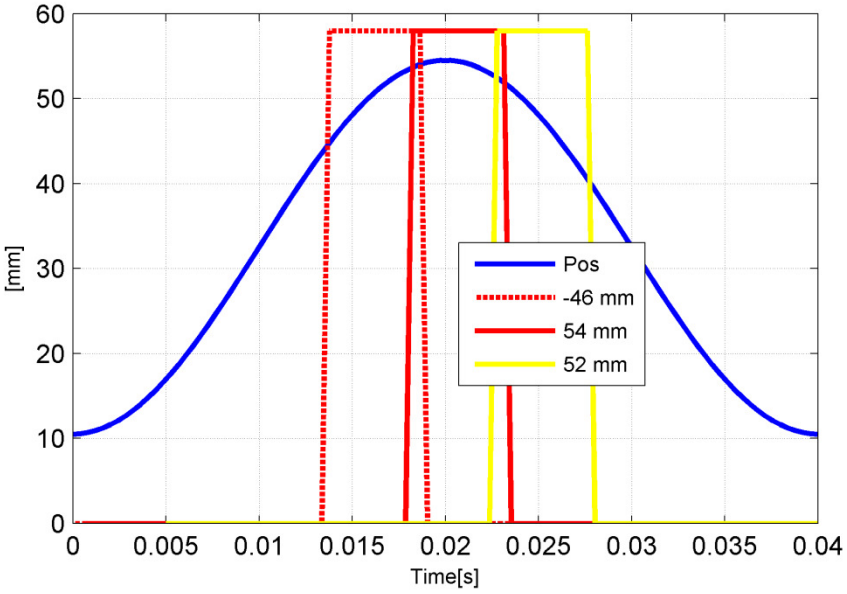

Fig. 4.18 Fuel injection timing signal with respect to piston motion

Fig. 4.19 shows the combustion data of fuel injection timing at -46 mm. The rapid rate of heat release indicates a well mixed in-cylinder gas. However, the low peak value also indicates a lean mixture, which is due to fuel scavenging through the exhaust port. Fig. 4.20 shows the combustion data of fuel injection timing at 54 mm. Based on the rate of heat release plot, large amount of energy was released in a short period, which indicates a well mixed in-cylinder gas with less fuel being lost to the exhaust port. To the contrary, the 52 mm injection produces highest rate of misfire cycles. When majority of the fuel was injected after intake and exhaust ports being closed, the injected fuel is not mixed properly with the fresh air, therefore, the air-fuel mixture around the spark plug was not rich enough to start a flame.

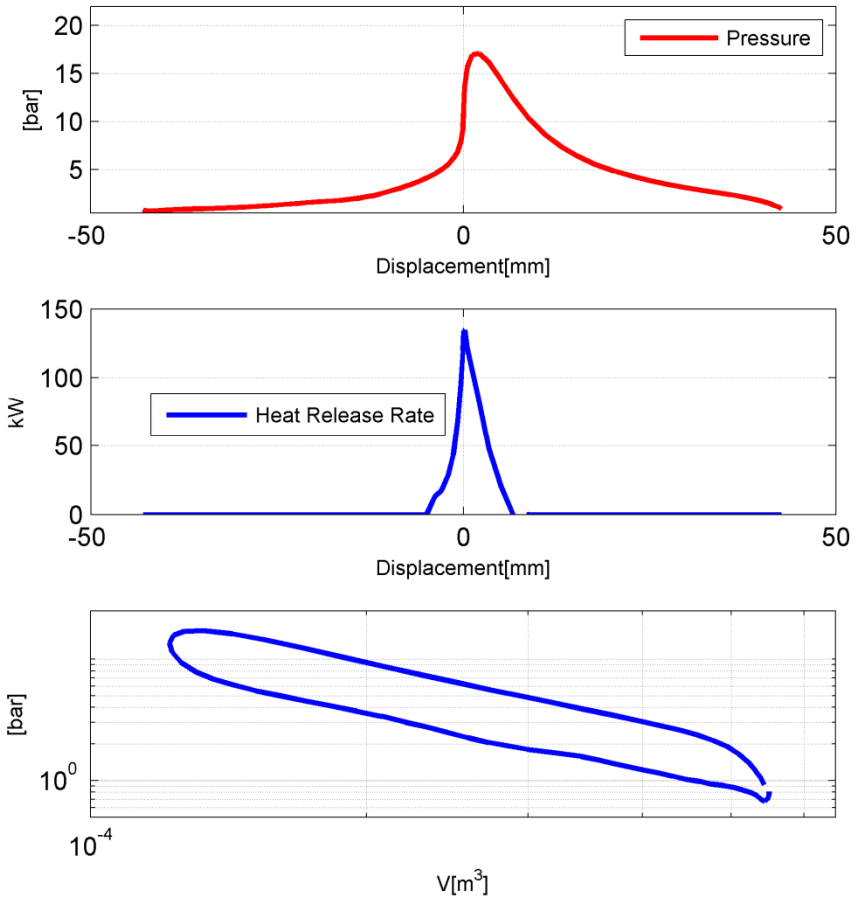

Fig. 4.19 Combustion data at -46 mm fuel injection timing (from top to bottom: combustion chamber pressure versus displacement, heat release rate versus displacement, and pressure versus volume)

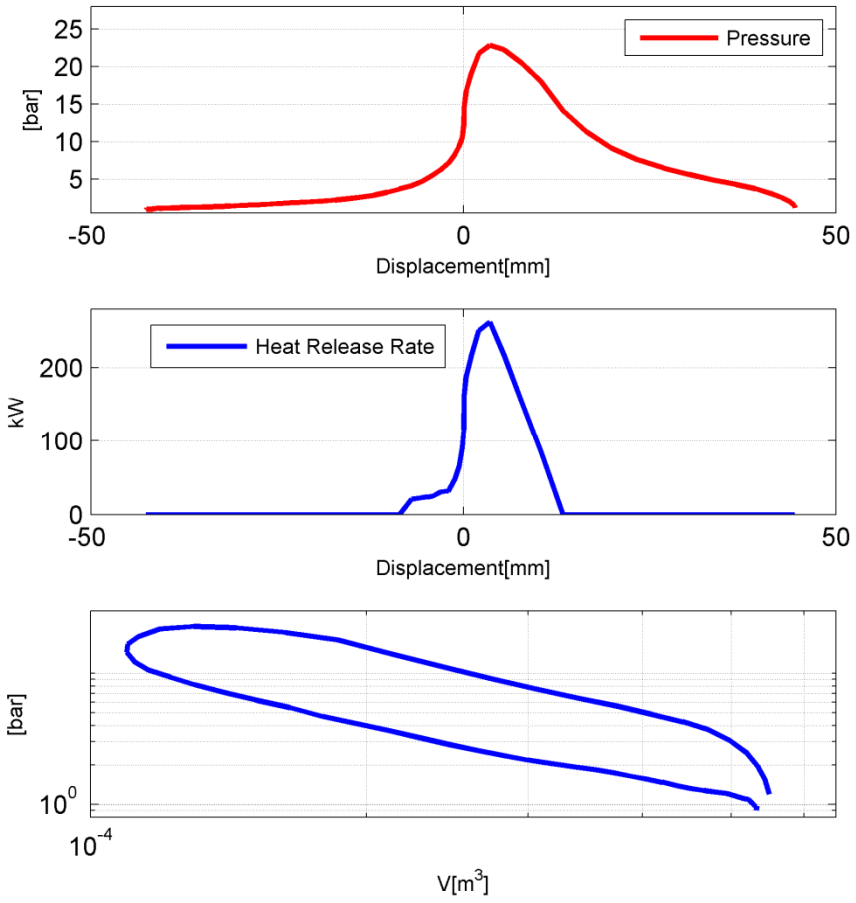

Fig. 4.20 Combustion data at 54 mm fuel injection timing (from top to bottom: combustion chamber pressure versus displacement, heat release rate versus displacement, and pressure versus volume)

4.4.3 Centerline position

The opposed piston design of the FPE enables the uniflow scavenging pattern, which is the scavenging process with the highest efficiency [96]. Uniflow scavenging can be realized by single piston with exhaust valve design [97] or opposed piston design [98-100] which the hydraulic FPE utilizes. The locations of the intake and exhaust ports are shown in Fig. 4.21. The distance between intake ports and combustion chamber

centerline is almost the same with distance between exhaust ports and the centerline. This means the intake ports will be uncovered at the same time when the exhaust ports open. The hydraulic FPE was originally designed for the HCCI combustion mode where a certain amount of residual gas from the previous cycle is required for the gas mixture to autoignite during the compression stroke. Therefore, the scavenging ports were designed to trap the residual gas. However, having the intake and exhaust ports open at the same time implies the high pressure hot exhaust will enter the intake manifold which hinders the entrance of fresh air. As a result, we have a lean air fuel mixture with high percentage of residual gas, which is difficult to be spark ignited with the given compression ratio. However, as shown in Fig. 2.1(b), there is a pair of on-off values in the hydraulic circuit that controls the relative position of the inner and outer pistons. In other words, the centerline position can be adjusted such that the piston pair still moves in synchronization, but the inner piston uncovers the exhaust ports earlier than the outer piston uncovers the intake ports. Therefore, the exhaust blowdown will mainly go through the exhaust port and allow the fresh air flowing into the combustion chamber more smoothly. For the purpose of illustration, the centerline position as shown in Fig. 4.21 is denoted as 0, the negative sign indicates the centerline is shifted to the left, and positive sign represents a right shift of the centerline.

Table 4.1 documents the combustion data of three centerline positions with -46 mm, BDC (54 mm) and 52 mm fuel injection timings. When centerline is shifted towards the left (intake ports opens earlier than the exhaust ports) for 1.5 mm, the overall percentage of engine misfire is high regardless of the fuel injection timing. That is caused by the fact

that exhaust port only opens for a short duration and the opening area is small as well, the uniflow scavenging pattern cannot be formed so that air fuel mixing is poor inside the combustion chamber. When centerline is at 0, fuel injection around the BDC results in the lowest percentage of misfire. On the other hand, with late fuel injection at 52 mm, the percentage of misfire is at the highest. When centerline position is shifted towards the right (exhaust ports open earlier than the intake ports) for 2 mm, the best operating condition is found if fuel were to be injected around the BDC. Compared to the 0 centerline position, allowing the exhaust ports opening prior to the intake ports creates better air fuel mixing that not only increase the combustion occurrence, it also improves the efficiency of the engine cycle. Therefore, centerline position at 2 and fuel injection timing at BDC are chosen for the continuous engine operation test. However, the experimental results show that combustion strength varies significantly between two consecutive cycles.

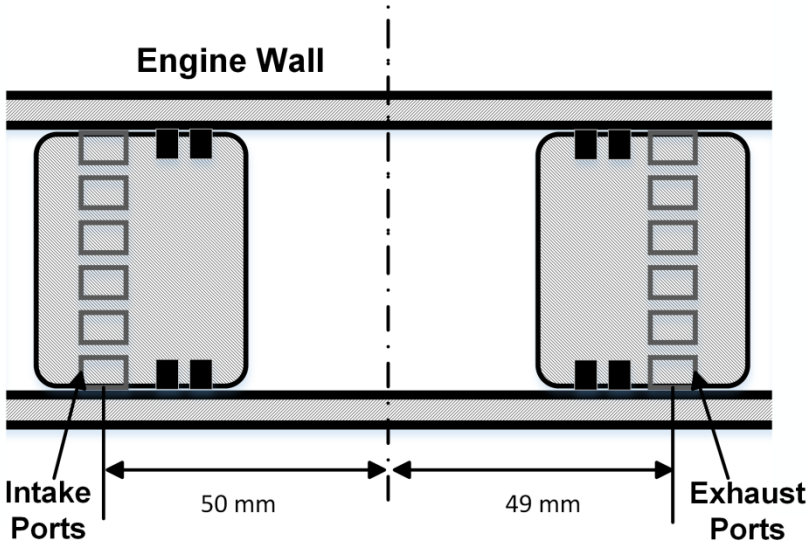

Fig. 4.21 Intake and exhaust ports location with respect to the combustion chamber centerline

Table 4.1 Combustion data of three centerline position at three fuel injection timings

	Centerline Position (mm)					
	-1.5		0		2	
Fuel Injection Timing (mm)	*% of Misfire*	*Average Work Output (J)*	*% of Misfire*	*Average Work Output (J)*	*% of Misfire*	*Average Work Output (J)*
-46	44	146	24	127	20	142
BDC	31	140	20	146	18	200
52	31	185	70	150	20	160

Fig. 4.22 shows the scavenging pump pressure of the engine with respect to the piston motion during the continuous operation (Fig. 4.14). The scavenging pump is designed to boost up the intake air pressure to the combustion chamber (a detailed schematic of the scavenging pump design is shown in Appendix 2). The first combustion occurs at 4.19s, and during the scavenging duration, a small jump of the scavenging pump pressure can be observed around 4.2s. At this time instant, the outer piston has just uncovered the intake ports, and the scavenging pump pressure is around 1.4 bar. However, the combustion chamber pressure is around 2.5 bar. This means the exhaust gas in the combustion chamber is entering the scavenging pump, which causes the pressure rise in the scavenging pump. Since the scavenging time duration is short, the entrance of exhaust gas reduces the amount of fresh air into the combustion chamber, so that weak combustion or misfire occurs in the following cycle. However, during the scavenging period of the next cycle (4.24s), the combustion chamber pressure is lower, and fresh air is able to enter and scavenge out the residual gas (see the scavenging pump pressure inside the circle). As expected, a strong combustion occurs at the end of the compression stroke that follows. This suggests that even though we can adjust the centerline position to influence the scavenging process, the effect is limited.

A potential solution is to utilize turbocharger. It is known that the intake pressure has a significant effect on the scavenging process in two stroke engines [96]. If the scavenging pump pressure can be boosted to be higher than 2.5 bar, the exhaust gas cannot enter the scavenging pump, thus allows for more fresh air flow. Meanwhile, the high pressure creates high speed intake flow that enhances the swirling effect and improves air fuel mixing. Therefore, continuous firing with less cycle-to-cycle variations can be achieved.

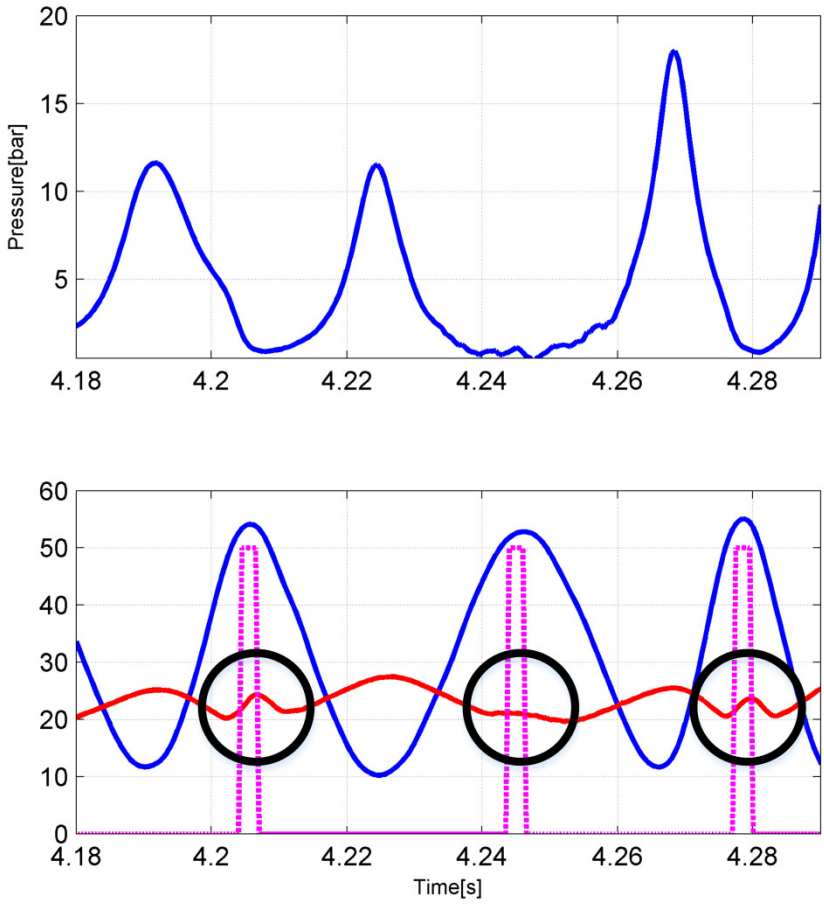

Fig. 4.22 Combustion chamber pressure and scavenging pump pressure during continuous engine operation

4.5 Conclusions

The focus of this chapter is on the combustion testing of the hydraulic FPE with the active motion control proposed in Chapter 3. The transient motion of the piston when switching from engine motoring to engine firing is first discussed and analysed. The transient motion is mainly caused by a mismatched coordination between the hydraulic force and the piston motion. Therefore, a transient control algorithm is created to restore the coordination, so that smooth engine operation can be achieved. The method is designed based on the active piston motion control that utilizes robust repetitive control to regulate the piston motion to follow a desired trajectory. The unique structure of repetitive control allows us to shift the future control signal to alter the hydraulic force. The algorithm consists of two parts: combustion detection and shifting (control signal shifting, reference shifting and tracking error shifting). The advantage of the transient control lies on the fact that it retains the repetitive learning mechanism but can adjust intelligently to nonrepetitive disturbances such as motoring to firing transition, misfire and cycle-to-cycle combustion variations.

The transient control is implemented on the hydraulic FPE for combustion tests, and its effectiveness has been demonstrated by various combustion scenarios. With the transient control, continuous firing tests are conducted. However, the results show that even with the similar fuel injection, spark timing and piston motion, the combustion outcomes are different. Therefore, detailed analyses of the combustion with various operating conditions are conducted. The results show that higher intake pressure boost is required to assist the scavenging process, so that continuous firing can be achieved.

Chapter 5

Summary and Future Work

5.1 Conclusions

The objective of the proposed research is on the modeling and control of the free piston engine (FPE) so that wide spread of this technology can be enabled. FPE as an alternative of the conventional internal combustion engines (ICE) offers the ultimate flexibility for variable compression ratio control by eliminating the crankshaft. The advantage of this setup lies in its simple design with few moving parts, giving a compact engine with low maintenance costs, reduced frictional losses and better fuel economy. However, the major technical barrier for application of this technology is the large cycle-to-cycle variation, especially during transient operation, which induces engine misfire. Previous works on free piston engine have shown limited success mainly due to the complex dynamic interactions between the combustion and the load in real-time. The research work in the thesis offers a unique and effective solution to the challenge.

The first part of the research focus on the modeling and analysis of the hydraulic free piston engine system to understand the characteristic of the engine operation. A comprehensive model of the hydraulic FPE system is developed. The piston dynamics of the FPE is compared with the conventional ICE. A calibration-based piston motion control is investigated using the model, and simulation results demonstrate the limitation of the calibration-based control when operating condition changes. The high order model developed earlier lead to the derivation of a cycle-to-cycle based model that is used for stability analysis of the engine operation. The model is validated and linearized around

equilibrium points with respect to a range of operating conditions for stability checking. The results demonstrate that feedback control is required to achieve stable engine operation.

In the second part of the research, an active piston motion control is proposed, designed and implemented. The motion control utilizes the energy in the storage unit to regulate the piston to follow a prescribed trajectory. Due to the repetitive motion of the piston, robust repetitive control is employed. Experimental results demonstrate the effectiveness of the proposed control. To further improve the tracking performance of the control system, a linear and nonlinear feedforward control are designed to assist the repetitive control. The combined control system demonstrates the tracking performance beyond the current state-of -the-art in electrohydraulic systems. Additionally, the control of a digital hydraulic FPE design is also investigated. The simulation results demonstrate the feasibility of piston motion control with fast response hydraulic on-off valves to reduce production cost.

The last part of the research focuses on the combustion testing of the hydraulic FPE with the regulation of the proposed motion control. A transient control algorithm which involves the modification of the repetitive control is developed. The transient control detects and automatically adjust the control signal to eliminate the transient piston motion caused by aperiodic phenomenon such as transition from motoring to firing or engine misfire (transition from firing to motoring), so that continuous engine operation can be achieved. Detailed analysis on the effects of operating conditions on the combustion processes is then conducted.

5.2 Contribution Summary

1. Study and analysis of the FPE operation. A comprehensive model of a hydraulic FPE is built to study the characteristics of the engine operation. Additionally, to study the stability of the FPE operation in a systematic way, a novel stability analysis has been conducted based on a cycle-to-cycle model that describes the states that governing the FPE operation.
2. Development of a key enabler for the FPE technology. The idea of piston trajectory tracking for FPE is proposed for the first time. An active piston motion control regulates the piston to follow a prescribed trajectory throughout the engine cycles. The uniqueness of the control is that it guarantees stable and reliable engine operation, and it also enables the design of distinct piston trajectories with respect to the operating conditions, so that engine efficiency can always be optimized.
3. Precise piston motion control is achieved. A feedfoward plus robust repetitive control structure is designed to guarantee stable and robust engine operation with precise trajectory control, the proposed motion control is implemented on a hydraulic FPE for engine motoring test, and the results show a performance beyond the current state-of-the-art.
4. Development of transient control for continuous engine operation. When switching from engine motoring to engine firing, a transient period after the combustion cycle, especially when a strong combustion occurs, prevents the continuous engine operation. A transient control algorithm is developed to

eliminate the transient period after the combustion cycle. The transient control modifies the control signal to alter the hydraulic force, and restore the coordination with the combustion chamber, so that piston motion will be maintained. Continuous engine operation is achieved with the proposed transient control.

5.3 Future Work

The research can be extended with three aspects in the future. First is on the design of the hydraulic free piston engine. Specifically, the location of the spark, fuel injector and scavenging ports can be redesigned to improve the mixing, and thus the combustion processes of the engine. Second is on the piston trajectory analysis and design, which is a brand new and exciting research frontier enabled by the proposed active piston motion. The information on the influence of piston trajectory on combustion is very limited, as well as the design of an optimal trajectory with various engine operating conditions. Third is to further explore the applications of the Hydraulic FPE. Hardware-in-the-loop tests can be done to evaluate the performance of the engine in real world applications. A flexible testing platform as shown in Fig. 5.1 can be built to emulate on-road or off-road vehicles powered by the HFPE. Models of various components of the vehicle as well as environmental conditions are developed and used to create a virtual vehicle interacting with the HFPE. This virtual system is run in real time parallel to the actual HFPE to emulate the loading conditions of the HFPE. This simulator outputs a hydraulic pressure and flow command to the loading system which adjusts its flow control valve to achieve the desired level of hydraulic fluid supply.

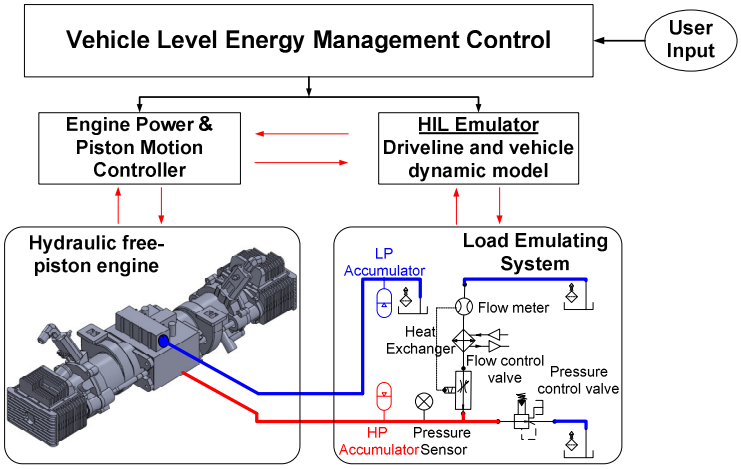

Fig. 5.1. Schematic diagram of the HFPE-in-the-loop test setup with load-emulating system.

Bibliography

[1] International Energy Agency, "Key World Energy Statistics," 2013.

[2] Heywood, J., "Internal Combustion Engine Fundamentals," New York: McGraw-Hill, 1988.

[3] Tanaka, Y., Hiyoshi, R., Takemura, S., Ikeda Y. et al., "A study of a Compression Ratio Control Mechanism for a Multiple-Link Variable Compression Ratio Engine," *SAE Technical Paper*, 2007-01-3547, 2007.

[4] Schwaderlapp, M., Habermann K. and Yapici, K., "Variable Compression Ratio – A Design Solution for Fuel Economy Concepts," *SAE Technical Paper*, 2002-01-1103, 2002.

[5] Rabhi, V., Beroff, J. and Dionnet, F., "Study of a Gear-Based Variable Compression Ratio Engine," *SAE Technical Paper*, 2004-01-2931, 2004.

[6] Van Blarigan, P., "Advanced Hydrogen Fueled Internal Combustion Engines," *Energy & Fuels*, vol. 12, no. 1, pp. 72-77, Jan. 1998.

[7] Pescara, R., Motor compressor apparatus, *US Patent*, 657,641, 1928.

[8] Mikalsen, R. and Roskilly, A., "A review of free-piston engine history and applications," *Applied Thermal Engineering*, Vol. 27 Issue 14-15, pp. 2339-2352, Oct 2007.

[9] Flynn, G.,"Observations on 25,000 hours of free-piston-engine operation", *SAE Technical Paper*, 1957:65:508-515, 1957.

[10] Noren, O and Erwin, R., "The future of the free-piston engine in commercial vehicles", *SAE Technical Paper*, 1958:66:305-314, 1958.

[11] London, A., and Oppenheim, A., "The free-piston engine development – Present status and design aspects," *Transactions of the ASME*, 1952:74(2):1349-1361, 1952.

[12] Van Blarigan, P., "Rapid Combustion Electrical Generator" in *Reciprocating Engines Peer Review*, April 23-24, Chicago, Illinois 2002.

[13] Achten, P., Van Den Oever, I., Potma J. and Vael, G., "Horsepower with brains: The design of the CHIRON Free Piston Engine," *SAE Technical Paper*, 2000-01-2545, 2000.

[14] Hibi, A. and Ito, T., "Fundamental test results of a hydraulic free piston internal combustion engine," in *Proc. Inst. Mech. Eng., Part D: J. Automobile Eng.*, vol. 218, no. 10, pp. 1149-1157, 2004.

[15] Hu, J., Wu, W., Yuan, S. and Jing, C., "On-off Motion of a Hydraulic Free-piston Engine," *Proceedings of the Institution of Mechanical Engineers, Part D: Journal of Automobile Engineering,* vol. 227, issue.3, pp. 323-333. Aug. 2012.

[16] Zhao, Z., Zhang, F., Huang, Y., Zhao, C. and Guo, F. "An Experimental Study of the Hydraulic Free Piston Engine". *Applied Energy*, volume (99), pp. 226-233,2012.

[17] Johansen, T., Egeland, O., Aa Johannessen, E. and Kvamsdal, R., "Free-piston diesel engine timing and control-toward electronic cam-and crankshaft," *IEEE Trans. Control syst. Technol*, vol. 10, no. 2, pp. 177-190, Mar. 2002.

[18] Mikalsen, R. and Roskilly, A., "The control of a free-piston engine generator. Part 2: Engine dynamics and piston motion control". *Applied Energy*, volume (87), pp. 1281-1287, 2010.

[19] Xu, Z. and Chang, S., "Prototype Testing and Analysis of a Novel Internal Combustion Linear Generator Integrated Power System," *Applied Energy,* vol.87,

issue. 4, pp. 1342-1348, April 2010.

[20] Kosaka, H., Akita, T., Moriya, K., Goto, S., Hotta, Y., Umeno, T. and Nakakita, K., "Development of Free Piston Engine Linear Generator System Part 1 – Investigation of Fundamental Characteristics," *SAE Technical Paper,* 2014-01-1203, 2014.

[21] Goto, S., Moriya, K., Kosaka, H, Akita, T., Hotta, Y., Umeno, T. and Nakakita, K., "Development of Free Piston Engine Linear Generator System Part 2 – Investigation of Control System for Generator," *SAE Technical Paper,* 2014-01-1193, 2014.

[22] Tikkanen, S., Lammila, and Vilenius, M. "Control of dual hydraulic free piston engine", *International Journal of Autonomous Systems,* volume (4), pp.3-23, 2006.

[23] Kock, F. and Ferrari, C., "Flatness-based high frequency control of a hydraulic actuator," *Journal of Dynamic Systems, Measurement, and Control*, vol. 134, 021003.

[24] Kock, F., Haag, J. and Friedrich, H., "The free piston linear generator – Development of an innovative, compact, highly efficient range-extender module," *SAE Technical Paper*, 2013-01-1727, 2013.

[25] Li, K. and Sun, Z., "Modeling and Control of a Hydraulic Free Piston Engine with HCCI Combustion," Proceedings of the 52nd National Conference on Fluid Power, 2011.

[26] Li, K., Sadighi, A. and Sun, Z. (2014). Active motion control of a hydraulic free piston engine. IEEE/ASME Transactions on Mechatronics, volume (19), pp. 1148-1159.

[27] Li, K. and Sun, Z., "Stability Analysis of a Hydraulic Free Piston Engine with HCCI Combustion," Proceedings of 2011 Dynamic Systems Control Conference, Arlington VA, 2011.

[28] Lin, J. and Chang, S., “Modeling and Simulation of a Novel Internal Combustion-linear Generator Integrated Power System Using Matlab/Simulink,” *Proceedings of 2012 IEEE International Conference on Power and Energy*, December, 2012.

[29] Li, L., Luan, Y., Wang, Z., Deng, J. et al., "Simulations of Key Design Parameters and Performance Optimization for a Free-piston Engine," *SAE Technical Paper*, 2010-01-1105, 2010.

[30] Goldsborough, S. and Van Blarigan, P., "A Numerical Study of a Free Piston IC Engine Operating on Homogeneous Charge Compression Ignition Combustion," *SAE Technical Paper*, 1999-01-0619, 1999.

[31] Atkinson, C., Petreanu, S., Clark, N., Atkinson, R. et al., "Numerical Simulation of a Two-Stroke Linear Engine-Alternator Combination," *SAE Technical Paper*, 1999-01-0921, 1999.

[32] Ba, H., Lim, O. and Iida, N., "Simulation Study of SI-HCCI Transition in a Two-Stroke Free Piston Engine Fuelled with Propane," *SAE Technical Paper*, 2014-01-1104, 2014.

[33] Xiao, J., Li, Q., and Huang, Z., "Motion characteristic of a free piston linear engine." *Applied Energy* 87.4 (2010): 1288-1294.

[34] Huang, L., "An Opposed-Piston Free-Piston Linear Generator Development for HEV," *SAE Technical Paper* , 2012-01-1021, 2012

[35] Zhao, Z., et al. "Modeling and simulation of a hydraulic free piston diesel engine". No. 2008-01-1528. SAE Technical Paper, 2008.

[36] Fredriksson, J., and Denbratt, I., "Simulation of a two-stroke free piston engine". No. 2004-01-1871. SAE Technical Paper, 2004.

[37] Li, Q., Xiao, J., and Huang, Z., "Simulation of a two-stroke free-piston engine for electrical power generation." Energy & fuels 22.5 (2008): 3443-3449.

[38] Mikalsen, R., and A. P. Roskilly. "Performance simulation of a spark ignited free-piston engine generator." Applied Thermal Engineering 28.14 (2008): 1726-1733.

[39] Larmi, M., et al. Performance simulation of a compression ignition free piston engine. No. 2001-01-0280. SAE Technical Paper, 2001.

[40] Aichlmayr, H., Kittelson, D., and Zachariah, M., "Miniature free-piston homogeneous charge compression ignition engine-compressor concept—Part I: performance estimation and design considerations unique to small dimensions." Chemical Engineering Science 57.19 (2002): 4161-4171.

[41] Aichlmayr, H., Kittelson, D., and Zachariah, M., "Miniature free-piston homogeneous charge compression ignition engine-compressor concept-Part II: modeling HCCI combustion in small scales with detailed homogeneous gas phase chemical kinetics." Chemical Engineering Science 57.19 (2002): 4173-4186.

[42] Chang, J., Guralp, O., Filipi, Z. and Assanis, D., "New Heat Transfer Correlation for an HCCI Engine Derived from Measurements of Instantaneous Surface Heat Flux," *SAE Technical Paper*, 2004-01-2996, 2004.

[43] Benson, R. and Bradham, P., " A new gas dynamic model for the gas exchange process in two-stroke loop and cross scavenged engines," *Int. J. Mech. Sci.*, vol. 19, no. 12, pp. 693-711, 1977.

[44] Merker, G. and Gerstle, M., "Evaluation on Two Stroke Engines Scavenging Models," *SAE Technical Paper*, 970358, 1997.

[45] Guzzella, L. and Onder, H., "Mean-Value Models," in *Introduction to Modeling and Control of Internal Combustion Engine System*, 2nd Ed. Berlin, Heidelberg: Springer-Verlag Berlin Heidelberg, 2010.

[46] Rausen, D., Stefanopoulou, A. and Kang, J., "A Mean-Value Model for Control of Homogeneous Charge Compression Ignition (HCCI) Engines," *ASME Trans. J. Dyn. Syst., Meas. Control*, vol. 127, no. 3, pp. 355-362, Sep. 2005.

[47] H. Janssen, "Electromagnetic servo valve strategy for controlling a free piston engine." U.S. Patent 6 971 339 B2, Dec. 6, 2005.

[48] Shaver, G. et al, "Dynamic modeling of residual-affected homogeneous charge compression ignition engines with Variable Valve Actuation," *ASME Trans. J. Dyn.* Syst., Meas. Control, vol. 127, no. 3, pp. 374-381, Sep. 2005.

[49] Chiang, C., and Stefanopoulou, A., "Dynamics of homogeneous charge compression ignition (HCCI) engines with high dilution." American Control Conference, 2007. ACC'07. IEEE, 2007.

[50] Chiang, C. and Stefanopoulou, A., "Sensitivity analysis of combustion timing of homogeneous charge compression ignition gasoline engines." Journal of Dynamic Systems, Measurement, and Control 131.1 (2009): 014506.

[51] Chiang, C., and Stefanopoulou. A., "Steady-state multiplicity and stability of thermal equilibria in homogeneous charge compression ignition (HCCI) engines." Decision and Control, 2004. CDC. 43rd IEEE Conference on. Vol. 2. IEEE, 2004.

[52] Chiang, C., and Stefanopoulou, A., "Stability analysis in homogeneous charge compression ignition (HCCI) engines with high dilution." Control Systems Technology, IEEE Transactions on 15.2 (2007): 209-219.

[53] Li, K., Sadighi, A. and Sun, Z., "Motion Control of a Hydraulic Free-Piston Engine", *American Control Conference*, pg. 2878-2883, 2012.

[54] Li, K, Zhang, C. and Sun, Z., "Precise piston trajectory control for a free piston engine." *Control Engineering Practice*, 34 (2015): 30-38.

[55] Tomizuka, M., Tsao, T.C. and Chew, K.K., "Analysis and synthesis of discrete-time repetitive controllers," *ASME Trans. J.Dyn. Syst., Meas. Control*, vol. 111, pp.353-358, Sep. 1989.

[56] Tsao, T. and Tomizuka, M., "Robust adaptive and repetitive digital tracking control and application to a hydraulic servo for noncircular machining," *ASME Trans. J.Dyn. Syst., Meas. Control*, vol. 116, pp.24-32, 1994.

[57] Sun, Z. and Kuo, T., "Transient control of electro-hydraulic fully flexible engine valve actuation system," *IEEE Trans. on control systems technology*, vol. 18, NO.3, May 2010.

[58] Mohanty, A. and Yao, B., "Indirect adaptive robust control of hydraulic manipulators with accurate parameter estimates". IEEE Transactions on Control Systems Technology, volume (19), pp. 567 - 575. , 2011.

[59] Sirouspour, M. and Salcudean, S., "Nonlinear control of hydraulic robots". *IEEE Transactions on Robotics and Automation*, volume (17), pp. 173 - 182, 2001.

[60] Sohl, G. and Bobrow, J. "Experiments and simulations on the nonlinear control of a hydraulic servosystem". *IEEE Transactions on Control Systems Technology*, volume (7), pp. 238 - 247, 1999

[61] Yao, B., Bu, F., Reedy, J. and Chiu, G.. "Adaptive robust motion control of single-rod hydraulic actuators: theory and experiments". *IEEE/ASME Transactions on Mechatronics*, volume (5), pp. 79-91,2000.

[62] Tomizuka, M., "Zero phase error tracking algorithm for digital control". *ASME Journal of Dynamic Systems, Measurement, and Control*, volume (109), pp. 65-68. ,1987.

[63] Tomizuka, M., "Design of digital tracking controllers for manufacturing applications. *ASME Manufacturing Review*, volume (2), pp. 134-141,1989.

[64] Shi, W. and Stelson, K., "Practical considerations for implementing adaptive zero phase error tracking control for a two-stage positioning system". *1990 Japan-USA Symposium on Flexible Automation*, pp. 559- 566, 1990.

[65] Gross, E., Tomizuka, M. and Messner, W., "Cancellation of discrete time unstable zeros by feedforward control". *ASME Journal of Dynamic Systems, Measurement, and Control*, volume (116), pp. 33-38, 1994.

[66] Fliess, M., Levine, J., Martin, P. and Rouchon, P., "Flatness and defect of nonlinear systems: Introductory theory and examples". *International Journal of Control*, volume (61), pp. 1327-1361, 1995.

[67] Martin, P., "Aircraft control using flatness. Proceedings of the symposium on control, optimization and supervision", *CESA 1996 IMACS multiconference, computational engineering in systems applications*, pp. 194-199, 1996.

[68] Chelouah, A., Borrelli, F., Glielmo, L. and Vasca, F., "Hybrid control of dry clutch engagement". *Proceedings of the European control conference 2001*, pp. 635-639,2001.

[69] Horn, J., Bamberger, J., Michau, P. and Pindl, S., "Flatness-based clutch control for automated manual transmissions". *Control Engineering Practice*, volume (11), pp. 1353-1359, 2003.

[70] Mitchell, D. M, *DC-DC Switching Regulator Analysis*, McGraw-Hill,New York, 1988.

[71] Barth, E., Zhang, J. and Goldfarb, M., "Control design for relative stability in a PWM-controlled pneumatic system". *ASME Journal of Dynamic Systems, Measurement, and Control*, volume (116), pp. 33-38, 1994.

[72] Shen, X., Zhang, J., Barth, E. J., & Goldfarb, M., "Nonlinear averaging applied to the control of pulse width modulated (PWM) pneumatic systems". *American Control Conference, 2004. Proceedings of the 2004*, 2004.

[73] Noritsugu, T. "Pulse-width modulated feedback force control of a pneumatically powered robot hand." Proc. of International Symposium of Fluid Control and Measurement. 1985.

[74] Shih, M., and Hwang, C., "Fuzzy PWM control of the positions of a pneumatic robot cylinder using high speed solenoid valve." JSME international journal. Series C, dynamics, control, robotics, design and manufacturing 40.3 (1997): 469-476.

[75] Royston, T. and Singh, S., "Development of a Pulse-Width Modulated Pneumatic Rotary Valve for Actuator Position Control." *Journal of dynamic systems, measurement, and control*, 115.3 (1993): 495-505.

[76] Ahn, K., and Yokota, S., "Intelligent switching control of pneumatic actuator using on/off solenoid valves." *Mechatronics*, *IEEE/ASME Transactions on* , 15.6 (2005): 683-702.

[77] Shen, X., et al. "Nonlinear model-based control of pulse width modulated pneumatic servo systems." *Journal of dynamic systems, measurement, and control* 128.3 (2006): 663-669.

[78] Barth, E., Zhang, J., and Goldfarb, M., "Sliding mode approach to PWM-controlled pneumatic systems." *American Control Conference*, 2002.

[79] Van Varseveld, R.B.; Bone, G.M., "Accurate position control of a pneumatic actuator using on/off solenoid valves," *Mechatronics, IEEE/ASME Transactions on* , vol.2, no.3, pp.195-204, Sep 1997.

[80] Li, K., Zhang, C., Sun, Z., “Transient Control of a Hydraulic Free Piston Engine” Proceeding of 2013 Dynamic Systems Control Conference, Palo Alto, CA, 2011.

[81] Okude, K., Mori, K., Shiino, S. and Moriya, T., "Premixed Compression Ignition (PCI) Combustion for Simultaneous Reduction for NOx and Soot in Diesel Engine," SAE 2004-01-1907, 2004.

[82] Iwabuchi, Y., Kawai, K., Shoji, T. and Takeda, Y., "Trial of New Concept Diesel Combustion System – Premixed Compression-Ignited Combustion," SAE 1999-01-0185, 1999.

[83] He, X., Durret, R. and Sun, Z., "Late Intake Valve Closing as an Emission Control Strategy at Tie 2 Bin 5 Engine-Out NOx Level," SAE International Journal of Engines, vol.1, no. 1, pp.427-443, 2008.

[84] Pilling, M. J., "Low-Temperature Combustion and Auto-Ignition," vol.35, Elsevier Science, 1997.

[85] Allen, J. and Law, D., "Variable Valve Actuated Controlled Auto-Ignition: Speed Load Maps and Strategic Regimes of Operation," SAE 2002-01-0422, 2002.

[86] Oakley, A., Zhao, H., Ladommatos, N. and Ma T., "Experimental Studies on Controlled Auto-ignition (CAI) Combustion of Gasoline in a 4-Stroke Engine," SAE Technical Papers, 2001-01-1030, 2001.

[87] Kokjohn, S. L., Hanson, R. M., Splitter, D. A., and Reitz, R. D., "Experiments and Modeling of Dual-Fuel HCCI and PCCI Combustion Using In-Cylinder Fuel Blending," SAE International Journal of Engines vol.2, no. 2, pp.24-39, 2010.

[88] Tanaka, S, Ayala, F., Keck, J. C. and Heywood, J. B., "Two-Stage Ignition in HCCI Combustion and HCCI Control by Fuels and Additives," Combustion and flame vol.132, no. 1, pp. 219-239, 2003.

[89] Shaver, G. M., Caton, P. A., Edwards, C. F., Gerdes, J. C and Roelle, M. J, "Dynamic Modeling of Residual-Affected Homogeneous Charge Compression Ignition Engines with Variable Valve Actuation," ASME Trans., J. Dyn. Syst., Meas. Control, vol. 127, pp. 374-381, 2005.

[90] Shaver, G. M., Gerdes, J. C. and Roelle, M. J, "Physics-Based Modeling and Control of Residual-Affected HCCI Engines," J. Dyn. Sys. Meas., Control. 2009; vol.131, no. 2, 021002-021002-12.

[91] Lujan, J., Bermudez, V., Guardiola, C. and Abbad, A., "A methodology for combustion detection in diesel engines through in-cylinder pressure derivative signal", *Mechanical Systems and Signal Processing*, volume (24), pp. 2261-2275, 2010.

[92] Payri, F., Lujan, J., Martin, J. and Abbad, A., "Digital signal processing of in-cylinder pressure for combustion diagnosis of internal combustion engines", *Mechanical Systems and Signal Processing*, volume (24), pp. 1767-1784, 2010.

[93] Shiao, Y. and Moskwa, J., "Cylinder pressure and combustion heat release estimation for SI engine diagnostics using nonlinear sliding observers", *IEEE Transactions on Control Systems Technology*, volume (3), pp. 70- 78, 1995.

[94] Sellnau, M., Matekunas, F., Battiston, P., Chang, C. and Lancaster, D., "Cylinder-pressure-based engine control using pressure-ratio-management and low-cost non-intrusive cylinder pressure sensors", *SAE Technical Paper Series*, 2000-01-0932, 2000.

[95] Lapuerta, M., Armas, O. and Hernandez, J., "Diagnosis of DI diesel combustion from in-cylinder pressure signal by estimation of mean thermodynamic properties of the gas", *Applied Thermal Engineering*, volume (19), pp. 513-529, 1999.

[96] Blair, Gordon P., Design and simulation of two-stroke engines. Warrendale, PA: *Society of Automotive Engineers*, 1996.

[97] Goldsborough, S. Scott, and Van Blarigan, P. "Optimizing the scavenging system for a two-stroke cycle, free piston engine for high efficiency and low emissions: a computational approach". *SAE Technical Paper*, 2003-01-0001, 2003.

[98] Kalkstein, J., Röver, W., Campbell, B., Zhong, L. et al., "Opposed Piston Opposed Cylinder (opoc™) 5/10 kW Heavy Fuel Engine for UAVs and APUs," *SAE Technical Paper*, 2006-01-0278, 2006.

[99] Franke, M., Huang, H., Liu, J., Geistert, A. et al., "Opposed Piston Opposed Cylinder (opoc™) 450 hp Engine: Performance Development by CAE Simulations and Testing," *SAE Technical Paper*, 2006-01-0277, 2006.

[100] Hofbauer, P., "Opposed Piston Opposed Cylinder (opoc) Engine for Military Ground Vehicles," *SAE Technical Paper*, 2005-01-1548, 2005.

Appendix 1

An off-line piston trajectory optimization strategy was investigated. The combustion model in Chapter 2 was used in this case. The objective of the optimization is to find the trajectory that result in the maximum energy output and dynamic programming is utilized to solve for the optimal trajectory. Based on the algorithm, the calculated optimal piston trajectory is shown in Fig. A1.1. The optimal trajectory results in a 5% increase of power output compared to a modified sinusoid trajectory. It should be noted that the pressure profiles from the two piston trajectories are presented in time domain. In the FPE, the displacement is not related to time directly because the duration between two piston positions could be varied by the piston trajectories arbitrarily.

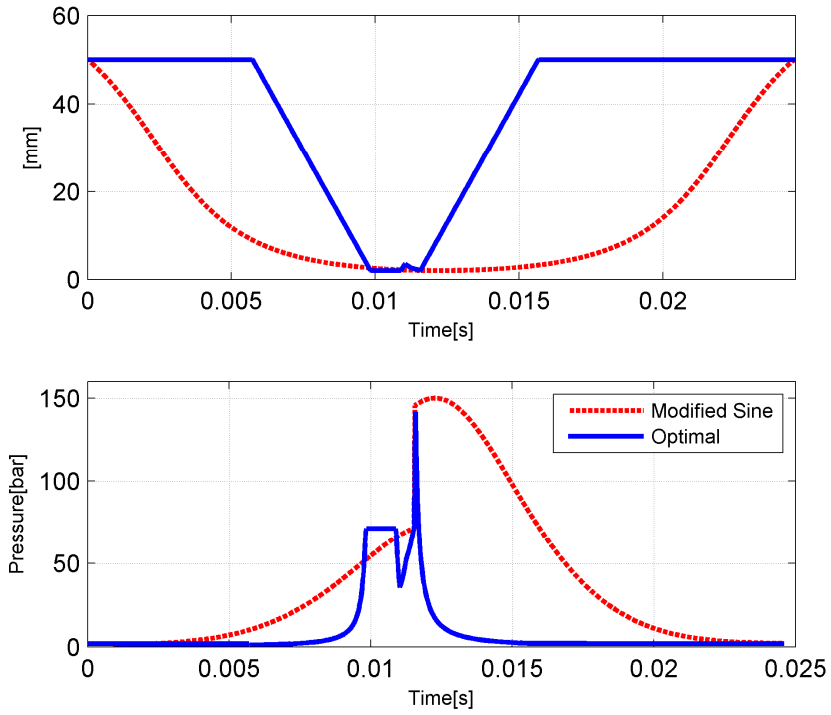

Fig. A1.1 Optimal piston trajectory compared to a modified sinusoid trajectory (position and chamber pressure)

Compared to the modified sinusoid trajectory, the optimal trajectory has a much faster compression and expansion stroke so that the piston staying at the TDC is minimized to reduce heat loss. Notice there is a "notch" on the pressure trace at TDC. This is because in the simplified model, heat release is assumed to be instantaneous after a combustion duration, which is only a function of temperature and pressure at start of combustion(SOC). Therefore, to reduce heat loss and ensure maximum power extraction, the piston expands first and then compresses the gas back to TDC at the moment of heat release (the "notch"). However, in real combustion process heat release is determined by the pressure, temperature and species concentration at every time instant after SOC, by using a model with chemical kinetics will result in a more accurate optimal solution. Also note the load dynamics are not considered in the above operation, which may set limitations on the piston trajectories.

Appendix 2

A detail drawing of the scavenging pump is shown in Fig. A2.1. The reed valves on the top ensure that the air flows from ambient to scavenging pump only. The reed valve on the bottom allows compressed gas flow from P1 to P2, but not in the opposite direction. When the outer piston is moving towards BDC (expansion stroke), pressure of P2 is decreasing while air in P1 is being compressed. When P1 is higher than P2, the compressed air overcomes the bottom reed valve and enters P2. Pressure in P1 and P2 continue to rise until the piston uncovers the intake port, where the high pressure air enters the combustion chamber.

When the outer piston is moving towards TDC (compression stroke), fresh air is drawn into P1 via the top reed valve while P2 is being compressed. Notice P2 does not consume any energy during the compression and expansion stroke. It is P1 that requires energy to boost the intake pressure and pushed the compressed air into the combustion chamber.

A pressure transducer is mounted on the scavenging pump to monitor the pressure of P2. In Fig. 4.22, the red line is the measured P2 pressure. A sudden increase of P2 pressure is observed when outer piston uncovers the intake port due to the pressure difference between P2 and combustion chamber. And the pressure drops only after piston reaches BDC, which suggests that during the scavenging process, the exhaust gas flows into P2, and then re-enters the combustion chamber. Therefore, when the outer piston covers the intake port, a large portion of the in-cylinder mixture is exhaust gas, which makes the combustion in the following cycle difficult to occur.

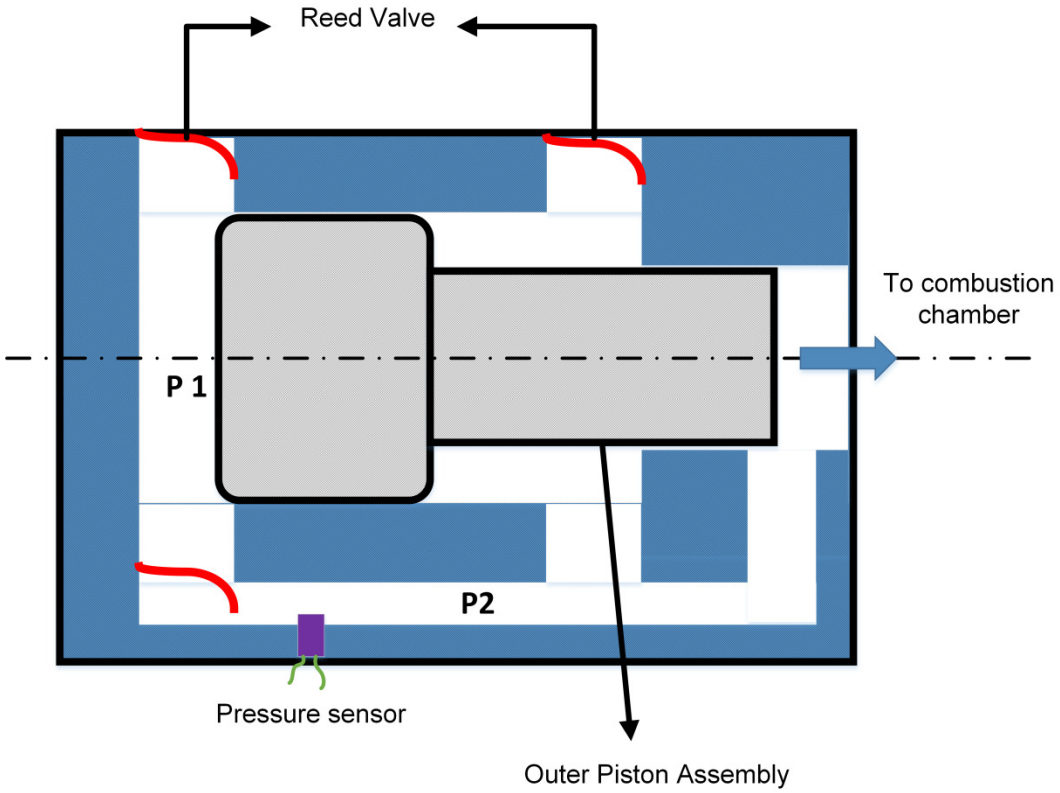

Fig. A2.1 Schematic of the scavenging pump